Internal Leaf CO_2 Transfer Conductance Diffusional Limitation and its Consequences for Modelling Photosynthesis in C_3 Plant Species

by

Gilbert J. Ethier
B.Sc., University of Victoria, 1996

A Dissertation Submitted in Partial Fulfilment of the
Requirements for the Degree of

DOCTOR OF PHILOSOPHY

in the Department of Biology

Internal Leaf CO_2 Transfer Conductance Diffusional Limitation and its Consequences for Modelling Photosynthesis in C_3 Plant Species

by

Gilbert J. Ethier
B.Sc., University of Victoria, 1996

Supervisory Committee

Dr. N.J. Livingston (Department of Biology)

Supervisor

Dr. T.A. Black (Faculty of Land and Food Systems, University of British Columbia)

Co-Supervisor

Dr. P.T. Gregory (Department of Biology)

Departmental Member

Dr. B.J. Hawkins (Department of Biology)

Departmental Member

Dr. M.J. Whiticar (Department of Earth and Ocean Sciences)

Outside Member

Dr. D.L. Spittlehouse (Research Branch, BC Ministry of Forest)

Additional Member

Dr. T.D. Sharkey (Department of Botany, University of Wisconsin)

External Examiner

Supervisory Committee

Dr. N.J. Livingston (Department of Biology)

Supervisor

Dr. T.A. Black (Faculty of Land and Food Systems, University of British Columbia)

Co-Supervisor

Dr. P.T. Gregory (Department of Biology)

Departmental Member

Dr. B.J. Hawkins (Department of Biology)

Departmental Member

Dr. M.J. Whiticar (Department of Earth and Ocean Sciences)

Outside Member

Dr. D.L. Spittlehouse (Research Branch, BC Ministry of Forest)

Additional Member

Dr. T.D. Sharkey (Department of Botany, University of Wisconsin)

External Examiner

ABSTRACT

Virtually all current estimates of the maximum carboxylation rate (V_{cmax}) of ribulose-1,5-bisphosphate carboxylase/oxygenase (Rubisco) and the maximum electron transport rate (J_{max}) for C_3 species used to parameterise Land Surface Models (LSMs) implicitly assume an infinite CO_2 transfer conductance from intercellular spaces to the sites of carboxylation (g_i). And yet, most measurements in perennial plant species or in ageing or stressed leaves show that g_i imposes a significant limitation on photosynthesis. In this study, I demonstrate that many current parameterisations of the photosynthesis model of Farquhar, von Caemmerer & Berry (1980) based on the leaf intercellular CO_2 concentration (C_i) are incorrect for leaves where g_i limits photosynthesis. I show how conventional A-C_i curve (net CO_2 assimilation rate of a leaf – A_n – as a function of C_i) fitting methods which rely on a rectangular hyperbola model under the assumption of infinite g_i can significantly underestimate V_{cmax} for such

leaves. Alternative V_{cmax} parameterisations of the conventional method based on a single, apparent Michaelis-Menten constant for CO_2 evaluated at C_i and used for all C_3 plants are also found to be inaccurate since the relationship between V_{cmax} and g_i is not conserved among species. To address this problem, I present an alternative A-C_i curve fitting method that accounts for g_i through a non-rectangular hyperbola version of the model of Farquhar *et al.* (1980).

Current estimates of a central Farqhuar *et al.* (1980) model parameter, $K_c(1+O/K_o)$ (*effective* Michaelis-Menten constant for CO_2), vary 4-fold, making it very difficult to justify any single value for the parameterisation of large scale, pan-species LSM studies. Following on previous work published over two decades ago, I demonstrate that the current range of $K_c(1+O/K_o)$ values chosen for LSMs is partly an artefact of many inaccurate *in vitro* determinations, and results in widely different estimates of A_n for given V_{cmac} values. Once corrected, the average $K_c(1+O/K_o)$ value determined *in vitro* for C_3 plants is essentially identical to the two *in vivo* values published to date, but considerable variation within the data set remains due to the poor accuracy of the *in vitro* determinations. The new A-C_i curve fitting method elaborated in this study suggests new ways of obtaining *in vivo* estimates of Rubisco's kinetic constants, as I demonstrate through a well-documented example.

The CO_2 transfer conductance was originally considered to be a constitutional property of a leaf related to its internal anatomy. This study provides the first estimates of g_i in a coniferous species and examines variation in g_i through time and space in relation to anatomical and physiological traits. Gas exchange measurements and subsequent novel A-C_i curve analyses, as well as stable carbon isotope, nitrogen (N), protein, and pigment analyses, were made on upper and lower canopy, current- to 4-year-old needles of 50-year-old *Pseudotsuga menziesii* trees. During the first growing season, needle thickness and leaf mass per area decreased by 30% from the top to bottom of the canopy. These anatomical changes were accompanied by modest variation in area-based estimates of g_i, but no causal link could be established between anatomical traits and mass-based estimates of g_i, whether in current-

year or older foliage. Both g_i and the stomatal conductance of leaves were closely coupled to V_{cmax}, J_{max} and A_n with all variables decreasing with increasing leaf age. The N content of leaves, as well as the amount of Rubisco and other proteins, increased during the first three growing seasons, then stabilised afterwards. Thus, the age-related photosynthetic nitrogen use efficiency decline of leaves was not a consequence of decreased allocation of nitrogen towards Rubisco and other proteins. Rather, loss of photosynthetic capacity was the result of the decreased activation state of Rubisco and proportional down-regulation of electron transport towards the photosynthetic carbon reduction and photorespiratory cycles in response to a reduction of CO_2 supply to the chloroplasts' stroma.

TABLE OF CONTENTS

LIST OF TABLES

Chapter 1

Chapter 2

Chapter 3

Appendix A

LIST OF FIGURES

Chapter 1

Chapter 2

Chapter 3

Appendix A

LIST OF SYMBOLS AND ABBREVIATIONS

a	carbon isotope fractionation due to diffusion through stomata (4.4‰)
a_b	carbon isotope fractionation due to diffusion through the boundary layer (2.9‰)
a_i	carbon isotope fractionation due to the dissolution and diffusion of CO_2 in water (1.8‰)
A_c	RuBP-saturated CO_2 assimilation rate (μmol CO_2 m^{-2} s^{-1})
A_j	RuBP-limited CO_2 assimilation rate (μmol CO_2 m^{-2} s^{-1})
A_{max}	maximal RuBP-limited gross CO_2 assimilation rate (μmol CO_2 m^{-2} s^{-1})
A_n	net CO_2 assimilation rate (also denoted "A") (μmol CO_2 m^{-2} s^{-1})
ATP	adenosine triphosphate
b	net carbon isotope fractionation caused by Rubisco and PEP carboxylation (30‰)
C	gas phase CO_2 concentration (μmol mol^{-1}) or partial pressure (μbar) in an *in vitro* assay media
C_a	CO_2 concentration (μmol mol^{-1}) or partial pressure (μbar) of the ambient air
C_c	chloroplastic CO_2 concentration (μmol mol^{-1}) or partial pressure (μbar)
C_i	CO_2 concentration (μmol mol^{-1}) or partial pressure (μbar) in the substomatal intercellular air spaces
C_s	CO_2 concentration (μmol mol^{-1}) or partial pressure (μbar) at the leaf surface
C_i*	intercellular CO_2 photocompensation point (μmol mol^{-1} or μbar)
C_3	photosynthetic pathway producing 3-carbon sugars
C_4	photosynthetic pathway producing 4-carbon sugars
CO_2	carbon dioxide
Chl	chlorophyll
E	energy of activation from the Arrhenius temperature function (kJ K^{-1} mol^{-1})
ELISA	enzyme-linked immunosorbtion assay

g_i	CO_2 transfer conductance from the substomatal intercellular air spaces to the stromal carboxylation sites (mol CO_2 m^{-2} s^{-1})
g_s	stomatal conductance (mol m^{-2} s^{-1})
g_{sc}	stomatal conductance to CO_2 (mol CO_2 m^{-2} s^{-1})
g_{sw}	stomatal conductance to water vapour (mol H_2O m^{-2} s^{-1})
HCO_3^-	bicarbonate ion
I	incident irradiance (μmol quanta m^{-2} s^{-1})
J	photochemical electron transport rate (μmol electrons m^{-2} s^{-1})
J_{max}	maximal photochemical electron transport rate (μmol electrons m^{-2} s^{-1})
k_{cat}	catalytic turnover rate of Rubisco
K_c	Michaelis-Menten constant for RuBP carboxylation (μmol mol^{-1} or μbar)
K_o	Michaelis-Menten constant for RuBP oxygenation (mmol mol^{-1} or mbar)
$K_c(1+O/K_o)$	effective Michaelis-Menten constant for CO_2 evaluated in the presence of O_2 (μmol mol^{-1} or μbar)
$K_m(CO_2)_i$	apparent Michaelis-Menten constant for CO_2 evaluated at C_i (μmol mol^{-1} or μbar)
Lsu	large subunit of Rubisco
LMA	leaf dry mass allocated per unit area (g m^{-2})
LSM	Land Surface Model
N	nitrogen
N_{area}	leaf nitrogen content per unit area (g m^{-2})
N_{mass}	leaf nitrogen content per unit mass (mg g^{-1})
NADPH	nicotinamide adenine dinucleotide phosphate, reduced form
O	O_2 concentration (mmol mol^{-1}) or partial pressure (mbar)
O_2	oxygen
pK_a	negative logarithm of the dissociation constant of carbonic acid (dimensionless)
PCR	photosynthetic carbon reduction

PCO	photosynthetic carbon oxidation (photorespiration)
PDB	Pee Dee Belemnite
PEP	phosphoenolpyruvate
PNUE	photosynthetic nitrogen use efficiency (μmol CO_2 mol^{-1} N s^{-1})
PPFD	photosynthetic photon flux density (μmol photons m^{-2} s^{-1})
R	universal gas constant (8.314 J K^{-1} mol^{-1})
R_d	mitochondrial respiration in the light (μmol CO_2 m^{-2} s^{-1})
RuBP	ribulose-1,5-bisphosphate
Rubisco	ribulose-1,5-bisphosphate carboxylase/oxygenase
$S_{c/o}$	Rubisco specificity factor (bar bar^{-1})
SD	standard deviation of the sample
SDS	sodium dodecyl sulfate
SE	standard error of the sample mean
T	temperature (°C or °K)
TPU	rate of triose phosphates utilisation
V_{cmax}	maximal carboxylation rate (μmol CO_2 m^{-2} s^{-1})
W_c	RuBP-saturated carboxylation rate (μmol CO_2 m^{-2} s^{-1})
α	leaf absorptance (dimensionless)
β	fraction of absorbed light that reaches photosystem II (dimensionless)
Γ	CO_2 compensation point (μmol mol^{-1} or μbar)
Γ^*	chloroplastic CO_2 photocompensation point (μmol mol^{-1} or μbar)
$\delta^{13}C$	stable carbon isotope composition (‰)
$\delta^{13}C_a$	carbon isotope composition of the ambient air (‰)
$\delta^{13}C_p$	carbon isotope composition of the plant sugar extract (‰)
Δ	carbon isotope discrimination (‰)
Θ	curvature factor of the non-rectangular hyperbola describing the light response of J or A_j (dimensionless)

μ	ionic strength of the *in vitro* assay medium (μM)
Φ	quantum yield of photochemical electron flow (mol electrons mol^{-1} quanta)
Φ_{CO2}	quantum yield of CO_2 assimilation (mol CO_2 mol^{-1} quanta)

ACKNOWLEDGMENTS

I feel very fortunate to have met my supervisor, Dr. Nigel J. Livingston. His youthful curiosity and enthusiasm for the field of plant ecophysiology have been a great source of inspiration to me. He has supported me financially and encouraged me morally since my first undergraduate years at UVIC, showed great patience and understanding during my prolonged illness, and, above all, gave me his trust and friendship.

This dissertation represents only a fraction of the work I put in my doctorate project. My research was originally inspired by discussions with Drs. Ray Leuning, T. Andrew Black, and David L. Spittlehouse about the validity of current "big leaf' canopy model assumptions in coniferous canopies. I would like to thank them for their intellectual input and encouragement, and also I extend this gratitude to the other members of my graduate committee, Drs. Louis A. Hobson, Patrick T. Gregory and Michael J. Whiticar. Special thanks to my friend & colleague, Dr. Charles Warren, for his collaboration on the CO_2 transfer conductance work.

This project generated a tremendous amount of field and laboratory work, which required the involvement of great number of people. I am truly indebted to the Natural Sciences and Engineering Research Council of Canada for funding my research; to my close friends Steeve & Edgar who came many times to my rescue in the woods; to Rob, Dale, and Rick, who joined us three to built the tall canopy access tower; to William R. Hook who advised me on TDR operation; to the many researchers, Drs. Barbara J. Hawkins, D.L. Spittlehouse, André Granier, Phil Comeau, Alan Mitchell, and Fred Peet, who generously lent their scientific equipment; to the UVIC machinists and technicians, Messrs. Patrick Kerfoot, Brad Binges, Gordon Davies, and David Smith, who built anything else I needed; to my field and lab assistants, John Christian, Tracy Rennie, Ian Jacobs, John Moran, Matthew Mitchell, Lindsay White, Derek Harrison and, most of all, Samantha Robbins and Ivan Petrovic. Warmest thanks are also due to my UBC friends & colleagues, Elyn Humphreys, Gordon Drewitt, and Zoran Nesic.

Most importantly, my love and gratitude to my parents, Monique et Jean, and to Andrea.

Dedication

Je tiens à dédier cette thèse à mon très cher ami Dr. Steeve Pepin, un homme de coeur et d'honneur comme il s'en fait peu et à qui je dois l'aboutissement final de ce travail.

A.

General introduction

The closing decades of the 20th century have been marked by growing concerns in the scientific community about the rising of the atmospheric CO_2 concentration and its effect on the global climate (Houghton *et al.* 2001). Considerable research effort has recently been given to the prediction of plant responses to future CO_2-enriched and warmer climates (e.g. Drake, Gonzàlez-Meler & Long 1997; Norby *et al.* 1999; Long *et al.* 2004, 2006; Körner *et al.* 2005) put in the context of the potential moderating capacity of natural terrestrial carbon sinks (e.g. Cox *et al.* 2000; Friedlingstein *et al.* 2001) and of the acceleration of human-induced land-cover changes and their impact on local surface–atmosphere interactions (e.g. Snyder, Delire & Foley 2004; Pitman *et al.* 2004). As a result, several large scale Land Surface Models (LSMs) have now been developed and coupled to existing climate models to explore the possible effects of the future terrestrial carbon cycle on the Earth's climate (e.g. Cramer *et al.* 2001; Dai, Dickinson & Wang 2004; Friend & Kiang 2005; Matthews *et al.* 2005).

The typical framework of modern (post-1980s) LSMs treats the vegetation cover over specified spatial grids as one "big leaf" suspended above the ground, rather than considering the land surface as a single, physical boundary exchanging energy, heat, and momentum with the atmosphere (Sellers *et al.* 1997; Pitman 2003). Initially, the big leaf analogy was introduced to allow the calculation of a canopy-scale estimate of the resistance to sensible (convection) and latent (evapotranspiration) heat transfer to the atmosphere based on the analytical integration of an empirical leaf-level equation relating the stomatal conductance to water vapour (g_{sw}) to microclimatic variables such as light, temperature, and atmospheric and soil moisture content (e.g. Dickinson *et al.* 1986; Sellers *et al.* 1986). Then, during the 1990s, following on the seminal work of Farquhar and colleagues on modelling leaf photosynthesis according to the C_3 and C_4 metabolic pathways (Berry & Farquhar 1978; Farquhar, von Caemmerer & Berry 1980; von Caemmerer & Farquhar 1982; see also Sharkey 1985 and

Harley & sharkey 1991) and that of Ball, Woodrow & Berry (1987), which led to the realisation that equations describing the supply of CO_2 through stomata and biochemical demand for CO_2 could be solved simultaneously to derive coupled leaf-level estimates of photosynthesis and transpiration (Leuning 1990; Collatz *et al.* 1991; Collatz, Ribas-Carbo & Berry 1992), new big leaf formulations linking canopy-level CO_2 and water vapor fluxes were introduced and soon were incorporated into a new, third generation of LSMs capable of simulating ecosystem photosynthetic responses to rising atmospheric CO_2 and air temperatures (e.g. Bonan 1995; Sellers *et al.* 1996; Cox, Huntingford & Harding 1998).

Within the big leaf model, the fundamental active components exchanging energy, carbon, and water with their surroundings and needing to be mathematically integrated are unit elements of leaf surface area whose physiological properties correspond to that of a reference model leaf from a plant species that has been parameterised *a priory* according to the Farquhar-von Caemmerer-Berry leaf photosynthesis model (the subject of my dissertation being a particularity of plants sharing the C_3 photosynthetic pathway, I will focus on this particular group for the remainder of my discussion). In close analogy, within the individual leaf, the fundamental photosynthetic units whose catalytic properties are being collectively fitted to the Farquhar *et al.* (1980) model are the enzymes ribulose-1,5-bisphosphate carboxylase/oxygenase (Rubisco) clustered inside individual chloroplasts. In both cases, the total, integrated CO_2 flux of the photosynthetic units can be inferred from reference, above surface conditions (i.e. incident radiation, air temperature, and atmospheric CO_2 and O_2 concentrations), provided that the resistances to mass (i.e. gases) and heat transfer are accounted for. For the big leaf model, which is scaled up from individual leaf-level parameterisations, the spatial gradients of irradiance *vs.* photosynthetic potentials also need to be defined.

The equations derived by Farquhar *et al.* (1980) and further elaborated in Farquhar & von Caemmerer (1982), Sharkey (1985), and Harley & Sharkey (1991) synthesise the stoichiometry of sub-cellular, rate-limiting biochemical processes related to photosynthetic

carbon assimilation in C_3 plant species. Since the Rubisco catalytic sites for CO_2 fixation are confined within the chloroplast stroma, the original equations of Farquhar *et al.* (1980) are formulated in terms of the CO_2 concentration found inside the chloroplasts (C_c). The present coupled leaf photosynthesis-stomatal conductance models incorporated into LSMs retain the original "chloroplastic" formulation of Farquhar *et al.* (1980), yet their converging solution for the CO_2 concentration to be used as model input goes no further than the intercellular air spaces immediately below the stomata.

The first *in vivo* estimates of the CO_2 transfer conductance from the substomatal air spaces to the stromal carboxylation sites (g_i) were obtained by Evans *et al.* (1986) based on online measurements of carbon isotope discrimination during gas exchange of herbaceous crops. Measurements performed on wheat and barley yielded g_i values above 0.4 mol m^{-2} s^{-1} bar^{-1}, which more or less confirmed the earlier assumption that g_i was large enough in C_3 plants to be ignored when modelling leaf photosynthesis (e.g. Farquhar *et al.* 1980; von Caemmerer & Farquhar 1981; Farquhar & Wong 1984). It was only in the next decade when g_i measurements were performed on several other C_3 plant species of various leaf morphologies and growth habits that this assumption first began to be contested (e.g. Lloyd *et al.* 1992; Epron *et al.* 1995; Roupsard, Gross & Dreyer 1996).

This dissertation addresses the problem met when seeking to parameterise the Farquhar-von Caemmerer-Berry leaf photosynthesis model for C_3 plant species for which g_i imposes a significant limitation on photosynthesis (i.e. the majority of woody species). In Chapter 1, I review the classic enzyme kinetics theory upon which the Farquhar *et al.* (1980) model is based to 1) demonstrate the inappropriateness of the current methodology used to parameterise the model for leaves where g_i limits photosynthesis and 2) derive an alternative model formulation and parameter estimation method that accounts for g_i.

In Chapter 2, I highlight an additional problem encountered in large scale LSMs; that of decoupling the two most important Farquhar *et al.* (1980) model parameters (the effective Michaelis-Menten constant for the carboxylation reaction in the presence of oxygen,

$K_c(1+O/K_o)$, and the maximal leaf carboxylation rate, V_{cmax}) describing the CO_2 response of leaf photosynthesis under Rubisco-limited conditions. Because this problem is often compounded by the use of inaccurate (or inappropriate) $K_c(1+O/K_o)$ values in the modelling community, much of the chapter is devoted to correcting previously biased *in vitro* estimates of K_c (Michaelis-Menten constant for the carboxylation reaction in the absence of oxygen) and to demonstrate how the theory and method presented in Chapter 1 can be used to estimate all the parameters describing Rubisco-limited photosynthesis in the model of Farquhar *et al.* (1980) simultaneously *in vivo* using a variation of the approach of von Caemmerer *et al.* (1994). I conclude Chapter 2 by suggesting which "chloroplastic" $K_c(1+O/K_o)$ value is most appropriate for pan-species parameterisations and which "intercellular" equivalent of $K_c(1+O/K_o)$ is best suited for LSMs.

Chapter 3 presents a Farquhar *et al.* (1980) model parameterisation for the dominant tree species (*Pseudotsuga menziesii* (Mirb.) Franco) of a 52-year-old, even-aged coastal British Columbia forest that is part of the Fluxnet-Canada research network. The parameterisation is based on the analysis of CO_2 and light responses curves performed according to the theory and recommendations made in the previous two chapters. Combined with protein and pigment assays, this analysis sheds light on the biochemistry behind the observed age-related photosynthetic decline of this evergreen species and reveals how the degree of activation of Rubisco remains closely coordinated with the stomatal and internal conductances to CO_2 through time to maintain the operational C_c of leaves close to the level established during the first growing season.

Lastly, in appendix, I include the study that started it all, an examination of the variation of g_i with canopy depth in *P. menziesii* trees and its relationships to the anatomical and physiological traits of foliage. This study was conducted and co-written with a post-doctoral fellow (Dr. Charles Warren) and is presented here in its original journal publication format. Chapters 1 and 3, which have also been published in the same journal, were written following the same format.

REFERENCES

Ball J.T., Woodrow I.E. & Berry J.A. (1987) A model predicting stomatal conductance and its contribution to the control of photosynthesis under different environmental conditions. In *Progress in Photosynthesis Research Vol. IV* (ed J. Biggins), pp. 221-224. Martinus Nijhoff Publishers, Dordrecht.

Berry J.A. & Farquhar G.D. (1978) The CO2 concentrating function of C_4 photosynthesis: a biochemical model. In *The Proceedings of the Fourth International Congress on Photosynthesis* (eds D. Hall, J. Coombs & T. Goodwin), pp 119–131. Biochemical Society of London, London, UK.

Bonan G.B. (1995) Land–atmosphere CO_2 exchange simulated by a land surface process model coupled to an atmospheric general circulation model. *Journal of Geophysical Research* **100,** 2817–2831.

Collatz G.J., Ball J.T., Grivet C. & Berry J.A. (1991) Physiological and environmental regulation of stomatal conductance, photosynthesis and transpiration: a model that includes a laminar boundary layer. *Agricultural and Forest Meteorology* **54,** 107–136.

Collatz G.J., Ribas-Carbo M. & Berry J.A. (1992) A coupled photosynthesis–stomatal conductance model for leaves of C_4 plants. *Australian Journal of Plant Physiology* **19,** 519–538.

Cox P.M., Betts R.A., Jones C.D., Spall S.A. & Totterdell I.J. (2000) Acceleration of global warming due to carbon-cycle feedbacks in a coupled climate model. *Nature* **408**, 184–187.

Cox P.M., Huntingford C. & Harding RJ. (1998) A canopy conductance and photosynthesis model for use in a GCM land surface scheme. *Journal of Hydrology* **212–213,** 79–94.

Cramer W., Bondeau A., Woodward F.I., Prentice I.C., Betts R.A., Brovkin V., Cox P.M., Fisher V., Foley J.A., Friend A.D., Kucharik C., Lomas M.R., Ramankutty N., Sitch S., Smith B., White A. & Young-Molling C. (2001) Global response of terrestrial ecosystem structure and function to CO_2 and climate change: results from six dynamic global vegetation models. *Global Change Biology* **7,** 357–373.

Dai Y., Dickinson R.E. & Wang Y.-P. (2004) A two-big-leaf model for canopy temperature, photosynthesis, and stomatal conductance. *Journal of Climate* **17,** 2281–2299.

Dickinson R.E., Henderson-Sellers A., Kennedy P.J. & Wilson M.F. (1986) Biosphere–Atmosphere Transfer Scheme (BATS) for the NCAR Community Climate Model. NCAR Technical Note TN-275 + STR.

Drake B.G., Gonzàlez-Meler M.A. & Long S.P. (1997) More efficient plants: A consequence of rising atmospheric CO_2? *Annual Review of Plant Physiology and Plant Molecular Biology* **48,** 609–39.

Epron D., Godard D., Cornic G. & Genty B. (1995) Limitation of net CO_2 assimilation rate by internal resistances to CO_2 transfer in the leaves of two tree species (*Fagus sylvatica* L. and *Castanea sativa* Mill.). *Plant, Cell and Environment* **18,** 43–51.

Evans J.R., Sharkey T.D., Berry J.A. & Farquhar G.D. (1986) Carbon isotope discrimination measured concurrently with gas exchange to investigate CO_2 diffusion in leaves of higher plants. *Australian Journal of Plant Physiology* **13,** 281–292.

Farquhar G.D. & von Caemmerer S. (1982) Modelling of photosynthetic response to environmental conditions. In *Physiological Plant Ecology II.* Encyclopedia of Plant Physiology, new series (eds O.L. Lange, P.S. Nobel, C.B. Osmond & H. Ziegler) Vol. 12B, pp. 550–587. Springer-Verlag, Heidelberg.

Farquhar G.D., von Caemmerer S. & Berry J.A. (1980) A biochemical model of photosynthetic CO_2 assimilation in leaves of C_3 species. *Planta* **149,** 78–90.

Farquhar G.D. & Wong S.C. (1984) An empirical model of stomatal conductance. *Australian Journal of Plant Physiology* **11,** 191–210.

Friedlingstein P., Bopp L., Ciais P., Dufresne J.-L., Fairhead L., LeTreut H., Monfray P. & Orr J. (2001) Positive feedback between future climate change and the carbon cycle. *Geophysical Research Letters* **28**, 1543–1546.

Friend A.D. & Kiang N.Y. (2005) Land surface model development for the GISS GCM: effects of improved canopy physiology on simulated climate. *Journal of Climate* **18,**

2883–2902.

Harley P.C. & Sharkey T.D. (1991) An improved model of C_3 photosynthesis at high CO_2: reversed O_2 sensitivity explained by lack of glycerate reentry into the chloroplast. *Photosynthesis Research* **27,** 169–178.

Houghton J.T., Ding Y., Griggs D.J., Noger M., van der Linden P.J., Dai X., Maskell K. & Johnson C.A. (2001) Climate Change, 2001, The Scientific Basis. Contribution of Working Group 1 to the Third Assessment Report of the Intergovernmental Panel on Climate Change. Cambridge University Press, Cambridge, UK.

Körner C., Asshoff R., Bignucolo O., Hättenschwiler S., Keel S.G., Peláez-Riedl S., Pepin S., Siegwolf R.T.W. & Zotz G. (2005) Carbon flux and growth in mature deciduous forest trees exposed to elevated CO_2. *Science* **309,** 1360–1362.

Leuning R. (1990) Modelling stomatal behaviour and photosynthesis of *Eucalyptus grandis*. *Australian Journal of Plant Physiology* **17,** 159–175.

Lloyd J., Syvertsen J.P., Kriedemann P.E. & Farquhar G.D. (1992) Low conductances for CO_2 diffusion from stomata to the sites of carboxylation in leaves of woody species. *Plant, Cell and Environment* **15,** 873–899.

Long S.P., Ainsworth E.A., Leakey A.D.B., Nösberger J. & Ort D.R. (2006) Food for thought: lower-than-expected crop yield stimulation with rising CO_2 concentrations. *Science* **312,** 1918–1921.

Long S.P., Ainsworth E.A., Rogers A. & Ort D.R. (2004) Rising atmospheric carbon dioxide: plants FACE the Future. *Annual Review of Plant Physiology and Plant Molecular Biology* **55,** 591–628.

Matthews H.D., Eby M., Weaver A.J. & Hawkins B.J. (2005) Primary productivity control of simulated carbon cycle–climate feedbacks. *Geophysical Research Letters* **32,** doi:10.1029/2005GL022941.

Norby R.J., Wullschleger S.D., Gunderson C.A., Johnson D.W. & Ceulemans R. (1999) Tree responses to rising CO_2 in field experiments: implications for the future forest. *Plant, Cell*

and Environment **22,** 683–714.

Pitman A.J. (2003) The evolution of, and revolution in, land surface schemes designed for climate models. *International Journal of Climatology* **23,** 479–510.

Pitman A.J., Narisma G.T., Pielke R.A. Sr. & Holbrook N.J. (2004) The impact of land cover change on the climate of south west western Australia. *Journal of Geophysical Research* **109,** doi:10.1029/2003JD004347.

Roupsard O., Gross P. & Dreyer E. (1996) Limitation of photosynthetic activity by CO_2 availability in the chloroplasts of oak leaves from different species and during drought. *Annales des Sciences Forestières* **53,** 243–254.

Sellers P.J., Dickinson R.E., Randall D.A., Betts A.K., Hall F.G., Berry J.A., Collatz G.J., Denning A.S., Mooney H.A., Nobre C.A., Sato N., Field C.B. & Henderson-Sellers A. (1997) Modeling the exchanges of energy, water, and carbon between continents and the atmosphere. *Science* **275,** 502–509.

Sellers P.J., Mintz Y., Sud Y.C. & Dalcher A. (1986) A Simple Biosphere model (SiB) for use within general circulation models. *Journal of the Atmospheric Sciences* **43,** 505–531.

Sellers P.J., Randall D.A., Collatz G.J., Berry J.A., Field C.B., Dazlich D.A., Zhang C., Collelo G.D. & Bounoua L. (1996) A revised land parameterization (SiB2) for atmospheric GCMs. Part I: model formulation. *Journal of Climate* **9,** 676-705.

Sharkey T.D. (1985) Photosynthesis in intact leaves of C_3 plants: physics, physiology and rate limitations. *The Botanical Review* **51,** 53–105.

Snyder P.K., Delire C. & Foley J.A. (2004) Evaluating the influence of different vegetation biomes on the global climate. *Climate Dynamics* **23,** 279–302.

von Caemmerer S., Evans J.R., Hudson G.S. & Andrews T.J. (1994) The kinetics of ribulose-1,5-bisphosphate carboxylase/oxygenase in vivo inferred from measurements of photosynthesis in leaves of transgenic tobacco. *Planta* **195,** 88–97.

von Caemmerer S. & Farquhar G.D. (1981) Some relationships between the biochemistry of photosynthesis and the gas exchange of leaves. *Planta* **153,** 376–387.

Chapter 1

On the need to incorporate sensitivity to CO_2 transfer conductance into the Farquhar-von Caemmerer-Berry leaf photosynthesis model

INTRODUCTION

Over the past two decades, the photosynthetic CO_2 responses of numerous C_3 plant species have been evaluated at the whole-leaf level in relation to the CO_2 concentration in the intercellular airspace subtending the stomata (C_i) and fitted to the photosynthesis model of Farquhar, von Caemmerer & Berry (1980). These "A-C_i curve" (net CO_2 assimilation rate of a leaf – A_n – as a function of C_i) analyses have been invaluable for elucidating and quantifying *in vivo* the fundamental biochemical processes underlying the photosynthetic responses of plants to various environmental conditions (von Caemmerer 2000). Several comparative studies document the species variability and the temperature or CO_2 sensitivity of two key model parameters derived from A-C_i curves: V_{cmax}, the maximum carboxylation rate of ribulose-1,5-bisphosphate carboxylase/oxygenase (Rubisco), and J_{max}, the maximum electron transport rate (e.g. Wullschleger 1993; Leuning 1997, 2002; Wohlfart *et al.* 1999; Medlyn *et al.* 1999, 2002; Bunce 2000). Such studies are particularly useful to global climate change modellers since the latest generation of surface carbon exchange models incorporate the equations of Farquhar *et al.* (1980) (Sellers *et al.* 1997; Pitman 2003). However, these estimates of V_{cmax} and J_{max}, and indeed all current canopy or landscape scale carbon exchange models, implicitly assume that once CO_2 has been transported into the leaf's internal airspace subtending the stomata, the diffusional resistance that remains between this point and the carboxylation sites is insignificant and can be ignored. Recent research has shown that this is often not the case. In perennial plants, for example, most reported values of leaf internal CO_2 transfer conductance (g_i) fall below 0.2 mol m^{-2} s^{-1} (Table 1.1), which is sufficiently

Table 1.1 Literature survey of CO_2 transfer conductance (g_i) measurements in C_3 plant species

Species	g_i range[a] (mol m^{-2} s^{-1})	Species	g_i range[a] (mol m^{-2} s^{-1})
Herbaceous annuals		Deciduous, cont'd	
Monocots		*Populus deltoides* x *nigra*[8]	0.50
Oryza sativa[1]	0.39 – 0.50	*Prunus persica*[3]	0.27 – 0.43
Triticum aestivum[1]	0.32 – 0.53	*Quercus petraea*[8]	0.24
Triticum durum[6]	0.35 – 0.60	*Quercus robur*[8, 12]	0.07 – 0.27
Triticum spp.[4]	0.638	*Quercus rubra*[2, 4]	0.10 – 0.18
Dicots		*Vitis vinifera*[16]	0.07 – 0.21
Xanthium strumarium[4]	0.37 – 0.60	Evergreens	
Beta vulgaris[4]	0.34	*Arbutus unedo*[4]	0.16
Cucumis sativus[4]	0.45	*Camellia japonica*[11]	0.07 – 0.12
Glycine max[12]	0.32	*Castanopsis sieboldii*[11, 15]	0.02 – 0.11
Nicotiana tabacum[1, 5, 12]	0.19 – 0.50	*Cinnamomum camphora*[11]	0.06
Phaseolus vulgaris[1]	0.17 – 0.29	*Citrus aurantium*[4]	0.02
Raphanus sativus[1]	0.25 – 0.38	*Citrus limon*[3]	0.15 – 0.18
Spinacia oleracea[10]	0.40	*Citrus paradisi*[3]	0.15 – 0.26
Vicia faba[4, 18]	0.34 – 0.46	*Eucalyptus blakelyi*[1]	0.16 – 0.19
Herbaceous perennials		*Eucalyptus globulus*[2, 4]	0.11– 0.12
Polygonum cuspidatum[14]	0.08 – 0.19	*Hedera helix*[4]	0.15
Woody perennials		*Ligustrum lucidum*[11]	0.07 – 0.11
Deciduous		*Macadamia integrifolia*[3]	0.11 – 0.13
Acer mono[13]	0.07 – 0.15	*Nerium oleander*[4]	0.22
Alnus japonica[13]	0.08 – 0.13	*Olea europea*[19]	0.06 – 0.12
Castanea sativa[7, 9]	0.02 – 0.15	*Pseudotsuga menziesii*[20]	0.14 – 0.20
Fagus sylvatica[7]	0.10	*Quercus glauca*[11]	0.07 – 0.08
Juglans nigra x *regia*[17]	0.09 – 0.19	*Quercus ilex*[4, 8]	0.10 – 0.11
Juglans regia[17]	0.08 – 0.22	*Quercus phillyraeoides*[11]	0.14
Populus maximowiczii[13]	0.04 – 0.20	*Simmondsia chinensis*[4]	0.03

[1]von Caemmerer & Evans (1991); [2]Harley *et al.* (1992a); [3]Lloyd *et al.* (1992); [4]Loreto *et al.* (1992); [5]Evans *et al.* (1994); [6]Loreto *et al.* (1994); [7]Epron *et al.* (1995); [8]Roupsard *et al.* (1996); [9]Lauteri *et al.* (1997); [10]Delfine *et al.* (1999); [11]Hanba, Miyazawa & Terashima (1999); [12]Gillon & Yakir (2000); [13]Hanba *et al.* (2001); [14]Kogami *et al.* (2001); [15]Miyazawa & Terashima (2001); [16]Flexas *et al.* (2002); [17]Piel *et al.* (2002); [18]Terashima & Ono (2002); [19]Centritto *et al.* (2003); [20]Warren *et al.* (2003).

[a]Values given are for well-watered plants, neither salt-stressed nor senescing. All g_i measurements were done at 25 °C leaf temperature except: [8, 20] (22 °C), [12] (23–29 °C), [6] (25–30 °C), [1]*Oryza sativa* and [4]*Simmondsia chinensis* (27 °C), [16] (30 °C).

small, given the photosynthetic capacity of the leaves, to impose a significant limitation on photosynthesis (e.g. Lloyd *et al.* 1992; Epron *et al.* 1995; Roupsard, Gross & Dryer 1996; Miyazawa & Terashima 2001; Warren *et al.* 2003). Furthermore, Bernacchi *et al.* (2002) have recently shown that g_i is strongly dependent on leaf temperature (see also Makino, Nakano & Mae 1994) and becomes increasingly limiting to photosynthesis as temperature rises. In such cases, failure to account for the finite g_i when estimating V_{cmax} from A-C_i curves results in erroneously low values (Epron *et al.* 1995; Centritto, Loreto & Chartzoulakis 2003; Warren *et al.* 2003).

As with stomatal conductance (g_s), g_i decreases in response to water or salinity stress (Roupsard *et al.* 1996; Delfine *et al.* 1999; Flexas *et al.* 2002; Centritto *et al.* 2003; Loreto, Centritto & Chartzoulakis 2003), the response being just as rapid and reversible as for g_s (Delfine *et al.* 1999; Centritto *et al.* 2003). As gas exchange studies of stomatal *vs.* non-stomatal limitations to photosynthesis during drought are typically based on A-C_i curve analyses carried out without considering g_i (e.g. Wilson, Baldocchi & Hanson 2000a and references therein), they overestimate the proportion of non-stomatal limitation attributed to a drought-induced loss of biochemical photosynthetic capacity (i.e. they underestimate V_{cmax}). Indeed, Centritto *et al.* (2003) recently showed that both V_{cmax} and J_{max} in olive (*Olea europea*) saplings remained unaffected by salt stress, the increased photosynthesis limitation being entirely due to simultaneous decreases in g_i and g_s. Similarly, the age-related decline of photosynthesis in annual and deciduous perennial species does not appear to be due solely to the reduction of g_s and loss of biochemical photosynthetic capacity. For example, Loreto *et al.* (1994) found that g_i decreased in parallel to A_n and g_s in maturing, well-watered wheat plants (*Triticum durum*) and that the relative contribution of g_i to photosynthetic limitation increased continuously throughout the maturation process. Similar results have also been found in spinach (Delfine *et al.* 1999), suggesting that g_i is an important factor causing the photosynthetic decline of leaves during ageing (Loreto *et al.* 1994) and thereby confounds the actual change of

biochemical photosynthetic capacity (i.e. V_{cmax}) throughout this process. This last fact has so far been overlooked in studies concerned with measuring the seasonal variability of V_{cmax} in annual crops and deciduous forests (e.g. Grossman-Clarke *et al.* 1999; Wilson, Baldocchi & Hanson 2000b; Kosugi, Shibata & Kobashi 2003).

This paper provides both a review and a critique of the current A-C_i curve analysis method which relies on fixed values for the kinetic constants of Rubisco under the assumption of infinite g_i. My objectives are 1) to explain why this method fails to properly estimate V_{cmax}, given a set of Rubisco kinetic constants, in leaves with low g_i relative to their photosynthetic capacity and 2) to present a new approach to estimate V_{cmax} or J_{max} that accounts for g_i. I start by reviewing the fundamental Michaelis-Menten theory upon which the photosynthesis model of Farquhar *et al.* (1980) is based to introduce the concepts and equations of the new A-C_i curve analysis method. I then illustrate the limitations of the existing approach using examples of incorrect V_{cmax} determinations and show how these errors are eliminated when using the new method.

THEORY

Rubisco-limited photosynthesis

The equations describing the original biochemical model of C_3 leaf photosynthesis of Farquhar *et al.* (1980) and its subsequent refinements (von Caemmerer & Farquhar 1981; Farquhar & von Caemmerer 1982; Harley & Sharkey 1991) have been presented on numerous occasions (see von Caemmerer 2000 for a detailed review). Here I review the equations describing Rubisco-limited photosynthesis through a series of theoretical CO_2 responses curves starting with the predicted enzyme kinetics of fully activated Rubisco *in vitro* in O_2-free media, then successively add the components that lead to the final formulation of whole-leaf net photosynthesis in relation to C_i. Such an approach emphasises the applicability of the fundamental Michaelis-Menten equation across all levels (enzyme to leaf) except at C_i. It also highlights the gradual apparent "burial" of

initial model parameters following the inclusion of the mitochondrial respiratory flux and the internal diffusion resistance.

Curve 1 of Fig. 1.1 illustrates the CO_2 response of a fully activated Rubisco preparation assayed *in vitro* under saturating concentrations of ribulose-1,5-bisphosphate (RuBP) and in O_2-free media. The curve follows the classical Michaelis-Menten equation

$$W_c = \frac{CV_{c\,max}}{C + K_c} \tag{1.1}$$

which describes the kinetic relationship between an enzyme and its substrate (x) as a rectangular hyperbola with asymptotes at V_{xmax} (ordinate) and $-K_x$ (abscissa). Following the notation of Farquhar *et al.* (1980), W_c denotes the RuBP-saturated carboxylation rate, V_{cmax} is the maximal carboxylation rate, and K_c is the Michaelis-Menten constant for CO_2; here C denotes the gas phase CO_2 concentration in the media. The Michaelis-Menten relation is fundamentally a function of diminishing returns. Its derivative

$$\frac{dW_c}{dC} = \frac{V_{c\,max}K_c}{(C + K_c)^2} \tag{1.2}$$

decreases continuously with increasing C, thereby describing the monotonic loss of free enzyme catalytic sites available to take advantage of further additions of substrate. That is, Eqn 1.2 describes the monotonic loss of *carboxylation efficiency* by Rubisco with increasing C. As long as the activity of the enzyme is unchanged, the rate of carboxylation efficiency loss is predictable and is given by

$$\frac{d^2W_c}{dC^2} = -\frac{2V_{c\,max}K_c}{(C + K_c)^3} \tag{1.3}$$

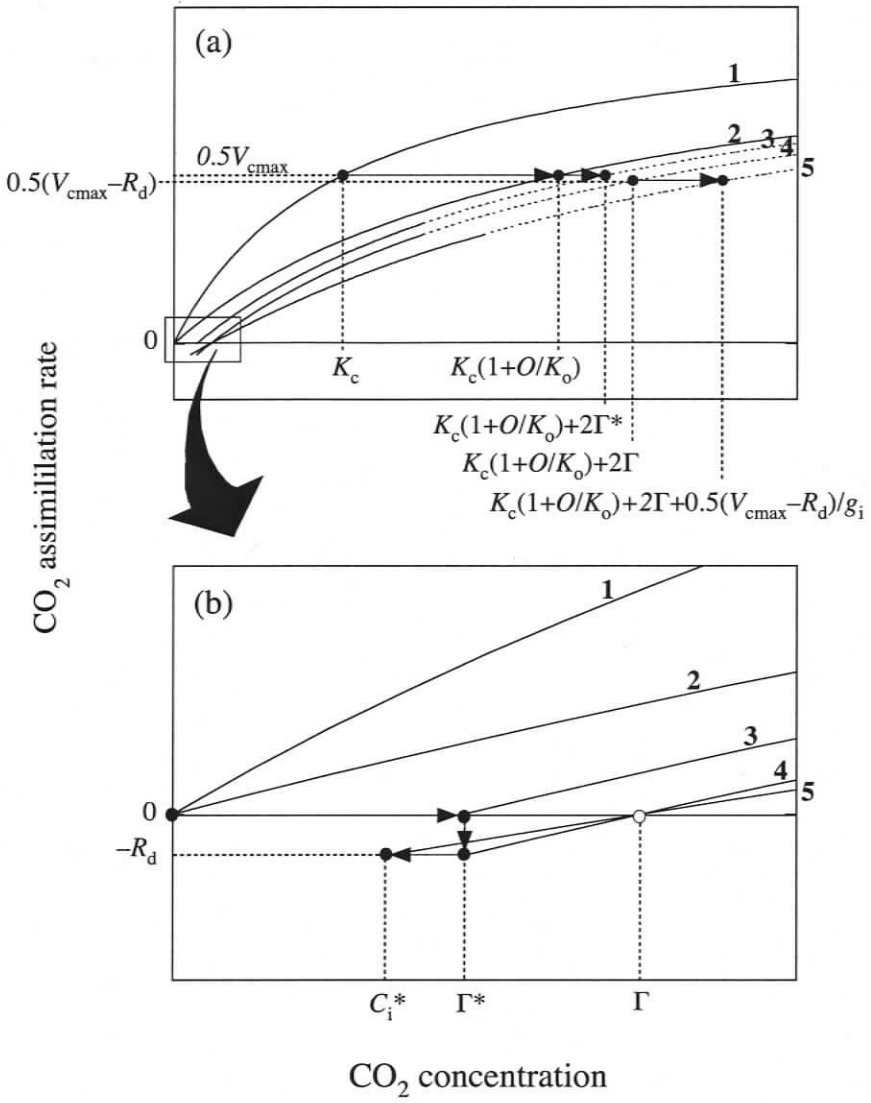

Figure 1.1 Hypothetical CO_2 response curves from purified Rubisco preparations and corresponding C_3 plant source leaves. Curves 1 and 2 illustrate the CO_2 response of the RuBP-saturated carboxylation rate (W_c) of fully activated Rubisco enzymes assayed *in vitro* in the absence or presence of O_2, respectively; curve 3 represents the whole-leaf CO_2 response of W_c minus photorespiration [$W_c(1–\Gamma^*/C_c)$] evaluated at C_c; and curves 4 and 5 are the corresponding CO_2 response of the net RuBP-saturated CO_2 assimilation rate (A_c) of the leaf evaluated at C_c and C_i, respectively. The upper panel (a) highlights the gradual change of the CO_2 concentration required to half-saturate the CO_2 response according to Michaelis-Menten theory while the lower panel (b) shows the corresponding change of the CO_2 concentration at which the gross RuBP-saturated CO_2 assimilation rate (W_c *in vitro*; W_c $(1–\Gamma^*/C_c)$ or A_c+R_d *in vivo*) equals zero. Broken lines sections indicate where CO_2 assimilation would normally no longer be Rubisco-limited in wild-type plants.

Thus, for a given V_{cmax}, the curvature of the CO_2 response function is entirely determined by K_c – the CO_2 concentration required to achieve a catalytic rate equal to $0.5V_{cmax}$.

Owing to the inherent bifunctionality of Rubisco with respect to CO_2 and O_2 (Andrews & Lorimer 1987), introduction of O_2 to the *in vitro* assay media inevitably diverts a portion of the enzyme's catalytic activity towards the oxygenation of RuBP (Bowes, Ogren & Hageman 1971; Bowes & Ogren 1972; Andrews, Lorimer & Tolbert 1973) and thereby decreases W_c at sub-saturating C (Fig. 1.1, curve 2). In the presence of the competitive inhibitor O_2, the Michaelis-Menten equation describing the CO_2 response of W_c becomes (Laing, Ogren & Hageman 1974)

$$W_c = \frac{CV_{cmax}}{C + K_c(1 + O/K_o)} \tag{1.4}$$

which shows that the effective CO_2 concentration required to half-saturate W_c – the *effective* Michaelis-Menten constant for CO_2 (von Caemmerer 2000) – is linearly dependent on the O_2 concentration in the media (O) and equals $K_c(1+O/K_o)$ (Fig. 1.1a), where K_o is the Michaelis-Menten constant for O_2 in the competitive oxygenation reaction. Graphically, the loss of carboxylation efficiency by Rubisco in the presence of O_2 is represented by the shift of the abscissa asymptote from $-K_c$ to $-K_c(1+O/K_o)$, which reduces the curvature of the rectangular hyperbola accordingly.

In intact, fully illuminated leaves from which Rubisco was presumably purified to perform the above-mentioned *in vitro* assays, the photorespiratory release of 0.5 mole of CO_2 which follows the oxygenation of each mole of RuBP (Tolbert 1971; Keys 1986) further depresses the gross yield of the photosynthetic process (Fig. 1.1, curve 3) by an amount equal to $W_c(\Gamma^*/C_c)$ (Farquhar & von Caemmerer 1982), where Γ^* is the *chloroplastic* CO_2 photocompensation point (Laisk 1977), that is the chloroplastic CO_2 concentration (C_c) at which W_c equilibriates with photorespiration (Fig. 1.1b). The

dependence of Γ* on O is related to Rubisco's relative specificity for CO_2 as opposed to O_2 ($S_{c/o}$); following Laing *et al.* (1974)

$$\Gamma^* = \frac{0.5O}{S_{c/o}} \tag{1.5}$$

Due to the photorespiratory flux, the CO_2 concentration required to half-saturate $W_c(1-\Gamma^*/C_c)$ inside the chloroplast increases to $K_c(1+O/K_o)+2\Gamma^*$ (Fig. 1.1a), as can be deduced from the denominator of the equation (written in Michaelis-Menten form) describing the CO_2 response of the net carboxylation rate following photorespiration:

$$W_c(1-\Gamma^*/C_c) = \frac{(C_c-\Gamma^*)V_{c\max}}{(C_c-\Gamma^*)+(K_c(1+O/K_o)+\Gamma^*)} \tag{1.6}$$

The new *effective* Michaelis-Menten constant for the combined carboxylation-photorespiration reaction is now equal to $K_c(1+O/K_o)+\Gamma^*$. Once again, we note that the curvature of the rectangular hyperbola is reduced accordingly.

As Woodrow & Berry (1988) remarked, one has to make a leap of faith to presume that the photosynthetic response of intact leaves can be interpreted in terms of the kinetic behaviour of Rubisco *in vitro*. The question is not so much the validity of the fundamental Michaelis-Menten model *in vivo*, but more the accuracy of the *in vitro* system and our ability to establish *in vitro* conditions that will not greatly affect the original *in vivo* Rubisco affinities for CO_2 and O_2 – otherwise the constants K_c, K_o, and $S_{c/o}$ will be affected (Kane *et al.* 1994).

Curve 4 of Fig. 1.1 represents the CO_2 response of a leaf's overall net RuBP-saturated CO_2 assimilation rate (A_c) evaluated at C_c. The curve is identical to curve 3 in all respects except that it is shifted down on the ordinate due to constant CO_2 input from the mitochondrial respiration of the illuminated cells (R_d) (Fig. 1.1b). Consequently, the

chloroplastic concentration at which all the respiratory processes of the leaf are in equilibrium with W_c no longer occurs at Γ^*, but further down the abscissa at Γ – the leaf's overall CO_2 compensation point (Fig. 1.1b). It follows that Γ^* is now found where A_c equals $-R_d$ (Fig. 1.1b).

Following Eqn 1.6, the Michaelis-Menten form of the equation describing the CO_2 response of A_c evaluated at C_c is given as

$$A_c = \frac{(C_c - \Gamma)(V_{c\max} - R_d)}{(C_c - \Gamma) + (K_c(1 + O/K_o) + \Gamma)} \tag{1.7}$$

Although the *effective* Michaelis-Menten constant for the overall net photosynthetic process is now increased to $K_c(1+O/K_o)+\Gamma$ (Fig. 1.1a), the curvature of the rectangular hyperbola describing curve 4 remains unchanged relative to curve 3 (Eqn 1.6) due to the lowering of the ordinate asymptote from V_{cmax} to "V_{cmax}–R_d" (Eqn 1.7). Equation 1.7 is the Michaelis-Menten equivalent of the commonly used equation of Farquhar *et al.* (1980)

$$A_c = \frac{(C_c - \Gamma^*)V_{c\max}}{C_c + K_c(1 + O/K_o)} - R_d \tag{1.8}$$

which of course is Eqn 1.6 minus R_d. Since there is a continuum of V_{cmax} and R_d combinations which will produce the ordinate asymptote "V_{cmax}–R_d", Eqn 1.8 requires that either Γ^* or R_d be known *a priori* to estimate V_{cmax} and "$K_c(1+O/K_o)$" accurately from a non-linear least-squares fit to the CO_2 response curve (knowledge of g_i is also required to express the A-C_i curve in terms of C_c). Equation 1.7, on the other hand, requires no *a priori* information (other than g_i) to properly estimate Γ, "V_{cmax}–R_d" and "$K_c(1+O/K_o)$" using non-linear regression methods. In both cases, the validity of the least-squares fit strongly depends on how well the curvature of the CO_2 response function follows the rectangular hyperbola model.

Under steady-state conditions

$$A_c = g_i(C_i - C_c) \tag{1.9}$$

Solving Eqn 1.9 for C_c and substituting in Eqn 1.7 or 1.8 gives a quadratic equation (von Caemmerer & Evans 1991) whose solution is the positive root

$$\begin{aligned} A_c &= \frac{-b + \sqrt{b^2 - 4ac}}{2a} \\ a &= -1/g_i \\ b &= (V_{c\max} - R_d)/g_i + C_i + K_c(1 + O/K_o) \\ c &= \begin{cases} -(V_{c\max} - R_d)(C_i - \Gamma) & \text{if using Eqn 1.7} \\ R_d(C_i + K_c(1 + O/K_o)) - V_{c\max}(C_i - \Gamma^*) & \text{if using Eqn 1.8} \end{cases} \end{aligned} \tag{1.10}$$

Equation 1.10 represents the CO_2 response of A_c evaluated at C_i (Fig. 1.1, curve 5). The A_c *vs.* C_i curve now follows a non-rectangular hyperbola. It shares the same ordinate asymptote (V_{cmax}–R_d) and x-intercept (Γ) as the A_c *vs.* C_c curve (Fig. 1.1, curve 4), but its curvature is decreased relative to the rectangular hyperbola model to a degree determined by the magnitude of g_i. Again, since there is a continuum of $K_c(1+O/K_o)$ and g_i combinations which will produce that curvature, Eqn 1.10, when derived from Eqns 1.7 and 1.9, requires that either $K_c(1+O/K_o)$ or g_i be known *a priori* to properly estimate the remaining parameters from a non-linear least-squares fit to the A_c *vs.* C_i curve. As mentioned above, *a priori* knowledge of either Γ^* or R_d is also required if the alternate form of Eqn 1.10 (based on Eqns 1.8 and 1.9) is used.

Equation 1.9 indicates that whenever there is a steady-state CO_2 flux through the leaf, there has to be a concentration gradient between C_i and C_c. Below Γ the flux is negative, so C_i is smaller than C_c, hence the appearance of an *intercellular* CO_2 photocompensation point (C_i^*) smaller than Γ^* at $-R_d$ (Fig. 1.1b). The difference between

Γ^* and C_i^* is rarely appreciated since g_i is usually assumed to be infinite in A-C_i curve analyses. Moreover, the CO_2 flux at $-R_d$ is usually very small so it is not expected to generate a significant drawdown between Γ^* and C_i^*. Still, Warren *et al.* (2003) estimated that this drawdown can be as high as 15 μbar in Douglas-fir (*Pseudotsuga menziesii*) and were able to use the measured differences between Γ^* and C_i^* to estimate g_i in this species using Eqn 1.9.

The validity of the non-rectangular hyperbola model (Eqn 1.10) rests on the assumption that g_i is purely diffusional and is therefore not affected by the changes in CO_2 concentration inside the leaf necessary to develop an A-C_i curve. This has been verified to some extent by both the isotopic (Evans *et al.* 1991) and the chlorophyll fluorescence (Harley *et al.* 1992a; Loreto *et al.* 1992) methods commonly used to estimate g_i. The recent evidence indicating a close association between carbonic anhydrase (Gillon & Yakir 2000) and aquaporin membrane channels (Terashima & Ono 2002) and g_i does not change this view since both proteins only act in facilitating the passive CO_2 diffusion process. Although Mächler, Müller & Dubach (1990) presented data suggesting the presence of an active CO_2 pump at the chloroplast envelope, I believe that their conclusion is due to calculation artefacts arising from using the rectangular hyperbola model to describe photosynthesis in relation to both C_c and C_i. Indeed, under this assumption, g_i will necessarily appear to scale in direct proportion to the carboxylation efficiency (dA_c/dC_c) which, as suggested in Eqns 1.2 and 1.3, rises increasingly sharply as C_c approaches Γ^* (substitute the appropriate terms from Eqn 1.6 into Eqns 1.2 and 1.3), thereby simulating, in the corresponding g_i case, an active transport system. No chloroplastic CO_2 concentrating mechanism has yet been identified in C_3 plants (Badger & Price 1994).

RuBP-limited photosynthesis

The half-asymptotic values of $W_c(1–\Gamma^*/C_c)$ and A_c on curves 3 to 5 (Fig. 1.1a) are shown on broken line portions of the Rubisco-limited CO_2 response curves to indicate that they are never reached under steady-state conditions in wild-type plants since the regeneration rate of the leaf's RuBP pool falls behind the potential rate of RuBP carboxylation/oxygenation by Rubisco and begins limiting photosynthesis at a lower C_c (Laisk & Oja 1974; Lilley & Walker 1975). Like A_c, the net RuBP-limited CO_2 assimilation rate (A_j) of a leaf can also be expressed in terms of an enzymatic Michaelis-Menten process whose overall efficiency diminishes with increasing C_c (i.e. a rectangular hyperbola model):

$$A_j = \frac{(C_c - \Gamma^*)J/4}{C_c + 2\Gamma^*} - R_d \qquad (1.11)$$

where J is the CO_2-saturated electron transport rate of the thylakoids reactions which ultimately supply the necessary energy in the form of ATP and NADPH for the regeneration of RuBP. Detailed treatments of the biochemical reactions involved in the process and of stoichiometric alternatives to Eqn 1.11 are given in Farquhar & von Caemmerer (1982) and von Caemmerer (2000). Equation 1.11 is given here in a form equivalent to Eqn 1.8, but it is understood that it can undergo the same derivations as outlined in Eqns 1.6 to 1.10 simply by replacing V_{cmax} by $J/4$ and $K_c(1+O/K_o)$ by $2\Gamma^*$. Following Farquhar & Wong (1984), the dependence of J on irradiance is given as

$$\theta J^2 - J(\alpha I + J_{max}) + \alpha I J_{max} = 0 \qquad (1.12)$$

where I is the incident irradiance, α is the quantum efficiency (number of electrons transfered per incident photon), and θ is the convexity (curvature factor) of the non-rectangular hyperbola.

CONVENTIONAL A-C_i CURVE FITTING METHOD

Disregarding the possible limitation imposed on photosynthesis at high CO_2 concentrations by the rate of triose phosphates utilisation (Harley & Sharkey 1991), the net CO_2 assimilation rate of a leaf is given as

$$A_n = \min\left\{A_c, A_j\right\} \tag{1.13}$$

where the appropriate equations describing A_c and A_j on the basis of C_i or C_c are given above. The conventional A-C_i curve fitting method commonly uses Eqns 1.8 and 1.11 to describe A_c and A_j, respectively, and assumes g_i to be infinite; thus

$$A_c = \frac{(C_i - \Gamma^*)V_{c\max}}{C_i + K_c(1 + O/K_o)} - R_d \tag{1.14}$$

and

$$A_j = \frac{(C_i - \Gamma^*)J/4}{C_i + 2\Gamma^*} - R_d \tag{1.15}$$

Equations 1.14 and 1.15 require that a total of six parameters be estimated from non-linear regression techniques, which, for reasons explained earlier, is beyond the iterative power of such techniques. Here, however, the leap of faith mentioned by Woodrow & Berry (1988) is taken and values for the kinetic constants of Rubisco ($S_{c/o}$ or Γ^*, K_c, K_o)

are chosen *a priori* from previously published estimates to constrain the least-squares fits to Eqns 1.14 and 1.15.

There are many $S_{c/o}$, K_c, and K_o estimates to choose from in the literature (see among others the multispecies comparative studies of Yeoh, Badger & Watson 1980, 1981; Jordan & Ogren 1981, 1983; Bird, Cornelius & Keys 1982; Makino, Mae & Ohira 1985; Parry *et al.* 1989; Kane *et al.* 1994; Laisk & Loreto 1996), but as far as the parameterisation of the model of Farquhar *et al.* (1980) is concerned, these have largely been restricted to values found in spinach and tobacco. Table 1.2 lists commonly used choices for Γ^* (often taken as C_i^*), K_c, and K_o and for the activation energy of the Arrhenius function describing their respective temperature response (e.g. Harley *et al.* 1992b; Wullschleger 1993; De Pury & Farquhar 1997; Walcroft *et al.* 1997; Wang & Leuning 1998; Medlyn *et al.* 1999, 2002; Dreyer *et al.* 2001; Wilson, Baldocchi & Hanson 2001; Kosugi *et al.* 2003). The rationale behind this approach is that the kinetic properties of Rubisco are so fundamental to the efficiency of the photosynthetic process that they should be largely conserved among C_3 plant species (von Caemmerer 2000).

Given a set of Rubisco kinetic constants, Eqn 1.13 can easily be fitted to the overall A-C_i curve once the respective domain of the A_c and A_j functions is defined. Von Caemmerer & Farquhar (1981) noted on the basis of C_i that the transition from A_c to A_j consistently occurred between 200 and 250 μbar in *Phaseolus vulgaris* when measurements were performed at ambient O_2 concentration and high irradiance. Furthermore, this transition zone appeared conserved over a range of leaf temperatures and nitrogen nutrition. Since then, it has become established practice to use the 200–250 μbar transition zone of *P. vulgaris* as the cut-off point for fitting A_c to the lowest portion of A-C_i curves performed under standard conditions in any species (e.g. Wullschleger 1993; Wohlfart *et al.* 1999; Bunce 2000). This approach is usually justified by the fact that the theoretical transition point between A_c and A_j is determined by the balance

Table 1.2 Kinetic constants of Rubisco commonly used to parameterise the photosynthesis model of Farquhar *et al.* (1980)

Reference	Species	Parameter	Value at 25 °C	Units	E (kJ K^{-1} mol^{-1})
Farquhar *et al.* (1980)[a, c]	*Spinacia oleracea* (15–35 °C)	K_c	460	μbar	59.413
		K_o	330	mbar	35.982
Jordan & Ogren (1984)[a, d]	*S. oleracea* (7–35 °C)	Γ^*	45.146	μmol mol^{-1}	29.213
		K_c	274.22	μbar	70.372
		K_o	418.29	mbar	14.351
Brooks & Farquhar (1985)[b]	*S. oleracea* (15–35 °C)	C_i^*	42.382	μmol mol^{-1}	30.037
von Caemmerer *et al.* (1994)[b]	*Nicotiana tabacum* (25 °C)	C_i^*	36.9	μbar	–
		K_c	404	μbar	–
		K_o	248	mbar	–
Bernacchi *et al.* (2001)[b]	*N. tabacum* (10–40 °C)	C_i^*	42.893	μmol mol^{-1}	37.83
		K_c	406.07	μmol mol^{-1}	79.43
		K_o	276.9	mmol mol^{-1}	36.38

The temperature response of the parameters was described by fitting the original data to the Arrhenius function normalised relative to 25 °C: $Parameter(T) = Parameter(25\ °C) \exp[(T - 298.15)\ E / 298.15\ RT]$

R *is* the gas constant (8.314 J K^{-1} mol^{-1}); T is the absolute temperature (T °C + 273.15) °K; E is the energy of activation; 1 cal = 4.184 J.

[a] Kinetic constants determined *in vitro*.

[b] Kinetic constants determined *in vivo* assuming $g_i = \infty$.

[c] Activation energies (E) for K_c and K_o are from Badger & Collatz (1977).

[d] After Harley *et al.* (1992b).

between J_{max} and V_{cmax} (von Caemmerer 2000) which have been found to correlate conservatively among species (Wullschleger 1993; Leuning 2002; Medlyn *et al.* 2002).

My studies on conifers revealed that the above-mentioned method repeatedly failed to properly fit the A-C_i curves I produced (n = 60) from shoots of 50-year-old Douglas-fir trees for which g_i was estimated to range (at least in current-year foliage) from 0.14 to 0.20 mol m^{-2} s^{-1} at 22 °C (Warren *et al.* 2003). Neither the Rubisco kinetic constants shown in Table 1.2 nor other recommended values (e.g. Collatz *et al.* 1991; Harley & Tenhunnen 1991; Bernacchi *et al.* 2002) produced acceptable results – the curvature of the fitted A_c function being always too pronounced to satisfy Eqn 1.13 (Fig. 1.2). Since my measurements were done using an integrating sphere at high diffuse irradiance (see Chapter 3), I considered it likely that the transition between A_c and A_j occurred at an appreciably higher C_i than 200–250 μbar (e.g. 300–400 μbar; Makino, Mae & Ohira 1988, Makino *et al.* 1994). However, I found that increasing the domain of the A_c function would solve the problem only if it were more than doubled and exclusively for sets of Rubisco kinetic constants that gave $K_c(1+O/K_o)$ values greater than 700 μbar.

Surprisingly, after over 20 years of use, to my knowledge there are no reports of similar difficulties with the standard A-C_i curve fitting method. For example, Wullschleger (1993) did a retrospective analysis of previously published A-C_i curves from 109 different C_3 plant species following the above-mentioned method, using the Rubisco kinetic contants values of Jordan & Ogren (1984) shown in Table 1.2, and reported no anomalies with the procedure. However, there are many cases in his report where V_{cmax} values were derived from invalid curve fits. Out of the 84 A-C_i curves that I analysed [V_{cmax} < 65 μmol m^{-2} s^{-1}, as estimated by Wullschleger (1993)], 15 could not be properly assessed due to insufficient C_i range or low light intensity, but a third of the remaining 69 gave wrong V_{cmax} estimates based on invalid curve fits. Two such examples

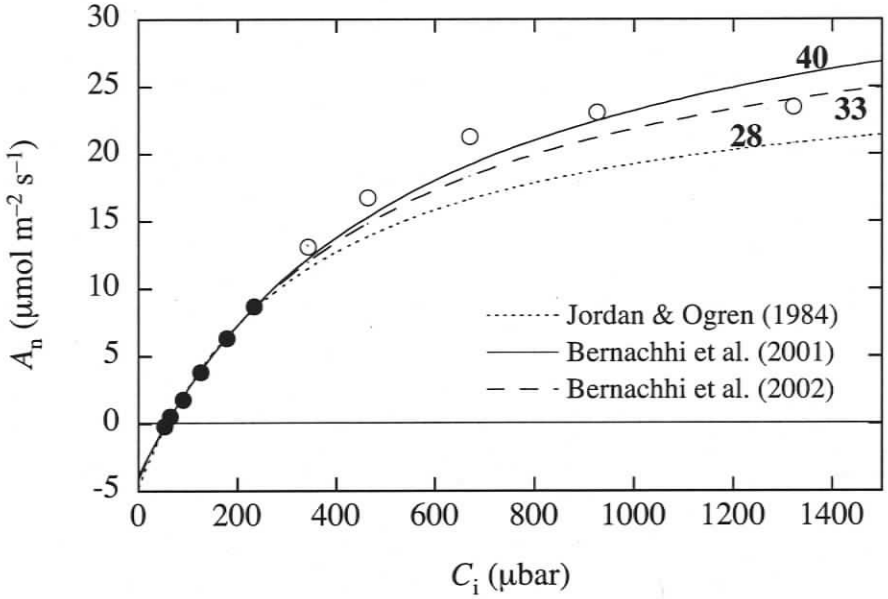

Figure 1.2 Typical CO_2 response of the net CO_2 assimilation rate (A_n) of a 1-year-old Douglas-fir shoot evaluated at C_i. Measurements were made at 22 °C and at saturating diffuse irradiance (1600 μmol m^{-2} s^{-1}) in an integrating sphere. Least-squares regression fits to the initial A-C_i curve portion (filled circles) were performed according to the standard A-C_i curve analysis method described in the text. The number beside each curve indicates the maximal carboxylation rate (V_{cmax}) obtained assuming infinite CO_2 transfer conductance (g_i) (Eqn 1.14), using popular Rubisco kinetic constant values (see Table 1.2 for Jordan & Ogren (1984) and Bernacchi *et al.* (2001); for Bernacchi *et al.* (2002) Γ^* = 33.86 μmol mol^{-1}, K_c = 195.41 μmol mol^{-1}, and K_o = 150.46 mmol mol^{-1} at 22 °C).

(Sun & Ehleringer 1986; Siebke *et al.* 1990) are reproduced in Fig. 1.3. The V_{cmax} values I obtained by following the procedure outlined above were within 1 μmol m^{-2} s^{-1} of those reported by Wullschleger (1993), that is 32 and 29 μmol m^{-2} s^{-1} for Sun & Ehleringer (1986) and Siebke *et al.* (1990), respectively, but it is clear from Fig. 1.3 that these were derived from invalid curve fits that underestimate the true V_{cmax} values which, according to the Rubisco kinetic constants of Jordan & Ogren (1984), would in both cases be about 56 μmol m^{-2} s^{-1} after accounting for g_i via Eqn 1.10 (see method outlined below).

NEW *A*-C_i CURVE FITTING METHOD

According to the non-rectangular hyperbola model (Eqn 1.10), A_c reaches its half-asymptotic value of $0.5(V_{cmax}-R_d)$ when C_i equals $K_c(1+O/K_o)+2\Gamma + 0.5(V_{cmax}-R_d)/g_i$ (Eqns 1.7 and 1.9) (Fig. 1.1a, curve 5). Under the assumption of infinite g_i, the least-squares rectangular hyperbola approximation to Eqn 1.10 that will produce the correct value for V_{cmax} is given by

$$A_c = \frac{(C_i - C_i^*)V_{cmax}}{C_i + K_m(CO_2)_i} - R_d \qquad (1.16)$$

The value $K_m(CO_2)_i$ is the *apparent* Michaelis-Menten constant for CO_2 evaluated at C_i. Since the value of C_i representing the half-asymptotic value of A_c in the initial non-rectangular hyperbola increases as g_i decreases, so will $K_m(CO_2)_i$. That is, the correct rectangular hyperbola approximation to Eqn 1.10 is one that keeps the ordinate asymptote at $V_{cmax}-R_d$ and increases the value of the abscissa asymptote in inverse proportion to g_i. The conventional *A*-C_i curve fitting method does the reverse; it fixes the abscissa asymptote at $-K_c(1+O/K_o)-\Gamma$ according to the Rubisco kinetic constants chosen *a priori*, and decreases the ordinate asymptote in inverse proportion to g_i. This leads to a

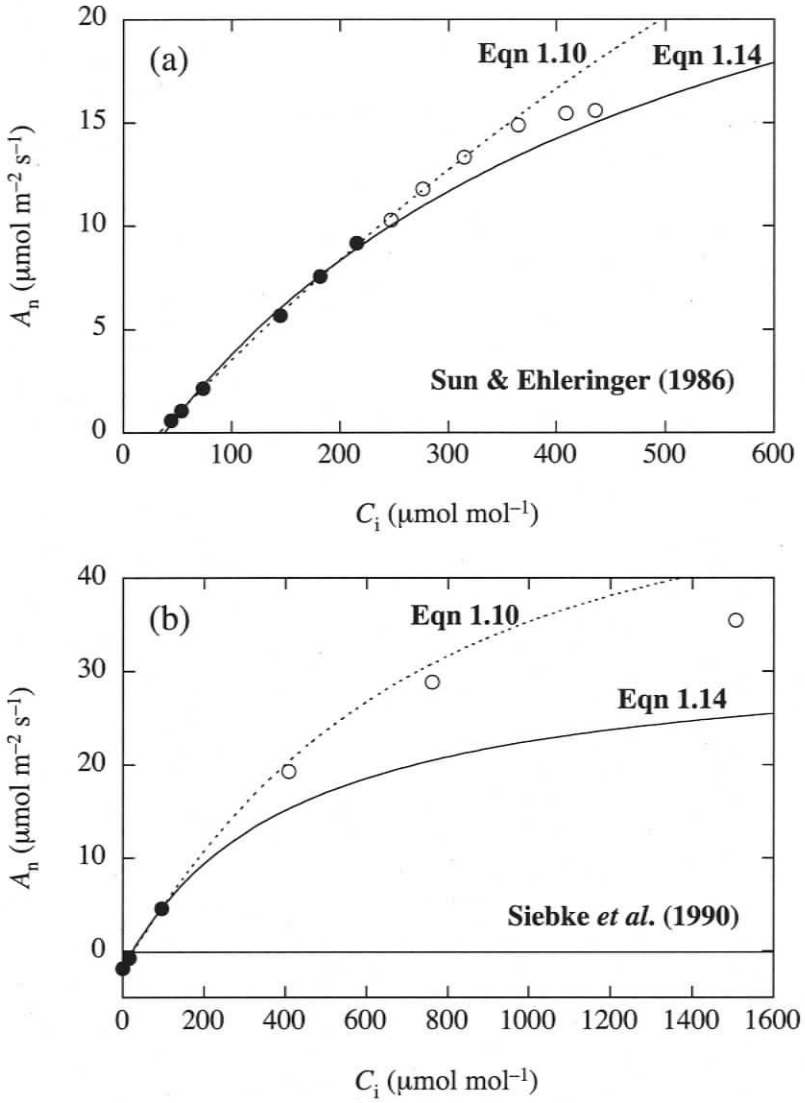

Figure 1.3 Least-squares regression fits to the initial portion (filled circles) of A-C_i curves reproduced from (a) Sun & Ehleringer (1986) and (b) Siebke *et al.* (1990). Curve fits of Eqn 1.14 assume infinite CO_2 transfer conductance (g_i) and were performed according to Wullschleger (1993). The maximal carboxylation rate (V_{cmax}) values obtained using the Rubisco kinetic constants of Jordan & Ogren (1984) (see Table 1.2) were (a) 33 and (b) 30 μmol m^{-2} s^{-1}. Curves fits of Eqn 1.10 were performed on the same data points using the same Rubisco kinetic constants. The values obtained were (a) 57 and (b) 56 μmol m^{-2} s^{-1} for V_{cmax} and (a) 0.1 and (b) 0.15 mol m^{-2} s^{-1} for g_i.

significant underestimation of V_{cmax} for leaves with low g_i relative to their photosynthetic capacity.

Figure 1.4a gives a graphical example of the extent of the V_{cmax} underestimation as g_i decreases and of the $K_m(CO_2)_i$ value required to restore V_{cmax} to its initial true value. The results shown in the figure were generated by fitting Eqn 1.14 (hollow circles) or Eqn 1.16 (filled circles) to a series of theoretical A-C_i curves obtained by combining a single A_n *vs.* C_c curve with different g_i values. Details about the curve fits and the parameters (mostly taken from Wullschleger 1993) used to construct the A_n *vs.* C_c curve are given in the figure legend. In reference to the aforementioned analysis of the A-C_i curves of Sun & Ehleringer (1986) and Siebke *et al.* (1990) which yielded underestimates of V_{cmax} of 54% and 58%, respectively, Fig. 1.4a shows that, given an initial "true" V_{cmax} value of 56 μmol m^{-2} s^{-1}, such an underestimation would be expected given g_i values close to 0.1 mol m^{-2} s^{-1} and that the $K_m(CO_2)_i$ value required to remove that underestimation would be approximately 880 μbar. This is over twice the original $K_c(1+O/K_o)$ value used by Wullschleger (1993). None of the recommended K_c and K_o combinations mentioned previously give a $K_c(1+O/K_o)$ value as high as this despite that the K_c and K_o values of von Caemmerer *et al.* (1994) and Bernacchi *et al.* (2001) shown in Table 1.2 were derived from *in vivo* measurements of $K_m(CO_2)_i$ and that the *in vitro* K_c value of Farquhar *et al.* (1980) is likely to be overestimated by approximately 85% due to a calculation error (wrong choice of dissociation constant (pK_a) for carbonic acid *vs.* CO_2 – see Yokota & Kitaoka 1985).

The new A-C_i curve fitting method I propose rests on the point emphasised throughout the theory section, that is, for a given V_{cmax}, the curvature of a CO_2 response function is entirely determined by its effective Michaelis-Menten constant. Since for A-C_i curves the curvature of the non-rectangular hyperbola is affected by both $K_c(1+O/K_o)$ and g_i, specifying $K_c(1+O/K_o)$ when fitting Eqn 1.10 to the initial A-C_i curve portion (as for Eqn 1.14 in the standard method) will automatically constrain the value of g_i to match the

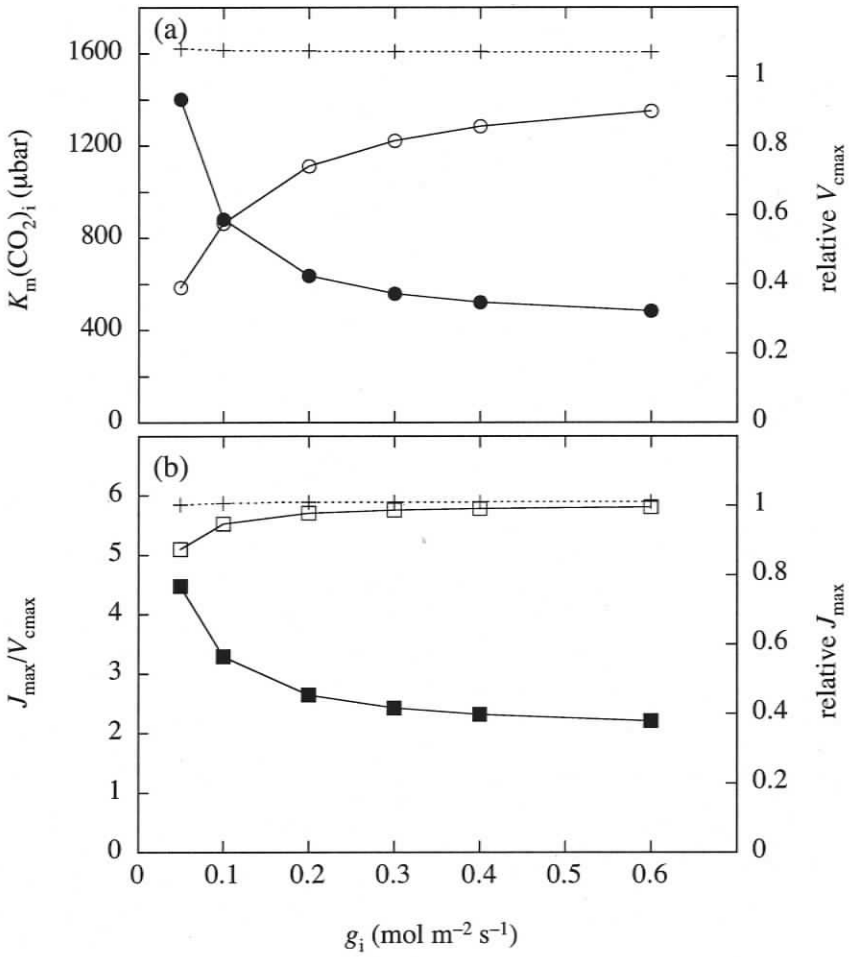

Figure 1.4 Influence of CO_2 transfer conductance (g_i) on (a) the maximal carboxylation rate (V_{cmax}) and apparent Michaelis-Menten constant for CO_2 evaluated at C_i [$K_m(CO_2)_i$] and (b) the maximal electron transport rate (J_{max}) and the J_{max}/ V_{cmax} ratio. Values of V_{cmax} and J_{max} were estimated by fitting Eqns 1.14 and 1.15 (standard A-C_i curve fitting method – see text for details) to a series of ideal A-C_i curves generated for various g_i values from a set of initial parameters valid at C_c. For Rubico-limited photosynthesis (Eqn 1.8) Γ^*, K_c, and K_o were taken from Jordan & Ogren (1984) (at 25 °C and 210 mbar O_2; see Table 1.2) and V_{cmax} and R_d were 56 and 0.6 μmol m^{-2} s^{-1}, respectively. For RuBP-limited photosynthesis (Eqns 1.11 and 1.12) ϕ = 0.18 mol e- mol quanta^{-1}, θ = 0.9, I = 1500 μmol quanta m^{-2} s^{-1}, and J_{max} = 112 μmol e$^-$ m^{-2} s^{-1}. Values of $K_m(CO_2)_i$ were determined by fitting Eqn 1.16 to the A-C_i curves, setting V_{cmax} and the mitochondrial respiration in the light (R_d) to their "true" value. The "+" symbols indicate values of (a) V_{cmax} and (b) J_{max} obtained when fitting Eqn 1.10 to the same set of A-C_i curves starting with $K_c(1+O/K_o)$ and Γ^* values that overestimate their "true" value by 20% and 10%, respectively.

curvature but will not change the value of the ordinate asymptote (V_{cmax}–R_d). Figure 1.4a ("+" symbols) shows an example of the relative constancy of the V_{cmax} parameter, with respect to g_i, estimated from curve fits based on Eqn 1.10 and initiated from overestimated Γ^* (10%) and $K_c(1+O/K_o)$ (20%) values. In this case, the V_{cmax} overestimates varied by less than 1% (59.3 to 59.8 μmol m^{-2} s^{-1}) across the g_i range explored (0.6 to 0.05 mol m^{-2} s^{-1}); the corresponding variation of the V_{cmax} estimates obtained from Eqn 1.14, following the standard A-C_i curve fitting method, is 57% (56.4 to 24.5 μmol m^{-2} s^{-1}). Graphical examples of this simulation are shown in Fig. 1.5. Note the 17% underestimation of V_{cmax} through Eqn 1.14 in Fig. 1.5a (g_i = 0.2 mol m^{-2} s^{-1}) despite the 20% overestimation of the $K_c(1+O/K_o)$ parameter and the apparent validity of the curve fit (compare with Fig. 1.5b and Figs. 1.2 and 1.3). In fact, when the correct Γ^* and $K_c(1+O/K_o)$ values are used to estimate V_{cmax} from Eqn 1.14, the latter can be underestimated by as much as 30% (g_i = 0.17 mol m^{-2} s^{-1}) from curve fits that still appear visually valid. Similar results are found for g_i of 0.1 mol m^{-2} s^{-1} (29% V_{cmax} underestimation) when the "true" V_{cmax} value used to generate the A-C_i curves is reduced by half (data not shown). Thus, according to these simulations, there could be considerably more significant V_{cmax} underestimates than I originally anticipated in the survey of Wullschleger (1993) and other C_3 species parameterisations which used the same Rubisco kinetic constants and curve fitting method (e.g. Harley & Baldocchi 1995; Centritto & Jarvis 1999; Le Roux *et al.* 1999; Bunce 2000; Warren Adams 2001; Wilson *et al.* 2001).

The A-C_i curve fitting method based on Eqn 1.10 is essentially insensitive to the above-mentioned biases (Fig. 1.5). This can easily be verified on any, reasonably well-defined, measured A-C_i curve simply by increasing the leaf internal resistance ($1/g_i$) in steps and by re-fitting the resulting A-C_i curves (re-computed from the original data using Eqn 1.9) according to the two methods described above. Another advantage of this new approach is that it reduces the sensitivity of the fitted value of V_{cmax} relative to the value

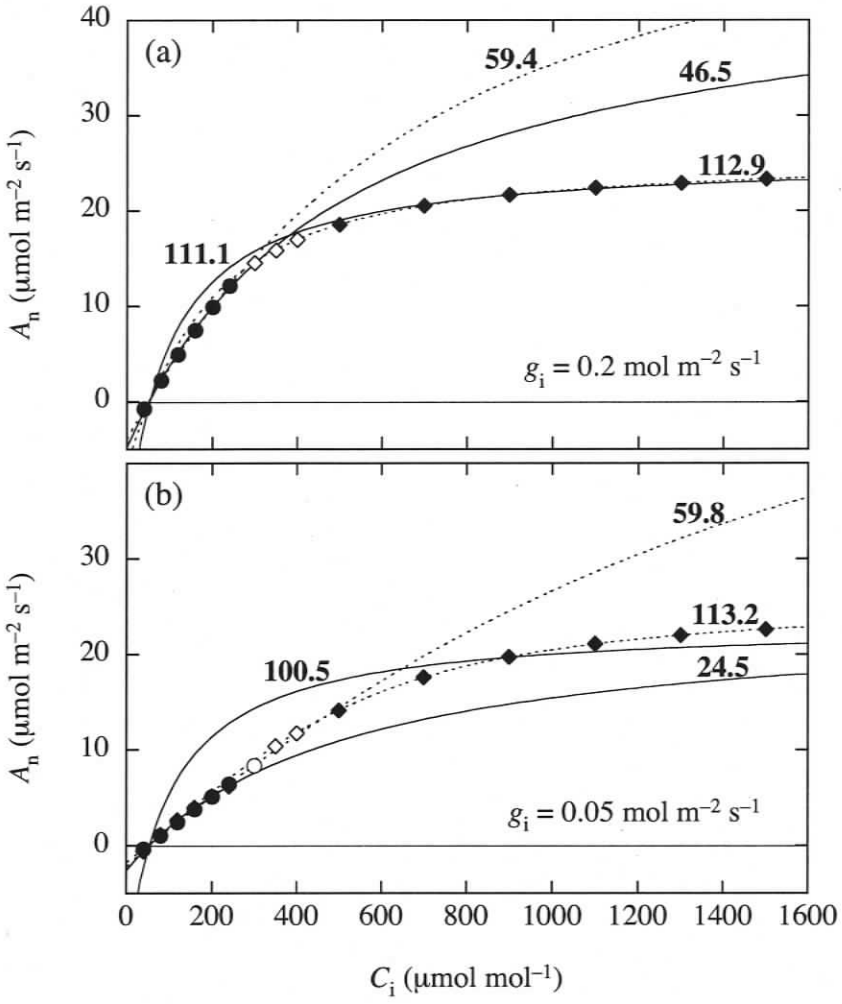

Figure 1.5 Examples of least-squares regression fits of Eqns 1.14 and 1.15 (standard method – see text for details; continuous lines) *vs.* Eqn 1.10 (new method; broken lines) performed on ideal A-C_i curves generated for g_i values of (a) 0.2 and (b) 0.05 mol m^{-2} s^{-1} from a set of initial parameters valid at C_c (see Fig. 1.4 legend for details). The number beside each curve indicates the maximal carboxylation rate (V_{cmax}) or the maximal electron transport rate (J_{max}) obtained by fitting the appropriate equation to the Rubisco-limited (Eqn 1.14 *vs.* Eqn 1.10; circles) and RuBP-limited (Eqn 1.15 *vs.* Eqn 1.10; diamonds) portion of the curves, respectively. Open symbols represent data points not used for the curve fits. All curve fits were done with $K_c(1+O/K_o)$ and Γ^* parameters that overestimated their "true" value by 20% and 10%, respectively.

of $K_c(1+O/K_o)$ chosen. For example, estimates of V_{cmax} in the above-mentioned simulation remained within 10% of the "true" V_{cmax} used initially to construct the A-C_i curves even when the $K_c(1+O/K_o)$ value chosen to initiate the curve fits was up to ±30% of the correct value; the corresponding uncertainty of the rectangular hyperbola model, corrected for g_i according to Eqn 1.16, was twice as high (Fig. 1.6).

The theoretical simulations described above suggest that it is possible for leaves of similar biochemical photosynthetic capacity (V_{cmax}) and intercellular operating point (C_i) to achieve very different A_n through significant variation in g_i. Yet, the commonly evoked positive relationship between A_n and g_i (Fig. 1.7a; von Caemmerer & Evans 1991; Lloyd *et al.* 1992; Epron *et al.* 1995; Evans & Loreto 2000; Warren *et al.* 2003) may lead one to conclude that V_{cmax} correlates conservatively with g_i among C_3 plant species. If so, one would expect the g_i limitation to photosynthesis to be similar among species, which would imply that the $K_m(CO_2)_i$ value required to compensate for that limitation is also conserved. However, the apparent convexity of the A_n vs. g_i relationship (Fig. 1.7a) suggests a general tendency towards "over-investment" in photosynthetic capacity as g_i falls below 0.2 mol m^{-2} s^{-1}; this is clearly indicated by the corresponding increasing drop in CO_2 concentration between C_i and C_c (Fig. 1.7b). Hence, the g_i limitation to photosynthesis can only be similar among species if the operating C_i is inversely proportional to A_n and g_i (in order to equalise C_c). On the contrary, the operating C_i is usually found to be remarkably conserved among species despite large differences in A_n (e.g. Yoshie 1985) or else positively related to A_n (e.g. Franks & Farquhar 1999). Thus, the correlation between A_n and g_i among species does not necessarily reflect the relationship between V_{cmax} and g_i for in theory A_n is fundamentally dependent on g_i but V_{cmax} is not (Eqn 1.10) – at least not necessarily to the same degree. This is shown explicitly in Fig. 1.7c for those data in Fig. 1.7a for which g_s was given alongside A_n and g_i (filled circles), thereby allowing the estimation of V_{cmax} on the basis of C_c via Eqns 1.8

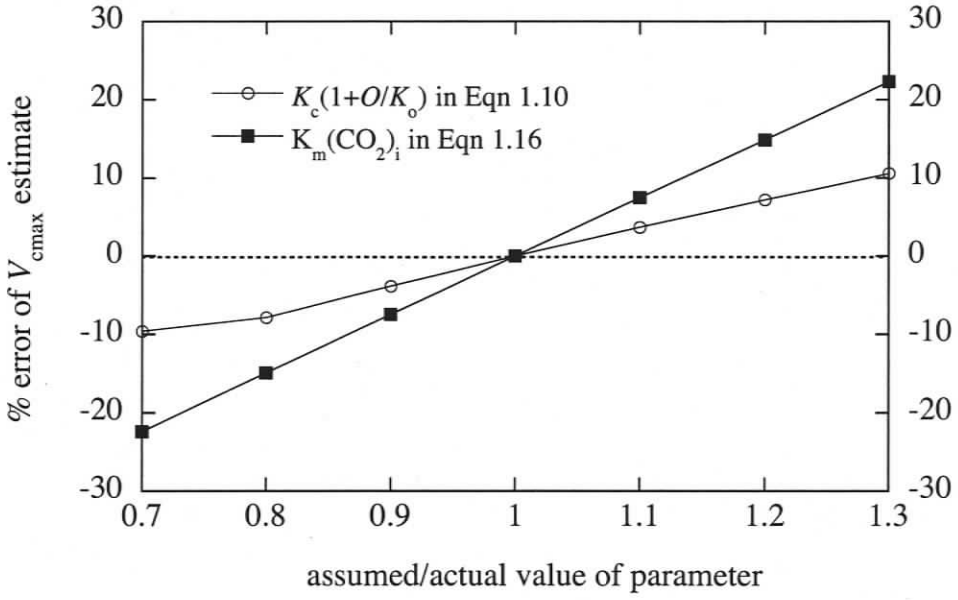

Figure 1.6 Errors in the estimates of the maximal carboxylation rate (V_{cmax}) caused by using up to ±30% of the actual value of $K_c(1+O/K_o)$ or $K_m(CO_2)_i$ when fitting Eqns 1.10 or 1.16, respectively, to the initial portion of an ideal A-C_i curve generated as described in the legend of Fig. 1.4 with a CO_2 transfer conductance (g_i) value of 0.2 mol m^{-2} s^{-1} (similar results were obtained using other g_i values). The correct value for $K_m(CO_2)_i$ was estimated to 635.3 μbar from the data shown in Fig. 1.4a.

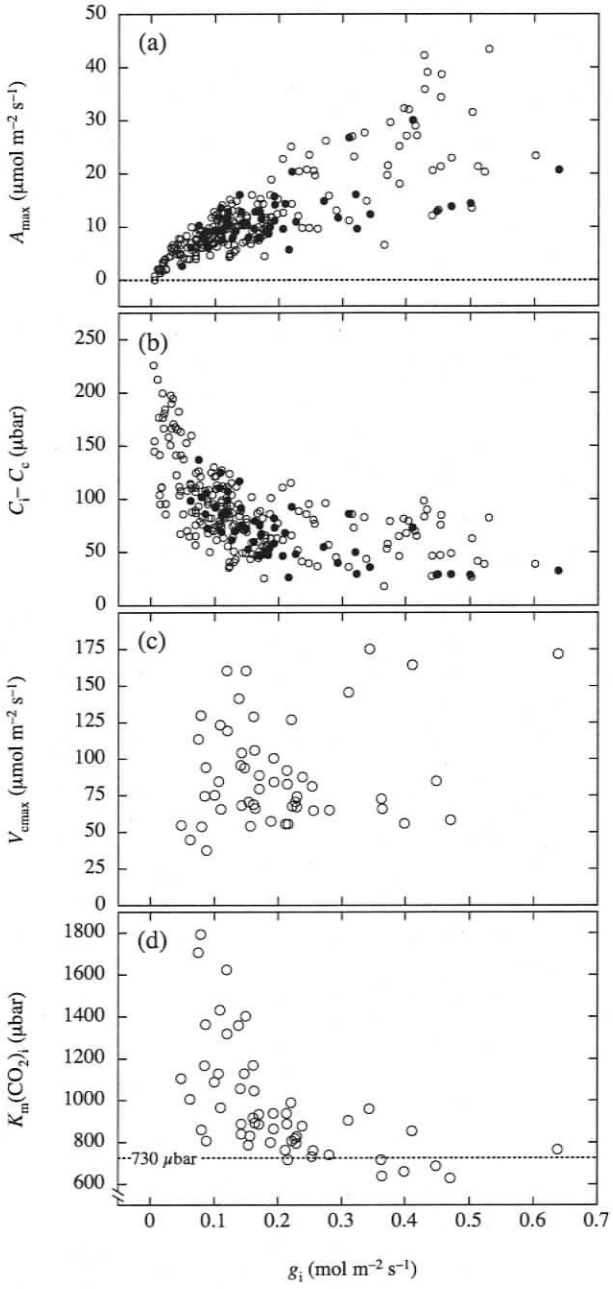

Figure 1.7 Relationship between the CO_2 transfer conductance (g_i) and (a) the net CO_2 assimilation rate (A_n), (b) the CO_2 concentration drawdown between the intercellular spaces subtending the stomata and the chloroplasts' carboxylation sites (C_i–C_c; from A_n/g_i), (c) the maximal carboxylation rate (V_{cmax}), and (d) the apparent Michaelis-Menten constant for CO_2 evaluated at C_i [$K_m(CO_2)_i$] among the C_3 plant species listed in Table 1.1 (n = 262; see references given therein for the data source). Filled circles in Figs. 1.7a, b represent the data subset (n = 53) for which the stomatal conductance (g_s) was given alongside g_i and A_n. From these, C_c was estimated at a reference leaf surface CO_2 concentration of 340 μbar [i.e. $C_c = (340 - 1.56A_n/g_s) - A_n/g_i$] and V_{cmax} was then solved using Eqn 1.8 (R_d = 0.8 μmol m^{-2} s^{-1} at 25 °C; otherwise adjusted for leaf temperature using the temperature response function of Bernacchi *et al.* 2001) parameterised with the Rubisco kinetic constants of von Caemmerer *et al.* (1994) evaluated at C_c (K_c = 259 μbar, K_o = 179 mbar, and Γ* = 38.6 μbar at 25 °C; otherwise adjusted for leaf temperature using the temperature response functions of Bernacchi *et al.* 2002); $K_m(CO_2)_i$ was subsequently estimated at 200 mbar O_2 from V_{cmax} using Eqn 1.16 (with C_i* determined from Eqn 1.9). The final V_{cmax} and $K_m(CO_2)_i$ values shown in Figs. 1.7c, d were adjusted to 25 °C using the temperature response functions of Bernacchi *et al.* (2001); other estimates derived from different leaf surface CO_2 concentrations gave different absolute values but similar trends (not shown). The dotted line in Fig. 1.7d represents the $K_m(CO_2)_i$ value found by von Caemmerer *et al.* (1994) for transgenic tobacco plants (see Table 1.2).

and 1.9 (see figure legend for details). Here, the tobacco Rubisco kinetic constants of von Caemmerer *et al.* (1994) determined *in vivo* on the basis of C_c (see Chapter 2) were used to calculate V_{cmax} so the corresponding $K_m(CO_2)_i$ values estimated from Eqn 1.16 could be compared with the value found by von Caemmerer *et al.* (1994) (730 μbar at 25 °C and 200 mbar O_2; see Table 1.2). The results clearly show that $K_m(CO_2)_i$ is not a conserved property among C_3 plant species (Fig. 1.7d). No single value can therefore be recommended for properly estimating V_{cmax} in all species. For example, the $K_m(CO_2)_i$ value of von Caemmerer *et al.* (1994) produced V_{cmax} estimates (Eqn 1.14) that varied from –24% to +10% (–8 ± 10%, mean ± SD, n = 24) of the "true" V_{cmax} (Eqn 1.8), as opposed to from –57% to –8% (–29 ± 14%, mean ± SD, n = 29), for leaves with a g_i above and below 0.2 mol m^{-2} s^{-1}, respectively.

According to Eqn 1.10 parameterised with the Rubisco kinetic constants of Jordan & Ogren (1984), the g_i value required to match the curvature of the real A-C_i curves shown in Fig. 1.3 is 0.1 and 0.15 mol m^{-2} s^{-1} for Sun & Ehleringer (1986) and Siebke *et al.* (1990), respectively. For the A-C_i curve of the Douglas-fir shoot shown in Fig. 1.2, the matching g_i value is 0.12 mol m^{-2} s^{-1} (corresponding to a V_{cmax} estimate of 44 mol m^{-2} s^{-1}, that is 1.6 times the value found with Eqn 1.14) – a close match to the g_i value found for this shoot based on the measured difference between C_i^* and Γ^* (0.15 mol m^{-2} s^{-1}; see Warren *et al.* (2003) for details about the technique). These estimates compare very well with the expected g_i value obtained from theory using the same Rubisco kinetic constants and assuming steady-state Rubisco activity (Fig. 1.4a). In Douglas-fir, I found that the curvature of the A-C_i curves sometimes increased significantly as C_i approached Γ and that I needed to remove these data from the curve fits to obtain reasonable g_i estimates (data not shown). This likely indicated a significant loss of Rubisco activity since it is known that the activation state of the enzyme can decrease when C_i falls below 100 μbar (e.g. von Caemmerer & Edmondson 1986; Sage, Sharkey & Seeman 1990). Such changes in the activation state of Rubisco may also explain the usual apparent linearity of the

initial A-C_i curve portion (e.g. von Caemmerer & Farquhar 1981; Brooks & Farquhar 1985). However, I emphasise that one consequence of the presence of significant g_i limitation in a leaf is that it effectively "linearises" the initial portion of its A-C_i curve (for example, compare Figs. 1.5a and 1.5b – note also the reduction of the overall slope of that initial A-C_i curve portion). In any case, when seeking estimates of g_i with this method, I recommend using a higher degree of measurement resolution for the Rubisco-limited A-C_i curve portion above a C_i of 100 μbar. In theory, if the $K_c(1+O/K_o)$ value chosen to initiate the least-squares fit of Eqn 1.10 remains within ±30% of its true value, the sensitivity of the g_i estimate to $K_c(1+O/K_o)$ is equivalent to that of the chlorophyll fluorescence techniques when the Γ^* value chosen to estimate g_i with this method is within ±10% of its true value (data not shown).

The effect of g_i on values of J_{max} estimated using the standard A-C_i curve fitting method (Eqn 1.15) is marginal over much of the range covered by the simulation (Fig. 1.4b). This is because 1) J_{max} is estimated from the saturating portion of the A-C_i curve and 2) the entire domain of the A_j function is almost entirely specified since its root (Γ^*, $-R_d$) is set *a priori*. There is, therefore, little need, other than improving the least-squares fit to better the delineation of the transition zone between the Rubisco-limited and the RuBP-limited portions of the A-C_i curve (see Fig. 1.5b), to account for varying g_i through Eqn 1.10 when estimating J_{max}. However, failure to correct V_{cmax} for g_i will increase the J_{max}/V_{cmax} ratio significantly when g_i is low relative to the leaf photosynthetic capacity (Fig. 1.4b).

CONCLUSION

I have shown that conventional A-C_i curve fitting methods can significantly underestimate V_{cmax} for plants photosynthetically limited by g_i and have provided a new approach to estimate V_{cmax} that accounts for g_i and which is less sensitive with respect to the absolute accuracy of the $K_c(1+O/K_o)$ value chosen to parameterise the model of

Farquhar *et al.* (1980). Alternative parameterisations of the conventional method based on a single $K_m(CO_2)_i$ value used for all C_3 plants are not acceptable since the relationship between V_{cmax} and g_i is not conserved among species.

The new A-C_i curve fitting method is based on the non-rectangular hyperbola version of the model of Farquhar *et al.* (1980) and gives reasonable estimates of g_i providing the $K_c(1+O/K_o)$ value chosen to parameterise the model is close to its true value. More C_3 species *in vivo* estimates of $K_c(1+O/K_o)$ properly evaluated at C_c are needed in this respect. In Chapter 2, I will demonstrate how the proposed new A-C_i curve fitting method can be used to derive such estimates.

The success of the photosynthesis model of Farquhar *et al.* (1980) cannot be understated. In the words of the authors, it "has had an impact and seen application that far exceeded our expectations" (Farquhar, von Caemmerer & Berry 2001). The wide use of the model is not only due to its solid theoretical basis, but also to its simplicity, a necessary prerequisite to make any model useful (von Caemmerer 2000). I suggest, however, that many present model parameterisations are incorrect for leaves with low g_i. Of course, such parameterisations remain useful to predict photosynthesis under the conditions used since they are empirically fitted to measured responses. They may, however, mislead us when it comes to evaluating the variability of V_{cmax} among C_3 plant species or interpreting the fundamental physiological processes underlying the measured photosynthetic responses of plants to various environmental conditions or through time. This, in effect, goes against "la raison d'être" of the theoretical mechanistic basis of the photosynthesis model of Farquhar *et al.* (1980). Considering the importance given to the V_{cmax} parameter in global climate change modelling, I believe it deserves better definition. By accounting for g_i through a non-rectangular hyperbola version of the model of Farquhar *et al.* (1980), the new V_{cmax} estimation method shows great potential for providing a more realistic view of the species variation and environmental regulation of photosynthetic capacity in C_3 plants. In doing so, the original simplicity of the original

rectangular hyperbola version of the model of Farquhar *et al.* (1980) need necessarily not be sacrificed since, following proper estimation of V_{cmax} with the non-rectangular hyperbola model parameterised with a set of Rubisco kinetic constants valid at C_c, it can be adjusted to account for g_i through Eqn 1.16.

REFERENCES

Andrews T.J. & Lorimer G.H. (1987) Rubisco: structure, mechanisms, and prospects for improvement. In *The Biochemistry of Plants* (eds M.D. Hatch & N.K. Boardman) Vol. 10, pp. 132–219. Academic press, New York.

Andrews T.J., Lorimer G.H. & Tolbert N.E. (1973) Ribulose diphosphate oxygenase. I. Synthesis of phosphoglycolate by fraction I protein of leaves. *Biochemistry* **12,** 11–18.

Badger M.R. & Collatz G.J. (1977) Studies on the kinetic mechanism of ribulose-1,5-bisphosphate carboxylase and oxygenase reactions, with particular reference to the effect of temperature on kinetic parameters. *Carnegie Institution of Washington Year Book* **76,** 355–361.

Badger, M.R. & Price, G.D. (1994) The role of carbonic-anhydrase in photosynthesis. *Annual Review of Plant Physiology and Plant Molecular Biology* **45,** 369–392.

Bernacchi C.J., Portis A.R., Nakano H., von Caemmerer S. & Long S.P. (2002) Temperature response of mesophyll conductance. Implications for the determination of Rubisco enzyme kinetics and for limitations to photosynthesis in Vivo. *Plant Physiology* **130,** 1–7.

Bernacchi C.J., Singsaas E.L., Pimentel C., Portis A.R. & Long S.P. (2001) Improved temperature response functions for models of Rubisco-limited photosynthesis. *Plant, Cell and Environment* **24,** 253–259.

Bird I.F., Cornelius M.J. & Keys A.J. (1982) Affinity of RuBP carboxylases for carbon dioxide and inhibition of the enzymes by oxygen. *Journal of Experimental Botany* **33,** 1004–1013.

Bowes G. & Ogren W.L. (1972) Oxygen inhibition and other properties of soybean ribulose-1,5-diphosphate carboxylase. *The Journal of Biological Chemistry* **247,** 2171–2176.

Bowes G., Ogren W.L. & Hageman R.H. (1971) Phosphoglycolate production catalysed by ribulose diphosphate carboxylase. *Biochemical and Biophysical Research Communications* **45,** 716–722.

Brooks A. & Farquhar G.D. (1985) Effects of temperature on the CO_2/O_2 specificity of ribulose-1,5-bisphosphate carboxylase/oxygenase and the rate of respiration in the light. Estimates from gas exchange measurements on spinach. *Planta* **165,** 397–406.

Bunce J.A. (2000) Acclimation of photosynthesis in eight cool and warm climate herbaceous C_3 species: temperature dependence of parameters of a biochemical photosynthesis model. *Photosynthesis Research* **63,** 59–67.

Centritto M. & Jarvis P.J. (1999) Long-term effects of elevated carbon dioxide concentration and provenance on four clones of Sitka spruce (*Picea sitchensis*). II. Photosynthetic capacity and nitrogen use efficiency. *Tree Physiology* **19,** 807–814.

Centritto M., Loreto F. & Chartzoulakis K. (2003) The use of low [CO_2] to estimate diffusional and non-diffusional limitations of photosynthetic capacity of salt-stressed olive saplings. *Plant, Cell and Environment* **26,** 585–594.

Collatz G.J., Ball J.T., Grivet C. & Berry J.A. (1991) Physiological and environmental regulation of stomatal conductance, photosynthesis and transpiration: a model that includes a laminar boundary layer. *Agricultural and Forest Meteorology* **54,** 107–136.

Delfine S., Alvino A., Villani M.C. & Loreto F. (1999) Restrictions to carbon dioxide conductance and photosynthesis in spinach leaves recovering from salt stress. *Plant Physiology* **119,** 1101–1106.

de Pury D.G.G. & Farquhar (1997) Simple scaling of photosynthesis from leaves to canopies without the errors of big-leaf models. *Plant, Cell and Environment* **20,** 537–557.

Dreyer E., Le Roux X., Montpied P., Daudet F.A. & Masson F. (2001) Temperature response of leaf photosynthesis capacity in seedlings from seven temperate tree species. *Tree Physiology* **21,** 223–232.

Epron D., Godard D., Cornic G. & Genty B. (1995) Limitation of net CO_2 assimilation rate by internal resistances to CO_2 transfer in the leaves of two tree species (*Fagus sylvatica* L. and *Castanea sativa* Mill.). *Plant, Cell and Environment* **18,** 43–51.

Evans J.R. & Loreto F. (2000) Acquisition and diffusion of CO_2 in higher plant leaves. In *Photosynthesis: Physiology and Metabolism* (eds R.C. Leegood, T.D. Sharkey & S. von Caemmerer), pp. 321–351. Kluwer Academic Publishers, Dordrecht, The Netherlands.

Evans J.R., von Caemmerer S., Setchell B.A. & Hudson G.S. (1994) The relationship between CO_2 transfer conductance and leaf anatomy in transgenic tobacco with a reduced content of Rubisco. *Australian Journal of Plant Physiology* **21,** 475–495.

Farquhar G.D. & von Caemmerer S. (1981) Some relationships between the biochemistry of photosynthesis and the gas exchange of leaves. *Planta* **153,** 376–387.

Farquhar G.D. & von Caemmerer S. (1982) Modelling of photosynthetic response to environmental conditions. In *Physiological Plant Ecology II.* Encyclopedia of Plant Physiology, new series (eds O.L. Lange, P.S. Nobel, C.B. Osmond & H. Ziegler) Vol. 12B, pp. 550–587. Springer-Verlag, Heidelberg.

Farquhar G.D., von Caemmerer S. & Berry J.A. (1980) A biochemical model of photosynthetic CO_2 assimilation in leaves of C_3 species. *Planta* **149,** 78–90.

Farquhar G.D., von Caemmerer S. & Berry J.A. (2001) Models of photosynthesis. *Plant Physiology* **125,** 42–45.

Farquhar G.D. & Wong S.C. (1984) An empirical model of stomatal conductance. *Australian Journal of Plant Physiology* **11,** 191–210.

Flexas J., Bota J., Escalona J.M., Sampol B. & Medrano H. (2002) Effects of drought on photosynthesis in grapevines under field conditions: an evaluation of stomatal and mesophyll limitations. *Functional Plant Biology* **29,** 461–471.

Franks P.J. & Farquhar G.D. (1999) A relationship between humidity response, growth form and photosynthetic operating point in C_3 plants. *Plant, Cell and Environment* **22,** 1337–1349.

Gillon J.S. & Yakir D. (2000) Internal conductance to CO_2 diffusion and $C^{18}OO$ discrimination in C_3 leaves. *Plant Physiology* **123,** 201–213.

Grossman-Clarke S., Kimball B.A., Hunsaker D.J., Long S.P., Garcia R.L., Kartschall Th., Wall G.W., Printer Jr. P.J., Wechsung F. & LaMorte R.L. (1999) Effects of elevated atmospheric CO_2 on canopy transpiration in senescent spring wheat. *Agricultural and Forest Meteorology* **93,** 95–109.

Hanba Y.T., Miyazawa S.-I., Kogami H. & Terashima I. (2001) Effects of leaf age on internal CO_2 transfer conductance and photosynthesis in tree species having different types of shoot phenology. *Australian Journal of Plant Physiology* **28,** 1075–1084.

Hanba Y.T., Miyazawa S.-I. & Terashima I. (1999) The influence of leaf thickness on the CO_2 transfer conductance and leaf stable carbon isotope ratio for some evergreen tree species in Japanese warm-temperate forests. *Functional Ecology* **13,** 632–639.

Harley P.C. & Baldocchi D.D. (1995) Scaling carbon dioxide and water vapour exchange from leaf to canopy in a deciduous forest. I. Leaf model parameterization. *Plant, Cell and Environment* **18,** 1149–1156.

Harley P.C., Loreto F., Di Marco G. & Sharkey T.D. (1992a) Theoretical considerations when estimating the mesophyll conductance to CO_2 flux by analysis of the response of photosynthesis to CO_2. *Plant Physiology* **98,** 1429–1436.

Harley P.C. & Sharkey T.D. (1991) An improved model of C_3 photosynthesis at high CO_2: reversed O_2 sensitivity explained by lack of glycerate reentry into the chloroplast. *Photosynthesis Research* **27,** 169–178.

Harley P.C. & Tenhunen J.D. (1991) Modeling the photosynthetic response of C_3 leaves to environmental factors. In *Modeling Crop Photosynthesis – from Biochemistry to Canopy* (eds K.J. Boote & R.S. Loomis), pp. 17–39. ASA, Madison, Wisconsin.

Harley P.C., Thomas R.B., Reynolds J.F. & Strain B.R. (1992b) Modelling photosynthesis of cotton grown in elevated CO_2. *Plant, Cell and Environment* **15,** 271–282.

Jordan D.B. & Ogren W.L. (1981) Species variation in the specificity of ribulose biphosphate carboxylase/oxygenase. *Nature* **291,** 513–515.

Jordan D.B. & Ogren W.L. (1983) Species variation in the kinetic properties of ribulose 1,5-bisphosphate carboxylase/oxygenase. *Archives of Biochemistry and Biophysics* **227,** 425–433.

Jordan D.B. & Ogren W.L. (1984) The CO_2/O_2 specificity of ribulose 1,5-bisphosphate carboxylase/oxygenase. Dependence on ribulose bisphosphate concentration, pH and temperature. *Planta* **161,** 308–313.

Kane H.J., Viil J., Entsch B., Paul K., Morell M.K. & Andrews T.J. (1994) An improved method for measuring the CO_2/O_2 specificity of ribulosebisphosphate carboxylase-oxygenase. *Australian Journal of Plant Physiology* **21,** 449–461.

Keys A.J. (1986) Rubisco: its role in photorespiration. *Philosophical Transactions of the Royal Society of London B* **313,** 325–336.

Kogami H., Hanba Y.T., Kibe T., Terashima I. & Masuzawa T. (2001) CO_2 transfer conductance, leaf structure and carbon isotope composition of *Polygonum cuspidatum* leaves from low and high altitudes. *Plant, Cell and Environment* **24,** 529–538.

Kosugi Y., Shibata S. & Kobashi S. (2003) Parameterization of the CO_2 and H_2O gas exchange of several temperate deciduous broad-leaved trees at the leaf scale considering seasonal changes. *Plant, Cell and Environment* **26,** 285–301.

Laing W.A., Ogren W.L. & Hageman R.H. (1974) Regulation of soybean net photosynthetic CO_2 fixation by the interaction of CO_2, O_2, and ribulose-1,5-diphosphate carboxylase. *PlantPhysiology* **54,** 678–685.

Laisk A. (1977) *Kinetics of photosynthesis and photorespiration in C_3 plants*. Nauka, Moscow (in Russian).

Laisk A. & Loreto F. (1996) Determining photosynthetic parameters from leaf CO_2 exchange and chlorophyll fluorescence. Ribulose-1,5-bisphosphate carboxylase/oxygenase specificity factor, dark respiration in the light, excitation distribution between photosystems, alternative electron transport rate, and mesophyll resistance. *Plant Physiology* **110,** 903–912.

Laisk A. & Oja V. (1974) Leaf photosynthesis in short pulses of CO_2. The carboxylation reaction *in vivo*. *Fiziologija Rastenij* **21,** 1123–1131 (in Russian).

Lauteri M., Scartazza A., Guido M.C. & Brugnoli E. (1997) Genetic variation in photosynthetic capacity, carbon isotope discrimination ands mesophyll conductance in provenances of *Castanea sativa* adapted to different environments. *Functional Ecology* **11,** 675–683.

Le Roux X., Grand S., Dreyer E. & Daudet F.-A. (1999) Parameterization and testing of a biochemically based photosynthesis model for walnut (*Juglans regia*) trees and seedlings. *Tree Physiology* **19,** 481–492.

Leuning R. (1997) Scaling to a common temperature improves the correlation between the photosynthesis parameters J_{max} and V_{cmax}. *Journal of Experimental Botany* **48,** 345–347.

Leuning R. (2002) Temperature dependence of two parameters in a photosynthesis model. *Plant, Cell and Environment* **25,** 1205–1210.

Lilley R.McC. & Walker D.A. (1974) Carbon dioxide assimilation by leaves, isolated chloroplasts, and ribulose bisphosphate carboxylase from spinach. *Plant Physiology* **55,** 1087–1092.

Lloyd J., Syvertsen J.P., Kriedemann P.E. & Farquhar G.D. (1992) Low conductances for CO_2 diffusion from stomata to the sites of carboxylation in leaves of woody species. *Plant, Cell and Environment* **15,** 873–899.

Loreto F., Centritto M. & Chartzoulakis K. (2003) Photosynthetic limitations in olive cultivars with different sensitivity to salt stress. *Plant, Cell and Environment* **26,** 595–601.

Loreto F., Di Marco G., Tricoli D. & Sharkey T.D. (1994) Measurements of mesophyll conductance, photosynthetic electron transport and alternative electron sinks of field grown wheat leaves. *Photosynthesis Research* **41,** 397–403.

Loreto F., Harley P.C., Di Marco G. & Sharkey T.D. (1992) Estimation of mesophyll conductance to CO_2 flux by three different methods. *Plant Physiology* **98,** 1437–1443.

Mächler F., Müller J. & Dubach M. (1990) RuBPCO kinetics and the mechanism of CO_2 entry in C_3 plants. *Plant, Cell and Environment* **13,** 881–899.

Makino A., Mae T. & Ohira K. (1985) Enzymic properties of ribulose-1,5-bisphosphate carboxylase/oxygenase purified from rice leaves. *Plant Physiology* **79,** 57–61.

Makino A., Mae T. & Ohira K. (1988) Differences between wheat and rice in the enzymic properties of ribulose-1,5-bisphosphate carboxylase/oxygenase and the relationship to photosynthetic gas exchange. *Planta* **174,** 30–38.

Makino A., Nakano H. & Mae T. (1994) Effects of growth temperature on the response of ribulose-1,5-bisphosphate carboxylase/oxygenase, electron transport components, and sucrose synthesis enzymes to leaf nitrogen in rice, and their relationship to photosynthesis. *Plant Physiology* **105,** 1231–1238.

Medlyn B.E., Badeck F.-W., De Pury D.G.G., Barton C.V.M., Broadmeadow M., Ceulemans R., De Angelis P., Forstreuter M., Jach M.E., Kellomäki S., Laitat E., Marek M., Philippot S., Rey A., Strassemeyer J., Laitinen K., Liozon R., Portier B., Roberntz P., Wang K. & Jarvis P.G. (1999) Effects of elevated [CO2] on

photosynthesis in European forest species: a meta-analysis of model parameters. *Plant, Cell and Environment* **22,** 1475–1495.

Medlyn B.E., Dreyer E., Ellsworth D., Forstreuter M., Harley P.C., Kirschbaum M.U.F., Le Roux X., Montpied P., Strassemeyer J., Walcroft A., Wang K. & Loustau D. (2002) Temperature response of parameters of a biochemically based model of photosynthesis. II. A review of experimental data. *Plant, Cell and Environment* **25,** 1167–1179.

Miyazawa S.-I. & Terashima I. (2001) Slow development of leaf photosynthesis in an evergreen broad-leaved tree, *Castanopsis sieboldii*: relationships between leaf anatomical characteristics and photosynthetic rate. *Plant, Cell and Environment* **24,** 279–291.

Parry M.A.J., Schmidt C.N.G., Cornelius M.J., Millard B.N., Burton S., Gutteridge S., Dyer T.A. & Keys A.J. (1989) Variations in properties of ribulose-1,5-bisphosphate carboxylase from various species related to differences in amino acid sequences. *Journal of Experimental Botany* **38,** 1260–1271.

Piel C., Frak E., Le Roux X. & Genty B. (2002) Effect of local irradiance on CO_2 transfer conductance of mesophyll in walnut. *Journal of Experimental Botany* **53,** 1–8.

Pitman A.J. (2003) The evolution of, and revolution in, land surface schemes designed for climate models. *International Journal of Climatology* **23,** 479–510.

Roupsard O., Gross P. & Dreyer E. (1996) Limitation of photosynthetic activity by CO_2 availability in the chloroplasts of oak leaves from different species and during drought. *Annales des Sciences Forestières* **53,** 243–254.

Sage R.F., Sharkey T.D. & Seemann J.R. (1990) Regulation of ribulose-1,5-bisphosphate carboxylase activity in response to light intensity and CO_2 in the C_3 annuals *Chenopodium album* L. and *Phaseolus vulgaris* L. *Plant Physiology* **94,** 1735–1742.

Sellers P.J., Dickinson R.E., Randall D.A., Betts A.K., Hall F.G., Berry J.A., Collatz G.J., Denning A.S., Mooney H.A., Nobre C.A., Sato N., Field C.B. & Henderson-Sellers A.

(1997) Modeling the exchanges of energy, water, and carbon between continents and the atmosphere. *Science* **275,** 502–509.

Siebke K., Laisk A., Oja V., Kiirats O., Raschke K. & Heber U. (1990) Control of photosynthesis in leaves as revealed by rapid gas exchange and measurements of the assimilatory force F_A. *Planta* **182,** 513–522.

Sun G.C. & Ehleringer J.R. (1986) Gas exchange in *Schima superba*, a subtropical monsoonal forest tree. *Photosynthetica* **20,** 158–163.

Terashima I. & Ono K. (2002) Effects of $HgCl_2$ on CO_2 dependence of leaf photosynthesis: evidence indicating involvement of aquaporins in CO_2 diffusion across the plasma membrane. *Plant and Cell Physiology* **43,** 70–78.

Tolbert N.E. (1971) Microbodies, peroxisomes and glyoxysomes. *Annual Review of Plant Physiology* **22,** 45–76.

von Caemmerer S. (2000) *Biochemical models of leaf photosynthesis*. Techniques in Plant Sciences N0. 2. CSIRO Publishing, Collingwood, Victoria, Australia.

von Caemmerer S. & Edmondson D.L. (1986) Relationship between steady-state gas exchange, *in vivo* ribulose bisphosphate carboxylase activity and some carbon reduction cycle intermediates in *Raphanus sativus*. *Australian Journal of Plant Physiology* **13,** 669–688.

von Caemmerer S. & Evans J.R. (1991) Determination of the average partial pressure of CO_2 in chloroplasts from leaves of several C_3 plants. *Australian Journal of Plant Physiology* **18,** 287–305.

von Caemmerer S., Evans J.R., Hudson G.S. & Andrews T.J. (1994) The kinetics of ribulose-1,5-bisphosphate carboxylase/oxygenase in vivo inferred from measurements of photosynthesis in leaves of transgenic tobacco. *Planta* **195,** 88–97.

von Caemmerer S. & Farquhar G.D. (1981) Some relationships between the biochemistry of photosynthesis and the gas exchange of leaves. *Planta* **153,** 376–387.

Walcroft A.S., Whitehead D., Silvester W.B. & Kelliher F.M. (1997) The response of photosynthetic model parameters to temperature and nitrogen concentration in *Pinus radiata* D. Don. *Plant, Cell and Environment* **20,** 1338–1348.

Wang Y.P. & Leuning R. (1998) A two-leaf model for canopy conductance, photosynthesis and partitioning of available energy I: model description and comparison with a multi-layer model. *Agricultural and Forest Meteorology* **91,** 89–111.

Warren C.R. & Adams M.A. (2001) Distribution of N, Rubisco and photosynthesis in *Pinus pinaster* and acclimation to light. *Plant, Cell and Environment* **24,** 597–609.

Warren C.R., Ethier G.J., Livingston N.J., Grant N.J., Turpin D.H., Harrison D.L. & Black T.A. (2003) Transfer conductance in second growth Douglas-fir (*Pseudotsuga menziesii* (Mirb.)Franco) canopies. *Plant, Cell and Environment* **26,** 1215–1227.

Wilson K.B., Baldocchi D.D. & Hanson P.J. (2000a) Quantifying stomatal and non-stomatal limitations to carbon assimilation resulting from leaf aging and drought in mature deciduous tree species. *Tree Phyisology* **20,** 787–797.

Wilson K.B., Baldocchi D.D. & Hanson P.J. (2000b) Spatial and seasonal variability of photosynthetic parameters and their relationship to leaf nitrogen in a deciduous forest. *Tree Phyisology* **20,** 565–578.

Wilson K.B., Baldocchi D.D. & Hanson P.J. (2001) Leaf age affects the seasonal pattern of photosynthetic capacity and net ecosystem exchange of carbon in a deciduous forest. *Plant, Cell and Environment* **24,** 571–583.

Wohlfahrt G., Bahn M., Haubner E., Horak I., Michaeler W., Rottmar K., Tappeiner U. & Cernusca A. (1999) Inter-specific variation of the biochemical limitation to photosynthesis and related leaf traits of 30 species from mountain grassland ecosystems under different land use. *Plant, Cell and Environment* **22,** 1281–1296.

Woodrow I.E. & Berry J.A. (1988) Enzymatic regulation of photosynthetic CO_2 fixation in C_3 plants. *Annual Review of Plant Physiology and Plant Molecular Biology* **39,** 533–594.

Wullschleger (1993) Biochemical limitations to carbon assimilation in C_3 plants – a retrospective analysis of the A/C_i curves from 109 species. *Journal of Experimental Botany* **44,** 907–920.

Yeoh H.-H., Badger M.R. & Watson L. (1980) Variations in $K_m(CO_2)$ of ribulose-1,5-bisphosphate carboxylase among grasses. *Plant Physiology* **66,** 1110–1112.

Yeoh H.-H., Badger M.R. & Watson L. (1981) Variations in the kinetic properties of ribulose-1,5-bisphosphate carboxylases among plants. *Plant Physiology* **67,** 1151–1155.

Yokota A. & Kitaoka S. (1985) Correct pK values for dissociation constant of carbonic acid lower the reported Km values of ribulose bisphosphate carboxylase to half. Presentation of a nomograph and an equation determining the pK values. *Biochemical and Biophysical Research Communications* **131,** 1075–1079.

Yoshie F. (1986) Intercellular CO_2 concentration and water-use efficiency of temperate plants with different life-forms and from different microhabitats. *Oecologia* **68,** 370–374.

Chapter 2

Towards a common Farquhar-von Caemmerer-Berry leaf photosynthesis model parameterisation in global scale studies

INTRODUCTION

Current parameterisations of "third generation" (Pitman 2003) Land Surface Models (LSMs) are based on the equations of the photosynthesis model of Farquhar, von Caemmerer & Berry (1980) formulated on the basis of C_i (intercellular CO_2 concentration) with single "pan-species" values for the Michaelis-Menten constants for the carboxylation (K_c) and oxygenation (K_o) reactions of ribulose-1,5-bisphosphate carboxylase/oxygenase (Rubisco). In these large spatial scale models, the parameter V_{cmax} (maximal carboxylation rate per unit leaf surface area) of dominant reference plant species is often taken from the literature independently from the value of K_c and K_o chosen for the simulations (e.g. Delire & Foley 1999; Kucharik *et al.* 2000; Dai, Dickinson & Wang 2004; Kothavala *et al.* 2005). Thus, in such cases, it is assumed that the magnitudes K_c and K_o have little effect on the predicted net CO_2 assimilation rate of a leaf (A_n) under Rubisco-limited conditions once the parameter V_{cmax} has been set. Yet, as I explained in Chapter 1, the curvature of the lower portion of A_n *vs.* C_i relationships (A-C_i curves) used to model photosynthesis under Rubisco-limited conditions depends in part on the $K_c(1+O/K_o)$ (*effective* Michaelis-Menten constant for CO_2) value chosen to describe the loss of CO_2 affinity by Rubisco in the presence of O_2 (O). Given that the current range of $K_c(1+O/K_o)$ values implemented in various LSMs is over 300 μbar (~ 1.8-fold variation – see Table 1.2), I find it necessary to verify whether, as suggested above, this variation has little consequence on predicting Rubisco-limited photosynthesis for vegetated surfaces of known V_{cmax} distribution.

The kinetic properties of Rubisco are generally considered to be largely conserved among C_3 species (von Caemmerer 2000; Bernacchi *et al.* 2001; Medlyn *et al.* 2002), hence

the unique pan-species $K_c(1+O/K_o)$ value implemented in various LSMs. Still, the aforementioned variation in $K_c(1+O/K_o)$ values reported in the literature and used in different LSMs hardly lends credibility to the conservativeness of Rubisco's affinity towards CO_2 relative to O_2. As explained in Chapter 1, much of this variability is due to the use of "chloroplastic" K_c and K_o values determined *in vitro* (where the CO_2 and O_2 gas concentrations are evaluated at the enzyme site) as opposed to values determined *in vivo* (where, in these cases, the CO_2 and O_2 gas concentrations are evaluated in the intercellular airspace subtending the stomata and are assumed to equal the gas concentrations inside the chloroplasts). Yet, the greatest $K_c(1+O/K_o)$ variation is still found among the *in vitro* studies (e.g. Badger & Andrews 1974; Jorden & Ogren 1981; Bird, Cornelius & Keys 1982; Whitney *et al.* 1999).

Over two decades ago, Yokota & Kitaoka (1985) suggested that the majority of previously reported *in vitro* Rubisco K_c values were incorrect and often largely overestimated due to failure to properly account for the ionic strength (μ) of the assay medium and its effect on the solubility of CO_2. Surprisingly, little effort has since been made to correct previous (and in some cases subsequent) *in vitro* K_c determinations accordingly. As a result, it is rarely appreciated that a great number of parameterisations (from leaf to global scale) of the photosynthesis model of Farquhar *et al.* (1980) published to date are based on uncorrected K_c values (e.g. von Caemmerer & Farquhar 1981; Harley *et al.* 1992; Wullschleger 1993; Friend *et al.* 1997; Walcroft *et al.* 1997; Leuning, Dunin & Wang 1998; Bunce 2000; Kothavala *et al.* 2005; Niinemets *et al.* 2006). Until previous *in vitro* studies of Rubisco kinetics constants are reviewed and corrected according to Yokota & Kitaoka (1985) where necessary, interspecific comparisons of $K_c(1+O/K_o)$ values based on data from different laboratories (e.g. von Caemmerer 2000; Medlyn *et al.* 2002) should not be considered as accurate.

In this study, I use a simple case study to demonstrate how the current practice of "decoupling" $K_c(1+O/K_o)$ and V_{cmax} parameterisations in global climate modelling may lead to significant errors in estimating A_n under Rubisco-limited conditions. I then proceed to re-

evaluate previous *in vitro* determinations of K_c and $K_c(1+O/K_o)$ values in C_3 species in the light of Yokota & Kitaoka's (1985) results to 1) adjust the values commonly used in LSMs and 2) evaluate which, if any, single pan-species $K_c(1+O/K_o)$ value is most appropriate for large scale modelling schemes. Finally, I demonstrate how the new A-C_i curve fitting method presented in Chapter 1 can be used to estimate all the parameters describing Rubisco-limited photosynthesis in the model of Farquhar *et al.* (1980) simultaneously *in vivo* using a variation of the approach of von Caemmerer *et al.* (1994).

METHODS

Evaluation of potential error in estimating A_n under Rubisco-limited conditions from "decoupled" $K_c(1+O/K_o)$ and V_{cmax} parameterisations

Following on the theory expounded in Chapter 1, the correct rectangular hyperbola formulation describing the photosynthetic response of C_3 plant leaves to variation in C_i under Rubisco-limited conditions is

$$A_c = \frac{(C_i - C_i^*)V_{c\max}}{C_i + K_m(CO_2)_i} - R_d \qquad (2.1)$$

where A_c is the RuBP (ribulose-1,5-bisphosphate)-saturated net CO_2 assimilation rate, R_d is the mitochondrial respiration in the light, C_i^* is the intercellular CO_2 photocompensation point, and $K_m(CO_2)_i$ is the *apparent* Michaelis-Menten constant for CO_2 evaluated at C_i whose value depends on $K_c(1+O/K_o)$ and on the magnitude of V_{cmax} relative to that of the CO_2 transfer conductance from the substomatal cavities to the stromal carboxylation sites (g_i). Because in LSMs, g_i is generally assumed to be infinite and the values of $K_c(1+O/K_o)$ and Γ^* (chloroplastic CO_2 photocompensation point) are fixed for all species, Eqn 2.1 is substituted by a single formula

$$A_c = \frac{(C_i - \Gamma^*)V_{c\max}}{C_i + K_c(1 + O/K_o)} - R_d \qquad (2.2)$$

from which A_c for different plant canopies is usually estimated using reference V_{cmax} values taken from the literature (R_d is generally considered a fixed fraction of V_{cmax} and C_i is the analytic solution that satisfies both Eqn 2.2 and an empirical equation relating the stomatal conductance (g_s) to A_c – see Leuning 1990 and Collatz *et al.* 1991 for details).

To evaluate the sensitivity of A_c estimates to $K_c(1+O/K_o)$ values currently implemented in various LSMs, I used a recent parameterisation of the Carbon-Canadian Land Surface Scheme (C-CLASS) for wheat (*Triticum aestivum*) fields described in Kothavala *et al.* (2005). The reference V_{cmax} value used therein (93 μmol m^{-2} s^{-1} at 25 °C) is taken from Wullschleger (1993) who based his 95% confidence limit V_{cmax} estimates on the A–C_i curve published in Kriedemann & Anderson (1988). The $K_c(1+O/K_o)$ value (412 μmol mol^{-1} at 25 °C and 21% O_2) originally used in Eqn 2.2 by Wullschleger (1993) is derived from the *in vitro* study of Jordan & Ogren (1984). By comparison, the big leaf photosynthesis model implemented in C-CLASS by Kothavala *et al.* (2005) is that of Wang & Leuning (1998) who instead used the $K_c(1+O/K_o)$ value originally published in Farquhar *et al.* (1980) (753 μmol mol^{-1} at 25 °C and 21% O_2). This value is similar to that used in the new National Aeronautics and Space Administration (NASA) Goddard Institute for Space Studies (GISS) land surface scheme (714 μmol mol^{-1} at 25 °C and 21% O_2) which follows the recent Farquhar *et al.* (1980) model parameterisation of Bernacchi *et al.* (2001) (see Friend & Kiang 2005). Another land surface scheme (Simple Biosphere Model II: SiB2) developed by NASA scientists (Sellers *et al.* 1996) and currently in use (e.g. Dai *et al.* 2004; Hanan *et al.* 2005) uses a $K_c(1+O/K_o)$ value equal to 510 μmol mol^{-1} at 25 °C and 21% O_2 (see Collatz *et al.* 1991). Thus, taking these various $K_c(1+O/K_o)$ estimates and the reference V_{cmax} value mentioned above as initial parameters, a set of A-C_i curves corresponding to that used in the aforementioned LSMs was generated using Eqn 2.2 to estimate the models' predicted

Rubisco-limited photosynthetic rate of fully illuminated wheat leaves (i.e. the sunlit big leaf in Wang & Leuning's 1998 model) for typical C_i values observed in the field at 25 °C.

Correction of Rubisco K_c *in vitro* estimates for errors in the calculation of dissolved CO_2 concentrations

According to the Henderson-Hasselbach equation, the concentration of CO_2 required to dissociate from carbonic acid to half-saturate the carboxylation rate of Rubisco in O_2-free media (i.e. K_c) is given by

$$K_c = \frac{[HCO_3^-]}{anti\log(pH - pK_a)} \tag{2.3}$$

where $[HCO_3^-]$ is the concentration of bicarbonate ions and pK_a is the negative logarithm of the dissociation constant of carbonic acid in solution of ionic strength μ and temperature T (°C) as given by Yokota & Kitaoka (1985)

$$pK_a = 0.175\log(1/\mu) + 0.2957\log(1/T) + 6.3572 \tag{2.4}$$

If K_c was originally determined from a double-reciprocal (Lineweaver-Burk) plot where CO_2 concentrations were calculated from Eqn 2.1 at various concentrations of carbonic acid using a possibly wrong pK_a value (pK_{a_1}), then, if needed, it can subsequently be corrected for the true pK_a of the solution (pK_{a_2}) according to

$$K_{c_2} = K_{c_1} \frac{anti\log(pH - pK_{a_1})}{anti\log(pH - pK_{a_2})} \tag{2.5}$$

where K_{c_1} and K_{c_2} are the original and corrected K_c value, respectively.

To determine μ (total concentration of dissociated ions in solution) from the buffer composition of previously published studies, I followed the calculation procedure described in Segel (1976) using a pK_a of 8.26, 8, 7.48, and 6.1 for Bicine, HEPPS, HEPES, and EDTA, respectively (for the ionisable salt $MgCl_2$, μ is 3 times its molarity).

RESULTS AND DISCUSSION

Sensitivity of A_c estimates to $K_c(1+O/K_o)$ value used in different LSMs

As expected from the Michaelis-Menten theory explained in detail in Chapter 1, the predicted A-C_i response of sunlit wheat leaves under standard (25 °C and no water stress) Rubisco-limited field conditions varied significantly according to the $K_c(1+O/K_o)$ parameter chosen for the photosynthesis model of representative LSMs (Fig. 2.1). Under such conditions, the operating C_i for fully illuminated wheat leaves has been shown to generally vary between 200 and 300 μbar and photosynthesis to remain Rubisco-limited throughout that range (Evans 1983, 1986; Evans *et al.* 1986; Makino, Mae & Ohira 1988; Renou *et al.* 1990). Figure 2.1 clearly illustrates that, over that range, the A_n value predicted by LSMs can differ from the original parameterisation by over 150% even when the same reference V_{cmax} value is used throughout. Similar results were obtained for other species having different reference V_{cmax} values (data not shown). That goes to show the importance of standardising the $K_c(1+O/K_o)$ value used for modelling photosynthesis in pan-species studies, not only when parameterising the original A-C_i response of the representative species under study (e.g. Wullschleger 1993; Medlyn *et al.* 2002), but also when subsequently predicting canopy photosynthesis from the published V_{cmax} parameters.

Literature survey of C_3 plant Rubisco K_c and $K_c(1+O/K_o)$ values determined *in vitro*

Of the 18 studies I reviewed, 15 provided sufficient information to allow the calculation of μ and subsequent correction of K_c according to Eqn 2.5, if needed. Of these, five originally overestimated K_c by almost 100% and four overestimated it by 18% (Table 2.1).

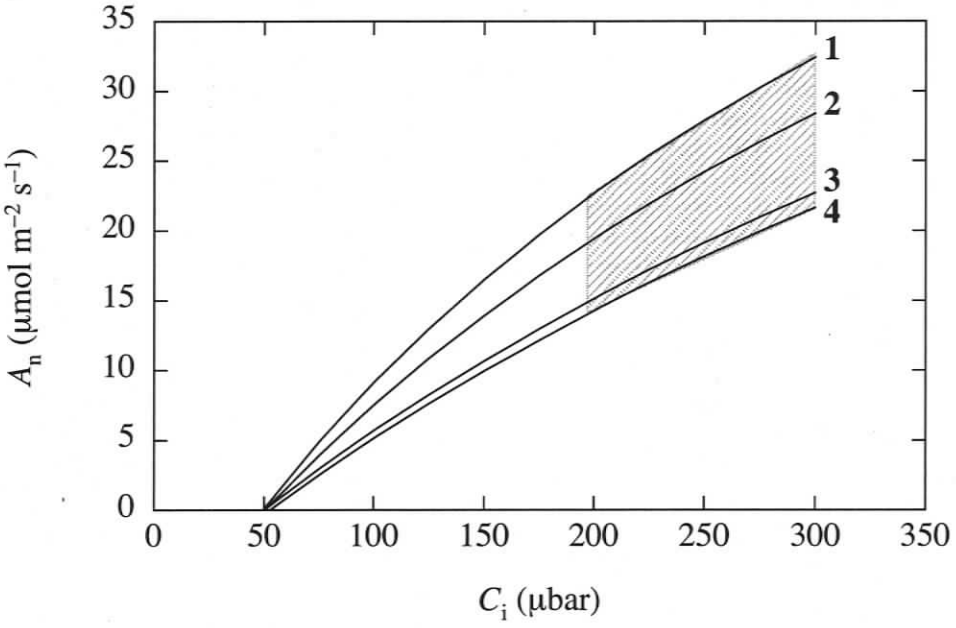

Figure 2.1 Photosynthetic CO_2 response – net CO_2 assimilation rate (A_n) as a function of the intercellular CO_2 concentration (C_i) – of a model wheat leaf under Rubisco-limited conditions. The A_n *vs.* C_i relationships numbered 1 to 4 were modelled from Eqn 2.2 using a same reference maximal carboxylation rate (V_{cmax}) value of 93 μmol m^{-2} s^{-1} (as per Kothavala *et al.* 2005), but different $K_c(1+O/K_o)$ values commonly implemented in Land Surface Models: (Curve 1) original Wullschleger (1993) $K_c(1+O/K_o)$ value from which the above reference V_{cmax} was determined; (Curve 2) value used in SiB2; (Curve 3) value used in the GISS GCM land surface scheme; (Curve 4) value used in CLASS. The shaded area corresponds to the range of C_i values expected for typical sunlit wheat leaves under standard field conditions (see text for details).

Table 2.1 Correction factors for previously reported Rubisco K_c values determined *in vitro* at 25 °C (see Eqn 2.5 for symbols definition)

Reference[a]	pH	pK_{a_1}	μ	pK_{a_2}	Correction Factor[b]
Badger & Andrews (1974)[1]	8.47	6.37	0.101	6.118	0.56
Badger & Collatz (1977)[2]	8.3	6.37	0.162	6.082	0.52
Yeoh, Badger & Watson (1980)[3]	8.0	6.37	0.111	6.111	0.55
Yeoh, Badger & Watson (1981)[4] species set #1	8.0	6.37	0.111	6.111	0.55
Yeoh, Badger & Watson (1981)[5] species set #2	8.0	6.37	0.146	6.090	0.52
McNeil *et al.* (1981)[6] Method B	8.2	6.10	0.127	6.101	1.00
Bird, Cornelius & Keys (1982)[7]	8.2	6.10	0.127	6.101	1.00
Jordan & Ogren (1981)[8]	8.3	6.23	0.056	6.163	0.86
Jordan & Ogren (1983)[9]	8.3	6.23	0.056	6.163	0.86
Jordan & Ogren (1984)[10] Method A	8.35	6.23	0.058	6.161	0.85
Meyers *et al.* (1983)[11]	8.35	6.23	0.058	6.161	0.85
Makino, Mae & Ohira (1985)[12]	8.0	6.11	0.111	6.111	1.00
Makino, Mae & Ohira (1988)[13]	8.15	6.12	0.104	6.116	1.00
Wessinger, Edwards & Ku (1989)[14]	8.0	6.09	0.112	6.111	1.00
Whitney *et al.* (1999)[15]	8.3	6.12	0.069	6.147	1.06

[a]Number in superscript cross-references to list of species in Table 2.2.

[b]Corresponds to $\frac{anti\log(pH - pK_{a_1})}{anti\log(pH - pK_{a_2})}$ in Eqn 2.5.

A total of 120 K_c determinations (of which 75% needed to be corrected) performed at 25°C were tabulated from the 76 C_3 plant species studied (Table 2.2). Following correction, the mean and variance of the overall data set were reduced by 32% and 73%, respectively. Despite the improvement, significant experimental bias among some research groups remained. For example, when comparing K_c measurements performed on herbaceous dicots, values obtained from pooled studies 6 & 7 (see numerical designation in superscript in Table 2.1) were consistently higher (22 to 50% greater sample mean value corresponding to 70–130 μbar offsets) than those generated by research groups 4 & 5, 8–11, and 12 & 13 ($P < 0.0001$, Kruskal-Wallis test) (differences among the latter studies were not significant; $P > 0.05$). This residual bias is in the same order as that reported by McNeil *et al.* (1981) (130 μbar) for repeated K_c measurements made on a single species but using two different common assay methods, hence illustrating the high sensitivity of *in vitro* K_c determinations to the conditions of assay. Under similar assay conditions, the accuracy of repeated K_c measurements made on a single species was at best 50 μbar (Jordan & Ogren 1981, 1983, 1984; Bird *et al.* 1982; Meyers *et al.* 1983). This is equivalent to the standard deviation of the sample from the two larger studies (Yeoh, Badger & Watson 1980, 1981) conducted using a single assay procedure. In the former, only herbaceous monocots were concerned ($n = 36$), and the sample mean did not differ significantly ($P = 0.9327$, Wilcoxon-Mann-Whitney test) from that of the second study which covered C_3 species that originated from widely different evolutionary lines ($n = 33$). Similarly, the sample means of the four general functional groups of higher vascular plants (all studies included – see Table 2.2) were found to be highly conserved ($P = 0.4642$, Kruskal-Wallis test) and also similar to that of bryophytes and lower vascular plants ($P = 0.3170$, Kruskal-Wallis test). Thus, in light of the above, and despite accuracy problems related to the use of different protein extraction and Rubisco assay protocols among *in vitro* studies, it seems reasonably safe to conclude that the average K_c value of Rubisco from the majority of C_3 plant species should fall within 50 μbar of the overall sample mean found in this study (317 μbar at 25 °C).

Table 2.2 Literature survey of Rubisco K_c (Michaelis-Menten constant for CO_2) values from C_3 plant species evaluated at 25 °C

Species	K_c (μbar)[a]	Species	K_c (μbar)[a]
Herbaceous annuals		Herbaceous perennials (n = 5)	
Monocots (n = 52)		Aciphylla glacialis	239[4]
Allium cepa	271[4]	*Cyperus eragrostis*	239[4]
Arundinaria sp.	415[3]	*Lupinus angustiflorius*	351[4]
Avena sativa	319[3]	*Microseris lanceolata*	351[4]
Bromus spp.	255 – 271[3]	*Rumex acetosella*	258[5]
Festuca spp.	303 – 319[3]	**Mean (SE)**	**292 (25)**
Hordeum vulgare	239[3], 368[7]	Woody perennials (n = 13)	
Lolium perenne	303[3], 397[8], 391 – 414[6], 405[7]	*Buddleia davidii*	303[4]
Oryza sativa	232 – 235[12, 13], 271[3]	*Clemantis sp.*	182[5]
Poa spp.	319 – 335[3, 4]	*Ginkgo biloba*	350[5], 518[7]
Triticum aestivum	239[3], 298[12], 324[13], 356[7]	*Gossypium hirsutum*	303[4]
Other *spp.* (n = 23)	207 – 399[3]	*Populus nigra*	289[5]
Mean (SE)	**308 (8)**	*Salix babylonica*	359[7]
Dicots (n = 41)		*Casuarina sp.*	213[5]
Atriplex patula	303[4]	*Chamaecyparis sp.*	486[7]
Beta vulgaris	321[7]	*Ilex aquifolium*	380[5]
Brassica napus	368[7]	*Macrozamia communis*	213[5]
Flaveria spp.	397 – 411[14]	*Magnolia grandiflora*	182[5]
Fragaria vesca	274[5]	*Pinus montezumae*	365[5]
Glycine max	223[8], 197[12]	**Mean (SE)**	**319 (30)**
Helianthus spp.	248[9], 272[12], 353[7]	Mosses and ferns (n = 9)	
Lactuca sativa	351[4]	*Atrichum undulatum*	446[7]
Lycopersicon esculentum	203[9]	*Funaria sp.*	367[4]
Medicago sativa	368 – 420[11], 389[9]	*Ceratopteris thalictroides*	255[4]
Mentha aquatica	351[4]	*Equisetum arvense*	460[7]
Nicotiana tabacum	273[8], 284[12], 329[15]	*Pellaea falcata*	289[5]
Papaver nudicaule	351[4]	*Psilotum nudum*	367[4]
Petroselinum crispum	288[9], 335[4], 363[7]	*Pteridium esculentum*	304[5]
Solanum tuberosum	271[4], 385[7]	*Pteris aquilina*	455[7]
Spinacia oleracea	271[4], 272[10], 295[7], 316[12], 340[1], 347[8], 360[11]	*Selaginella kraussiana*	274[5]
Tetragonium expansa	322[8]	**Mean (SE)**	**357 (27)**
Verbascum thapsus	271[4]		
Mean (SE)	**321 (9)**		

[a]Original micromolar concentration values converted to partial pressures assuming a Henry's law constant for CO_2 equal to 0.03454 mol bar^{-1} at 25 °C (Sander 1999). The numbers in superscript cross-reference to studies indicated in Table 2.1.

Compared to the carboxylase, the Michaelis-Menten constant for RuBP oxygenase (K_o) has been far less documented (only 20 species). Because of accuracy problems related to the use of different assay conditions, most researchers have preferred to determine K_o from the slope of the "apparent" increase of the Michaelis-Menten constant for CO_2 that results from increasing O_2, rather than from assaying the oxygenase separately (e.g. Jordan & Ogren 1981, 1984; McNeil *et al.* 1981; Bird *et al.* 1982; Whitney *et al.* 1999). Thus, in principle, if sufficient measurements are included to determine the slope of the O_2 response, the accuracy of these K_o determinations should be similar to that of K_c. In the majority of cases, however, only two points (O_2-free and ambient air) were used to determine the slope, so the resulting accuracy of the K_o estimates was found to be 2–3 times less than for K_c (e.g. McNeil *et al.* 1981; Bird *et al.* 1982). Consequently, current *in vitro* estimates of Rubisco $K_c(1+O/K_o)$ values are more variable: 550 ± 100 μbar (mean ± SD, n = 28) at 25 °C and 200 mbar O_2 (after applying the aforementioned correction for K_c) for those studies where K_o was estimated from the inhibitory constant on the carboxylase – but it is not clear at this stage if this variation truly reflects the species diversity.

Only two *in vitro* studies have determined the temperature response of K_c and K_o over an appreciably large range and have been used to parameterise the leaf photosynthesis models implemented in LSMs. The first study (Badger & Collatz 1977) measured the two Michaelis-Menten constants over a 5–35 °C temperature range for Rubisco purified from leaves of a C_4 species (*Atriplex glabriuscula*) while the second study (Jordan & Ogren 1984) used Rubisco purified from spinach (*Spinacia oleracea*) leaves and measured K_c and K_o from 7 to 35 °C. Details about the Arrhenius functions used to fit the above temperature responses are given in Table 1.2 of Chapter 1 (see also Medlyn *et al.* 2002). These equations, currently implemented in LSMs (e.g. Cramer *et al.* 2001; Dai *et al.* 2004; Hanan *et al.* 2005; Kothavala *et al.* 2005), are not exact as they come from studies where K_c determinations were performed using an incorrect pK_a for carbonic acid. The corrected temperature responses are shown in Fig. 2.2 and corresponding Arrhenius function parameters given in Table 2.3.

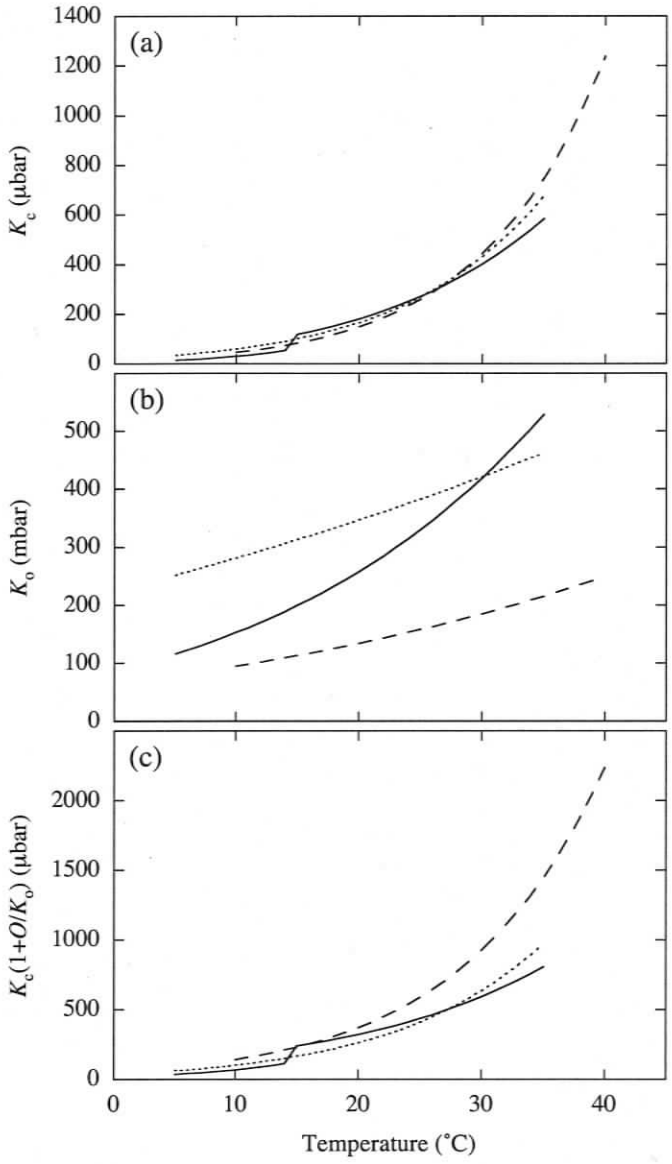

Figure 2.2 Temperature response of Rubisco's (a) Michaelis-Menten constant for CO_2 (K_c), (b) Michaelis-Menten constant for O_2 (K_o), and (c) effective Michaelis-Menten constant for CO_2 [$K_c(1+O/K_o)$] evaluated at 200 mbar O_2. Data are from Badger & Collatz (1977) (solid line) and Jordan & Ogren (1984) (dotted line) (*in vitro* studies), and Bernacchi *et al.* (2002) (dashed line) (*in vivo* study) (see Table 2.3). For the *in vitro* studies, original values were corrected for the calculated ionic strength of the assay medium following Eqn 2.5 (other details given in the text – see also Table 2.3 footnote).

Table 2.3 Temperature response of the Michaelis-Menten constants of ribulose-1,5-bisphosphate carboxylase (K_c) and oxygenase (K_o) commonly used to parameterise the photosynthesis model of Farquhar *et al.* (1980)

Reference	Species	Parameter	Value at 25 °C	Units	E (kJ K^{-1} mol^{-1})
Farquhar *et al.* (1980)[a, c]	*S. oleracea* (5 ≥ T °C < 15)	K_c	271	μbar	103.570
	(15 ≥ T °C < 35)				58.805
	(5–35 °C)	K_o	330	mbar	35.982
Jordan & Ogren (1984)[a, d]	*S. oleracea* (7–35 °C)	K_c	269	μbar	70.517
		K_o	383	mbar	14.435
Bernacchi *et al.* (2002)[b]	*N. tabacum* (10–40 °C)	K_c	272	μmol mol^{-1}	80.990
		K_o	166	mmol mol^{-1}	23.720

The temperature response of the parameters was described by fitting the original data to the Arrhenius function normalised relative to 25 °C: *Parameter* (T) = *Parameter*(25 °C) exp [(T – 298.15) E / 298.15 RT]. R *is* the gas constant (8.314 J K^{-1} mol^{-1}); T is the absolute temperature (T °C + 273.15) °K; E is the energy of activation; 1 cal = 4.184 Joules.

[a] Kinetic constants determined *in vitro*. Inter-conversions between micromolar concentrations and partial pressures at different temperatures were done using the Henry's law constants for CO_2 and O_2 given by Sander (1999).

[b] Kinetic constants determined *in vivo* as "chloroplastic" values.

[c] Activation energies (E) for K_c and K_o are from Badger & Collatz (1977). Values given for K_c were fitted after the original values were corrected for the ionic strength (μ) of the assay medium following Eqn 2.5.

[d] From Jordan & Ogren's (1984) Table 2. Original CO_2 and O_2 concentrations corrected for μ according to Eqn. 2.5 and to the solubility tables of O_2 in NaCl solutions of Smith (1928), respectively.

To present the corrected temperature functions of Badger & Collatz (1977), I followed many previous modelling studies (e.g. Friend *et al.* 1997; Walcroft *et al.* 1997; Wang & Leuning 1998; Kothavala *et al.* 2005) that used the K_c and K_o values of spinach Rubisco given at 25 °C in Farquhar *et al.* (1980) (originally a personal communication from M.R. Badger) but adjusted K_c to 271 μbar (originally 460 μbar – see Table 1.2), based on the corrected K_c value of spinach Rubisco from Yeoh *et al.* (1981) (see Table 2.2). Unlike before, the corrected values of K_c and $K_c(1+O/K_o)$ from both studies are now within the aforementioned measurement accuracy of *in vitro* methods across the measured temperature range (compare Fig. 2.2 with Fig. 1 in Medlyn *et al.* 2002). Also shown in Fig. 2.2 is the temperature response of the Michaelis-Menten constants of Rubisco assayed *in vivo* on transgenic tobacco (*Nicotiana tabacum*) leaves (Bernacchi *et al.* 2002). These differ from the Bernacchi *et al.*'s (2001) values shown in Medlyn *et al.* (2002) as, unlike the latter, they were evaluated on the basis of C_c (CO_2 concentration inside the chloroplasts) rather than C_i. The *in vivo* temperature response of $K_c(1+O/K_o)$ rises appreciably more sharply than the corresponding *in vitro* responses, resulting in significantly greater values at higher temperatures (2 to 3 times greater over the 25–35 °C temperature range, starting with a same $K_c(1+O/K_o)$ value at 10°C). Such discrepancies have important implications in modelling the photosynthetic response of C_3 plants in the face of climate change and should be addressed in future LSM simulations (Matthews *et al.* 2005). Particularly problematic is the uncertainty concerning the magnitude and temperature response of K_o (Fig. 2.2b). Current *in vitro* estimates of the inhibitory constant on the carboxylase determined at 25 °C range from 230 to 679 mbar (n = 28, compiled from studies 1, 6–8, 10, 12, and 15 indicated in Table 2.1) compared to the 166–179 mbar value of tobacco found by the *in vivo* studies (von Caemmerer *et al.* 1994; Bernacchi *et al.* 2002). In that respect, *in vitro* studies that have determined K_o from the Michaelis-Menten constant of the oxygenase (Badger & Andrews 1974; Badger & Collatz 1977; Makino *et al.* 1985, 1988) are in better agreement (143–299 mbar, n = 5) with the *in vivo* values, but the temperature function of the constant for the C_4 plant oxygenase derived

by Badger & Collatz (1977) differs significantly (i.e. rises far more sharply – see Fig. 2.2b) from that of the inhibitory constant of the C_3 plant carboxylase (*cf.* Jordan & Ogren 1984; Bernacchi *et al.* 2002). Whether this is due to the two different (direct *vs.* indirect) methodologies used to assay the oxidation of RuBP by Rubisco *in vitro*, or else reflects a possibly greater temperature sensitivity for the C_4-type oxygenase, remains to be determined.

Simultaneous determination of Rubisco kinetic constants *in vivo*

Despite the aforementioned accuracy problems related to the extraction of Rubisco and its re-solubilisation *in vitro* under different assay conditions (possibly resulting in alterations of the protein's secondary to quaternary structure), there are still very few published *in vivo* estimates for the kinetic constants of Rubisco that have been properly evaluated at C_c. This is because the domain of the A_c function is normally considered too small to allow an accurate extrapolation of the effective Michaelis-Menten constant for CO_2, $K_c(1+O/K_o)$, either from non-linear regression techniques or from linear Lineweaver-Burk plots. Von Caemmerer and colleagues (von Caemmerer *et al.* 1994; Bernacchi *et al.* 2002) circumvented this problem by using transgenic tobacco plants which had a reduced Rubisco content and were limited by Rubisco activity, as opposed to RuBP regeneration capacity, even at high CO_2 concentrations. The non-linear regression method they used for estimating $K_c(1+O/K_o)$ for leaves exposed to a range of O_2 concentrations is based on the theoretical principle described in Chapter 1. They fitted the transgenic tobacco CO_2 response curves (evaluated at C_c) with the following equation

$$A_c + R_d = \frac{(C_c - \Gamma^*)V_{c\max}}{(C_c - \Gamma^*) + (K_c(1 + O/K_o) + \Gamma^*)} \qquad (2.6)$$

(*cf.* Eqn 1.6) after having determined g_i, C_i*, and R_d *a priori* by independent methods (and assuming $\Gamma^* = C_i^* - R_d/g_i$), then subtracted Γ^* from the fitted "$K_c(1+O/K_o)+\Gamma^*$" parameter.

However, as I showed in Chapter 1, the equivalent expression

$$\begin{aligned} A_c &= \frac{-b+\sqrt{b^2-4ac}}{2a} \\ a &= -1/g_i \\ b &= (V_{c\max}-R_d)/g_i + C_i + K_c(1+O/K_o) \\ c &= -(V_{c\max}-R_d)(C_i-\Gamma) \end{aligned} \qquad (2.7)$$

(*cf.* Eqns 1.7, 1.9 & 1.10) can instead be used to solve for the CO_2 compensation point (Γ), "$K_c(1+O/K_o)$", and "V_{cmax}–R_d" simultaneously from the original A-C_i curves without having to rely on prior knowledge of Γ^* and R_d (g_i needs still be known). Figure 2.3 shows an example of this using the data of von Caemmerer *et al.* (1994) reproduced from their Fig. 4a. The O_2-response obtained for the three fitted parameters: Γ, $K_c(1+O/K_o)$, and V_{cmax}–R_d is shown in Fig. 2.4 (compare with Fig. 5 of von Caemmerer *et al.* 1994). As predicted from theory, the V_{cmax}–R_d values estimated are essentially the same across the O_2 concentration range (Fig. 2.4c).

According to Michaelis-Menten theory, the linear dependence of Γ on O (Fig. 2.4a) originates from the O_2-dependence of Γ^* and $K_c(1+O/K_o)$ (Fig. 2.4b) and is given as

$$\Gamma = \frac{O}{V_{c\max}-R_d}\left(\frac{0.5V_{c\max}}{S_{c/o}}+\frac{K_cR_d}{K_o}\right)+\frac{K_cR_d}{V_{c\max}-R_d} \qquad (2.8)$$

where the specificity factor of Rubisco ($S_{c/o}$) equals $O/2\Gamma^*$ (*cf.* Eqn 1.5). The y-intercept of Eqn 2.8 represents the residual CO_2 compensation point in the absence of RuBP oxygenation and photorespiration. It can be used to derive R_d from the estimated values of V_{cmax}–R_d and K_c (y-intercept of Fig. 2.4b). Following this, the value of V_{cmax} is readily obtained and can be used to solve $S_{c/o}$ (and therefore Γ^*) from the slope of Eqn 2.8 (K_o is given by the slope of Fig. 2.4b). The final sets of values derived from the least-squares fits of Eqn 2.7 to the A-C_i

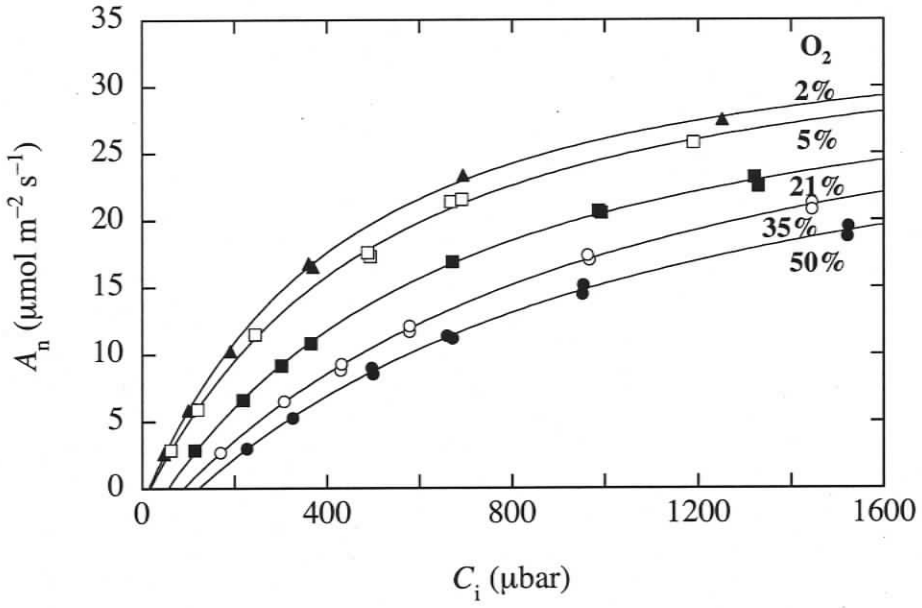

Figure 2.3 Least-squares regression fits of Eqn 2.7 (as derived from Eqns 1.7 and 1.9 – see Chapter 1) to the A-C_i curves of Fig. 4a from von Caemmerer *et al.* (1994). Measurements were done on a transgenic tobacco leaf with a reduced Rubisco content at 25 °C (I = 1500 μmol quanta m^{-2} s^{-1}) under five different O_2 concentrations. The CO_2 transfer conductance (g_i) for such leaves was estimated to be 0.27 ± 0.2 mol m^{-2} s^{-1} (Evans *et al.* 1994).

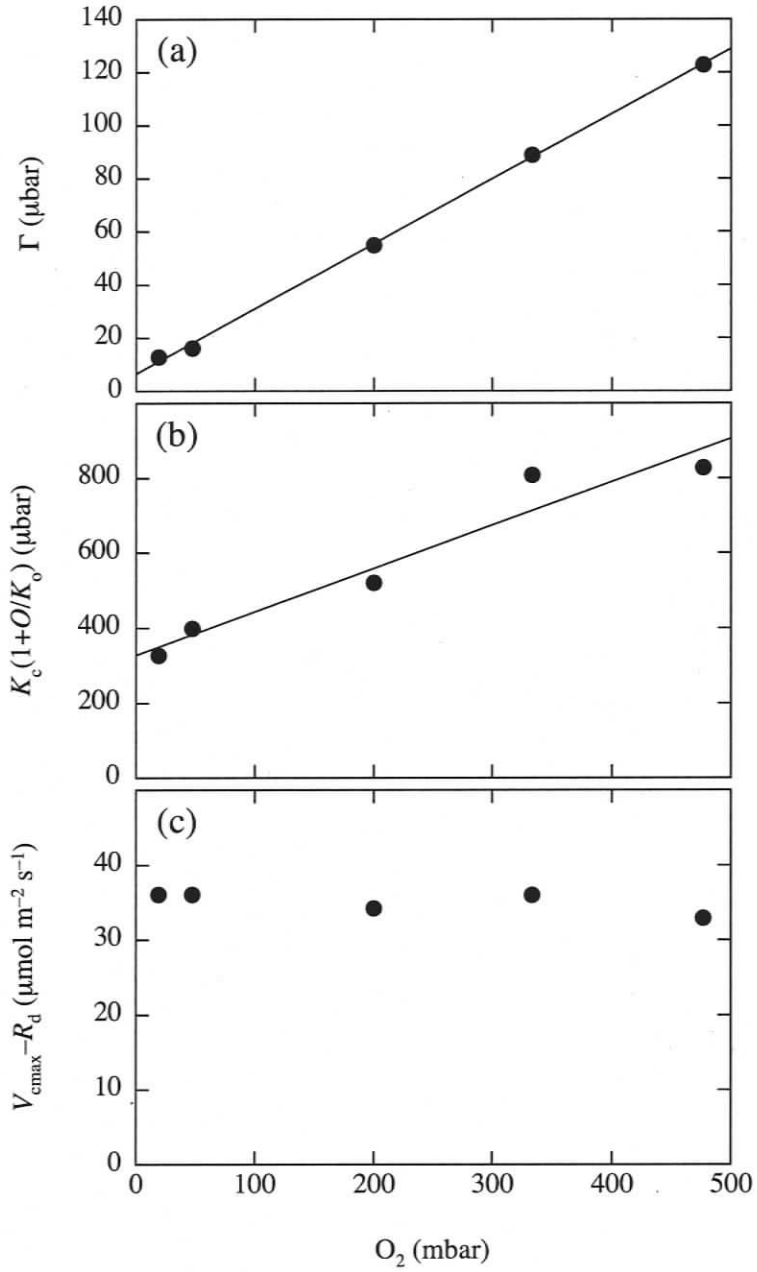

Figure 2.4 O_2-response of (a) the CO_2 compensation point (Γ), (b) the effective Michaelis-Menten constant for CO_2 [$K_c(1+O/K_o)$], and (c) the effective maximal carboxylation rate in the presence of mitochondrial respiration in the light (V_{cmax}–R_d) estimated from the least-squares regression fits of Eqn 2.7 to the A-C_i curves shown in Fig. 2.3.

curves shown in Fig. 2.3 are given in Table 2.4 for g_i values of 0.27 ± 0.2 mol m^{-2} s^{-1} determined for these transgenic tobacco plants using the isotopic method (Evans *et al.* 1994). The final $K_c(1+O/K_o)$ value I obtained for this particular leaf (550–566 μbar at 200 mbar O_2) is essentially identical to the average value reported by von Caemmerer *et al.* (1994) (549 μbar at 200 mbar O_2) and, surprisingly, also corresponds to the aforementioned average $K_c(1+O/K_o)$ value determined *in vitro* for C_3 plants. Interestingly, the K_c and K_o values I obtained are significantly greater than the corresponding estimates of von Caemmerer *et al.* (1994) and Bernacchi *et al.* (2002), yet they seem to be in better agreement with the *in vitro* estimates that von Caemmmerer & colleagues produced for this transgenic tobacco line (329 μbar and 236 mbar for K_c and K_o, respectively – see Whitney *et al.* 1999).

In principle, if g_i is known, it should be possible to estimate the overall value of $K_c(1+O/K_o)$ in wild-type plants from a least-squares fit of Eqn 2.7 to the Rubisco-limited portion of A-C_i curves, provided that a high degree of measurement resolution is used over the domain of interest (e.g. ≤ 25 μbar steps). Although the restricted measurable domain of the A_c function remains a concern in wild-type plants, my measurements on Douglas-fir (see Chapter 3) as well as those of Manter & Kerrigan (2004) performed on other woody plant species with low g_i are encouraging in that they indicate that the transition C_i between the Rubisco-limited and RuBP-limited A-C_i curve portions can be as high as 400-800 μbar or even higher (also compare Fig. 2.5a and 2.5c in next section). If so, then the aforementioned method may prove very useful to investigate the kinetic properties of Rubisco from this important, but so far rarely studied, C_3 plant functional group *in vivo*.

CONCLUSION

Which Michaelis-Menten constant for CO_2 is most appropriate for large scale pan-species studies?

I have showed that the current range of $K_c(1+O/K_o)$ values chosen for LSMs to model photosynthesis under Rubisco-limited conditions is unnecessarily large and results in widely

Table 2.4 Complete set of parameters obtained from estimating Γ, $K_c(1+O/K_o)$, and V_{cmax}–R_d from least-squares fits of Eqn 2.7 to A-C_i curves measured at different O_2 concentrations. Data from von Caemmerer *et al.* (1994) (see Figs. 2.3 and 2.4).

	$g_i = 0.25$ (mol m^{-2} s^{-1} bar^{-1})	$g_i = 0.27$ (mol m^{-2} s^{-1} bar^{-1})	$g_i = 0.29$ (mol m^{-2} s^{-1} bar^{-1})	Units
Γ	54.6	54.9	55.1	μbar
V_{cmax}–R_d	34.07	34.19	34.28	μmol m^{-2} s^{-1}
$K_c(1+O/K_o)$[a]	549.7	558.5	566.0	μbar
K_c	319.3	327.0	333.7	μbar
K_o	277.1	282.6	287.3	mbar
R_d	0.63	0.66	0.69	μmol m^{-2} s^{-1}
V_{cmax}	34.70	34.85	34.97	μmol m^{-2} s^{-1}
$S_{c/o}$	2275	2291	2304	bar bar^{-1}
Γ*[a]	44.0	43.7	43.4	μbar

[a] Evaluated at O = 200 mbar.

different estimates of A_c for given V_{cmac} values. According to the present analysis, the average C_3 species $K_c(1+O/K_o)$ value most appropriate for determining V_{cmax} in pan-species comparative studies is 550 μbar at 25 °C and 200 mbar O_2 – that is provided that g_i is accounted for in the A-C_i analyses. I therefore recommend the use of the *in vivo* K_c and K_o "chloroplastic" values of von Caemmerer *et al.* (1994), or the complete set of Rubisco kinetic constants shown in Table 2.4 (e.g. first column) which seems to better agree with current *in vitro* estimates of mean values for C_3 species (see previous discussion), along with the *in vivo* temperature responses of Bernacchi *et al.* (2002), for such large scale comparative studies.

For LSM simulations which require that the parameterisation of the photosynthesis model of Farquhar *et al.* (1980) be based on a simple rectangular hyperbola formulation that assumes g_i to be infinite, the aforementioned "chloroplastic" K_c and K_o values are inappropriate as they will correctly estimate A_c only for species with lowest V_{cmax}/g_i ratios (such as the wheat example used in Fig. 2.1, here reproduced in its original form in Fig. 2.5a based on the A_n *vs.* C_i measurements of Kriedemann & Anderson 1988). According to Fig. 1.7d, the V_{cmax}/g_i ratio of C_3 plants varies almost 3-fold, corresponding to $K_m(CO_2)_i$ values ranging from 630 μbar to over 1600 μbar (Fig. 2.5b). In the past, LSMs have inappropriately been parameterised with $K_c(1+O/K_o)$ values representing only the lowest V_{cmax}/g_i ratios observed in C_3 plants (Fig. 2.5b), or even lower ratios. Figure 2.5c shows that, to avoid significant underestimations of A_c and corresponding overestimations of the C_i at which the transition from Rubisco-limited to RuBP-limited photosynthesis takes place in species with high V_{cmax}/g_i ratios (typically leaves with higher longevity), a large $K_m(CO_2)_i$ value from the opposite end of the spectrum should be used. The example shown in Fig. 2.5 covers both extremes of the V_{cmax}/g_i variation observed in C_3 plants, yet Fig. 2.5a shows that both A_c and the C_i transition point can be modelled with good accuracy even when the $K_m(CO_2)_i$ value chosen to fit the A-C_i curve is over twice the correct value.

Thus, to improve their estimates of photosynthesis under Rubisco-limited conditions, I suggest that LSMs revise their reference (25 °C) V_{cmax} parameterisations based on a common

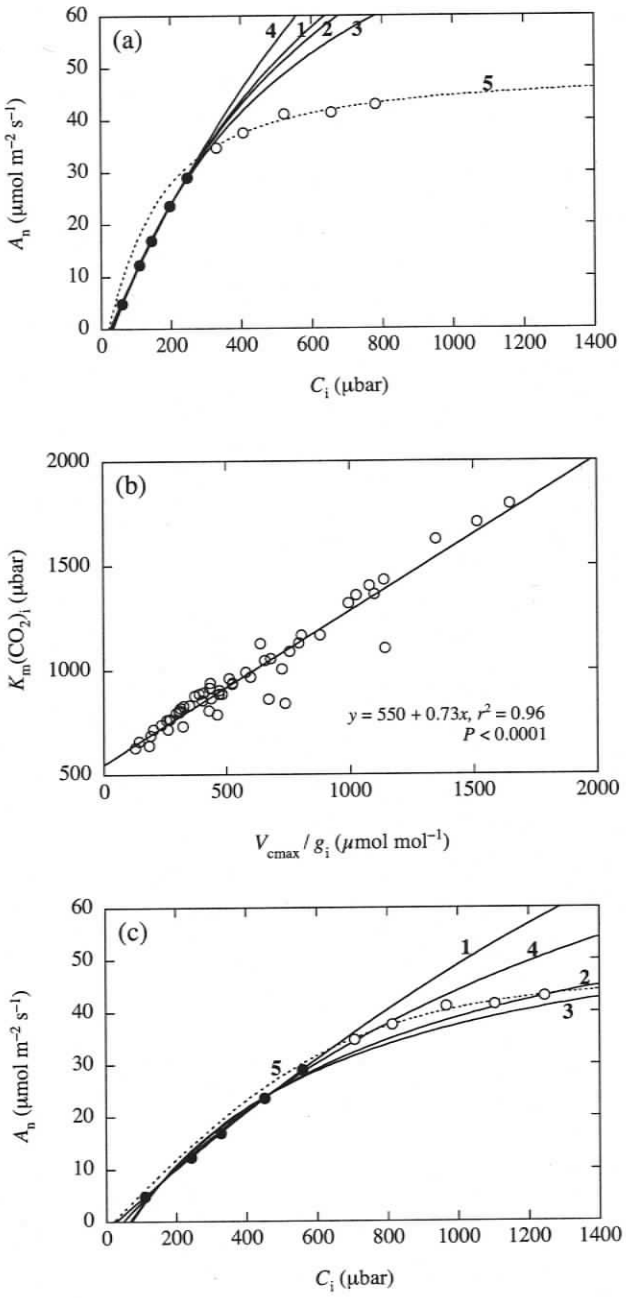

Figure 2.5 (a) Net CO_2 assimilation rate (A_n) of a wheat leaf as a function of its intercellular CO_2 concentration (C_i) (reproduced from Fig. 2 in Kriedemann & Anderson 1988). (b) Apparent Michaelis-Menten constant for CO_2 evaluated at C_i [$K_m(CO_2)_i$] of various C_3 plant leaves as a function of their V_{cmax} / g_i (maximal carboxylation rate to CO_2 tranfer conductance) ratio (reproduced from Fig. 1.7 – see details given in Chapter 1). (c) A_n *vs.* C_i relationship of the wheat leaf shown in panel (a) for which the V_{cmax} / g_i ratio was increased from 218 to 1600 μmol mol^{-1} [by decreasing g_i from 0.58 to 0.08 mol m^{-2} s^{-1} – note the increase (from panel a) of the C_i value marking the transition from Rubisco- to RuBP-limited photosynthesis]. In panels (a) and (c) data representing Rubisco-limited photosynthesis (●) were fitted with Eqn 2.7 (*c.f.* Eqn 3.2) using a $K_c(1+O/K_o)$ value of 550 μbar (Curve 1), or with Eqn 2.1 using a $K_m(CO_2)_i$ value of 695 μbar (Curve 2), 550 μbar (Curve 3), or 1600 μbar (Curve 4); other data representing Rubisco-limited photosynthesis (○) were fitted with Eqn 3.3 (see details in Chapter 3) using a chloroplastic CO_2 photocompensation point (Γ*) value of 44 μbar (see Table 2.4).

$K_m(CO_2)_i$ value that is large enough to prevent significant underestimation of A_c in those reference model species that have high V_{cmax} / g_i ratios. For modelling purposes, the overestimation of V_{cmax} for species with lower V_{cmax} / g_i ratios (e.g. crops) is of no concern and no worse than the reverse current situation. Because V_{cmax} / g_i is expected to increase with temperature (especially high temperatures – see Bernacchi *et al.* 2002), the temperature response of $K_m(CO_2)_i$ is expected to rise more sharply than that of $K_c(1+O/K_o)$. However, no such disparity was observed between the C_c- and C_i-based temperature responses of $K_c(1+O/K_o)$ published by Bernacchi and colleagues (Bernacchi *et al.* 2001, 2002). New determinations of $K_m(CO_2)_i$ (see Chapter 1) evaluated at various temperatures are needed to resolve this theoretical contradiction.

REFERENCES

Badger M.R. & Andrews T.J. (1974) Effects of CO_2, O_2 and temperature on a high-affinity form of ribulose diphosphate carboxylase-oxygenase from spinach. *Biochemical and Biophysical Research Communications* **60,** 204–210.

Badger M.R. & Collatz G.J. (1977) Studies on the kinetic mechanism of ribulose-1,5-bisphosphate carboxylase and oxygenase reactions, with particular reference to the effect of temperature on kinetic parameters. *Carnegie Institution of Washington Year Book* **76,** 355–361.

Bernacchi C.J., Portis A.R., Nakano H., von Caemmerer S. & Long S.P. (2002) Temperature response of mesophyll conductance. Implications for the determination of Rubisco enzyme kinetics and for limitations to photosynthesis in Vivo. *Plant Physiology* **130,** 1–7.

Bernacchi C.J., Singsaas E.L., Pimentel C., Portis A.R. & Long S.P. (2001) Improved temperature response functions for models of Rubisco-limited photosynthesis. *Plant, Cell and Environment* **24,** 253–259.

Bird I.F., Cornelius M.J. & Keys A.J. (1982) Affinity of RuBP carboxylases for carbon dioxide and inhibition of the enzymes by oxygen. *Journal of Experimental Botany* **33,** 1004–1013.

Bunce J.A. (2000) Acclimation of photosynthesis in eight cool and warm climate herbaceous C_3 species: temperature dependence of parameters of a biochemical photosynthesis model. *Photosynthesis Research* **63,** 59–67.

Collatz G.J., Ball J.T., Grivet C. & Berry J.A. (1991) Physiological and environmental regulation of stomatal conductance, photosynthesis and transpiration: a model that includes a laminar boundary layer. *Agricultural and Forest Meteorology* **54,** 107–136.

Cramer W., Bondeau A., Woodward F.I., Prentice I.C., Betts R.A., Brovkin V., Cox P.M., Fisher V., Foley J.A., Friend A.D., Kucharik C., Lomas M.R., Ramankutty N., Sitch S., Smith B., White A. & Young-Molling C. (2001) Global response of terrestrial ecosystem structure and function to CO_2 and climate change: results from six dynamic global vegetation models. *Global Change Biology* **7,** 357–373.

Dai Y., Dickinson R.E. & Wang Y.-P. (2004) A two-big-leaf model for canopy temperature, photosynthesis, and stomatal conductance. *Journal of Climate* **17,** 2281–2299.

Delire C. & Foley J. (1999) Evaluating the performance of a land surface ecosystem model with biophysical measurements from contrasting environments. *Journal of Geophysical Research* **104,** 16895–16909.

Evans J.R. (1983) Nitrogen and photosynthesis in the flag leaf of wheat (*Triticum aestivum* L.). *Plant Physiology* **72,** 297–302.

Evans J.R. (1986) The relationship between carbon-dioxide-limited photosynthetic rate and ribulose-1,5-bisphosphate-carboxylase content in two nuclear-cytoplasm substitution lines of wheat, and the coordination of ribulose-bisphosphate-carboxylation and electron-transport capacities. *Planta* **167,** 351–358.

Evans J.R., Sharkey T.D., Berry J.A. & Farquhar G.D. (1986) Carbon isotope discrimination measured concurrently with gas exchange to investigate CO_2 diffusion in leaves of higher

plants. *Australian Journal of Plant Physiology* **13,** 281–292.

Farquhar G.D., von Caemmerer S. & Berry J.A. (1980) A biochemical model of photosynthetic CO_2 assimilation in leaves of C_3 species. *Planta* **149,** 78–90.

Friend A.D. & Kiang N.Y. (2005) Land surface model development for the GISS GCM: effects of improved canopy physiology on simulated climate. *Journal of Climate* **18,** 2883–2902.

Friend A.D., Stevens A.K., Knox R.G. & Cannell M.G.R. (1997) A process-based, terrestrial biosphere model of ecosystem dynamics (Hybrid v3.0). *Ecological Modelling* **95,** 249–287.

Hanan N.P., Berry J.A., Verma S.B., Walter-Shea E.A., Suyker A.E., Burba G.G. & Denning A.S. (2005) Testing a model of CO2, water and energy exchange inGreat Plains tallgrass prairie and wheat ecosystems. *Agricultural and Forest Meteorology* **131,** 162–179.

Jordan D.B. & Ogren W.L. (1981) Species variation in the specificity of ribulose biphosphate carboxylase/oxygenase. *Nature* **291,** 513–515.

Jordan D.B. & Ogren W.L. (1983) Species variation in the kinetic properties of ribulose 1,5-bisphosphate carboxylase/oxygenase. *Archives of Biochemistry and Biophysics* **227,** 425–433.

Jordan D.B. & Ogren W.L. (1984) The CO_2/O_2 specificity of ribulose 1,5-bisphosphate carboxylase/oxygenase. Dependence on ribulose bisphosphate concentration, pH and temperature. *Planta* **161,** 308–313.

Harley P.C., Thomas R.B., Reynolds J.F. & Strain B.R. (1992) Modelling photosynthesis of cotton grown in elevated CO_2. *Plant, Cell and Environment* **15,** 271–282.

Kothavala Z., Arain M.A., Black T.A. & Verseghy D. (2005) The simulation of energy, water vapor and carbon dioxide fluxes over common crops by the Canadian Land Surface Scheme (CLASS). *Agricultural and Forest Meteorology* **133,** 89–108.

Kriedemann P.E. & Anderson J.E. (1988) Growth and photosynthetic responses to manganese and copper deficiencies in wheat (*Triticum aestivum*) and barley grass

(*Hordeum glaucum* and *H. leporinum*). *Australian Journal of Plant Physiology* **15,** 429–446.

Kucharik C.J., Foley J.A., Delire C., Fisher V.A., Coe M.T., Lenters J.D., Young-Molling C., Ramankutty N., Norman J.M. & Gower S.T. (2000) Testing the performance of a Dynamic Global Ecosystem Model: water balance, carbon balance, and vegetation structure. *Global Biogeochemical Cycles* **14,** 795–825.

Leuning R. (1990) Modelling stomatal behaviour and photosynthesis of *Eucalyptus grandis*. *Australian Journal of Plant Physiology* **17,** 159–175.

Leuning R., Dunin F.X. & Wang, Y.-P. (1998) A two-leaf models for canopy conductance, photosynthesis and partitioning of available energy II. Comparison with measurements. *Agricultural and Forest Meteorology* **91,** 113–125.

Makino A., Mae T. & Ohira K. (1985) Enzymic properties of ribulose-1,5-bisphosphate carboxylase/oxygenase purified from rice leaves. *Plant Physiology* **79,** 57–61.

Makino A., Mae T. & Ohira K. (1988) Differences between wheat and rice in the enzymic properties of ribulose-1,5-bisphosphate carboxylase/oxygenase and the relationship to photosynthetic gas exchange. *Planta* **174,** 30–38.

Manter D.K. & Kerrigan J.A. (2004) *A*/*C*i curve analysis across a range of woody plant species: influence of regression analysis parameters and mesophyll conductance. *Journal of Experimental Botany* **55,** 2581–2588.

Matthews H.D., Eby M., Weaver A.J. & Hawkins B.J. (2005) Primary productivity control of simulated carbon cycle–climate feedbacks. *Geophysical Research Letters* **32,** doi:10.1029/2005GL022941.

McNeil P.H., Foyer C.H., Walker D.A., Bird I.F., Cornelius M.J. & Keys A.J. (1981) Similarity of ribulose-1,5-bisphosphate carboxylases of isogenic diploid and tetraploid ryegrass (*Lolium perenne* L.) cultivars. *Plant Physiology* **67,** 530–534.

Medlyn B.E., Dreyer E., Ellsworth D., Forstreuter M., Harley P.C., Kirschbaum M.U.F., Le Roux X., Montpied P., Strassemeyer J., Walcroft A., Wang K. & Loustau D. (2002)

Temperature response of parameters of a biochemically based model of photosynthesis. II. A review of experimental data. *Plant, Cell and Environment* **25,** 1167–1179.

Meyers S.P., Brinegar A.C., Schrader L.E., Jordan D.B. & Ogren W.L. (1983) Ploidy effects in isogenic populations of alfalfa (*Medicago sativa* L.). *Plant Physiology* **71,** 966–968.

Niinemets Ü., Cescatti A., Rodeghiero M. & Tosens T. (2006) Complex adjustments of photosynthetic potentials and internal diffusion conductance to current and previous light availabilities and leaf age in Mediterranean evergreen species *Quercus ilex*. *Plant, Cell and Environment* **29,** 1159–1178.

Pitman A.J. (2003) The evolution of, and revolution in, land surface schemes designed for climate models. *International Journal of Climatology* **23,** 479–510.

Renou J.-L., Gerbaud A., Just D. & André M. (1990) Differing substomatal and chloroplastic CO_2 concentrations in water-stressed wheat. *Planta* **182,** 415–419.

Sander R. (1999) Compilation of Henry's Law Constants for Inorganic and Organic Species of Potential Importance in Environmental Chemistry (Version 3). http://www.mpch-mainz.mpg.de/~sander/res/henry.html

Segel I.H. (1976) *Biochemical Calculations* (2nd ed.) John Wiley & Sons Inc., New York.

Sellers P.J., Randall D.A., Collatz G.J., Berry J.A., Field C.B., Dazlich D.A., Zhang C., Collelo G.D. & Bounoua L. (1996) A revised land parameterization (SiB2) for atmospheric GCMs. Part I: model formulation. *Journal of Climate* **9,** 676-705.

Smith D.F. (1928) The solubility of gases in solutions. In *International Critical Tables* (ed E.W. Washburn) Vol. 3, pp. 271–280. McGraw-Hill, New York.

von Caemmerer S. (2000) *Biochemical models of leaf photosynthesis*. Techniques in Plant Sciences N0. 2. CSIRO Publishing, Collingwood, Victoria, Australia.

von Caemmerer S., Evans J.R., Hudson G.S. & Andrews T.J. (1994) The kinetics of ribulose-1,5-bisphosphate carboxylase/oxygenase in vivo inferred from measurements of photosynthesis in leaves of transgenic tobacco. *Planta* **195,** 88–97.

von Caemmerer S. & Farquhar G.D. (1981) Some relationships between the biochemistry of photosynthesis and the gas exchange of leaves. *Planta* **153,** 376–387.

Walcroft A.S., Whitehead D., Silvester W.B. & Kelliher F.M. (1997) The response of photosynthetic model parameters to temperature and nitrogen concentration in *Pinus radiata* D. Don. *Plant, Cell and Environment* **20,** 1338–1348.

Wang Y.P. & Leuning R. (1998) A two-leaf model for canopy conductance, photosynthesis and partitioning of available energy I: model description and comparison with a multi-layer model. *Agricultural and Forest Meteorology* **91,** 89–111.

Wessinger M.E., Edwards G.E. & Ku M.S.B. (1989) Quantity and kinetic properties of ribulose-1,5-bisphosphate carboxylase in C_3, C_4, and C_3–C_4 intermediate species of *Flaveria* (Asteraceae). *Plant and Cell Physiology* **30,** 665–671.

Whitney S.M., von Caemmerer S., Hudson G.S. & Andrews T.J. (1999) Directed mutation of the Rubisco large subunit of tobacco influences photorespiration and growth. *Plant Physiology* **121,** 579–588.

Wullschleger (1993) Biochemical limitations to carbon assimilation in C_3 plants – a retrospective analysis of the A/C_i curves from 109 species. *Journal of Experimental Botany* **44,** 907–920.

Yeoh H.-H., Badger M.R. & Watson L. (1980) Variations in $K_m(CO_2)$ of ribulose-1,5-bisphosphate carboxylase among grasses. *Plant Physiology* **66,** 1110–1112.

Yeoh H.-H., Badger M.R. & Watson L. (1981) Variations in the kinetic properties of ribulose-1,5-bisphosphate carboxylases among plants. *Plant Physiology* **67,** 1151–1155.

Yokota A. & Kitaoka S. (1985) Correct pK values for dissociation constant of carbonic acid lower the reported Km values of ribulose bisphosphate carboxylase to half. Presentation of a nomograph and an equation determining the pK values. *Biochemical and Biophysical Research Communications* **131,** 1075–1079.

Chapter 3

Low stomatal and internal conductance to CO_2 *vs.* Rubisco deactivation as determinants of the photosynthetic decline of aging evergreen leaves

INTRODUCTION

Gradual loss of photosynthetic activity is a commonly noted trait in aging foliage of evergreen tree species (Brooks, Sprugel & Hinckley 1996; Oleksyn *et al.* 1997; Kayama, Sasa & Koike 2002; Escudero & Mediavilla 2003); yet, the physiological basis of this age-related photosynthetic decline is still poorly understood. In herbaceous annuals and deciduous perennials, the age-related photosynthetic decline of leaves begins at the early phase of leaf senescence (e.g. Friedrich & Huffaker 1980; Jurik 1986) and proceeds with the degradation of chlorophylls and the breakdown of ribulose-1,5-bisphosphate carboxylase/oxygenase (Rubisco) and other chloroplast proteins into amino acids which are then exported as a source of nitrogen (N) to growing/storing organs (Kang & Titus 1980; Hörtensteiner & Feller 2002). Thus, in these species, declining photosynthetic capacity is closely coupled with the N economy of the plant (Chiba *et al.* 2003). In contrast, evergreen leaves with a long leaf life span often begin losing their photosynthetic capacity several years before the onset of leaf senescence and significant N resorption; correspondingly, their photosynthetic nitrogen use efficiency (PNUE) declines as they age (Kayama *et al.* 2002; Escudero & Mediavilla 2003; Niinemets, Tenhunen & Beyschlag 2004).

Few studies have investigated the physiological processes causing the age-related PNUE decline of evergreen leaves. Niinemets *et al.* (2004, 2005) recently suggested that there is a possible gradual decrease in fractional investment of leaf N in photosynthetic machinery and reallocation towards structural cell wall components. However, they did not measure the amount of N allocated to those components directly, but instead based their estimates on photosynthesis model parameters derived from gas exchange measurements. Still, Takashima,

Hikosaka & Hirose (2004) showed that low PNUE evergreen *Quercus* species allocated appreciably more N to cell wall proteins and less N to Rubisco than deciduous species of the same genus. In both groups, the amount of N allocated to cell wall proteins correlated positively with the amount of leaf dry mass allocated per unit area (LMA) whereas the trend was reversed for Rubisco. Although Takashima *et al.* (2004) made their measurements on current-year foliage only, the fact that LMA is generally found to increase with leaf age in evergreen species (Escudero & Mediavilla 2003; Niinemets *et al.* 2004, 2005) may indicate a concomitant increase in N investment to structural compounds.

This being said, Warren & Adams (2000) measured the N and Rubisco content of *Pinus pinaster* needles up to 5 years of age and did not observe any significant change in N allocation to Rubisco among the various foliar age classes. Moreover, Wendler *et al.* (1995) found no degradation of Rubisco in older, non-senescing *Eucalyptus globulus* leaves as they remobilised part of their N content to flushing new leaves during spring. In annual and perennial deciduous plants, excess Rubisco can be down-regulated and serve as a N storage protein until the onset of leaf senescence (Eichelmann & Laisk 1999; Cheng & Fuchigami 2000). Indeed, several studies have indicated that in evergreen species Rubisco may be synthesised in excess of what is required to support the realised photosynthetic rates under optimal field conditions (Warren, Adams & Chen 2000; Warren, Dreyer & Adams 2003a). However, in these studies the Rubisco requirement of leaves was calculated from their maximal carboxylation rate (V_{cmax}) estimated under the assumption that the CO_2 transfer conductance from the sub-stomatal cavities to the carboxylation sites in the chloroplasts (g_i) is sufficiently large to be ignored. Yet, most studies concerned with evergreen species have indicated that g_i is small enough in these plants to cause a significant drop in CO_2 concentration between the sub-stomatal cavities and the carboxylation sites (Loreto *et al.* 1992; Hanba, Miyazawa & Terashima 1999; Manter & Kerrigan 2004), a condition that leads to the underestimation of V_{cmax} if not accounted for (see Chapter 1).

The question arises, then, as to whether or not age-related changes in g_i may contribute appreciably to the photosynthetic decline of aging evergreen foliage. In senescing leaves of herbaceous annuals and deciduous perennials, g_i has been shown to decline in parallel to photosynthesis (Loreto *et al.* 1994; Delfine *et al.* 1999; Grassi & Magnani 2005). Although new studies (Niinemets *et al.* 2005, 2006; Warren 2006) confirmed that g_i also follows photosynthesis throughout its decline in aging evergreen leaves, they disagreed as to whether or not g_i contributes significantly to the loss of PNUE. For broadleaf evergreens, Niinemets *et al.* (2005, 2006) estimated that the photosynthetic limitation imposed by g_i increases with leaf age, whereas for *P. pinaster*, Warren (2006) argued that the age-related PNUE decline is solely due to the deactivation of Rubisco.

In Chapter 1, I presented a novel A-C_i curve analysis method that accounts for g_i through a non-rectangular hyperbola version of the photosynthesis model of Farquhar, von Caemmerer & Berry (1980). Here, I apply this new method 1) to assess age-related differences in photosynthetic capacity and g_i in Douglas-fir (*Pseudotsuga menziesii* (Mirb.) Franco), an evergreen conifer known to be photosynthetically limited by g_i under natural conditions (Warren *et al.* 2003b), and, by combining the photosynthesis model results with leaf protein assays, 2) to determine if age-related changes in PNUE are attributable to diffusive (i.e. stomatal conductance and g_i) or biochemical (e.g. Rubisco content and activity) causes.

MATERIALS AND METHODS

Site description and sampling

Measurements were made from late-September to mid-October 2001on twelve 52-year-old coastal Douglas-fir trees sampled (one tree per day) from an even-aged stand located on the east coast of Vancouver Island, British Columbia, Canada (49°52' N, 125°20' W). The stand is 300 m above sea level and covers an area of 130 ha on a 5–10°slope of north-eastern exposure. It is surrounded by other second-growth Douglas-fir forests at various stages of regeneration. The stand density is 1100 trees ha^{-1} with an estimated projected leaf area index of 9 (based on the

allometric equations of Standish, Manning & Demaerschalk 1985 and Turner *et al.* 2000). The overstorey canopy is 88% Douglas-fir, 10% western redcedar (*Thuja plicata* Donn) and 2% western hemlock (*Tsuga heterophylla* (Raf.) Sarg.) with tree heights ranging from 16 to 40 m. Understorey vegetation is composed of smaller western redcedar and western hemlock trees (12% of stand density) and a sparse ground flora dominated by salal (*Gaultheria shallon* Pursh), Oregon grape (*Berberis nervosa* Pursh), vanilla-leaf deer foot (*Achlys triphylla* (Smith) DC), and various ferns and mosses. Further details about the study site are given in Humphreys *et al.* (2003) and Morgenstern *et al.* (2004).

The trees were accessed via a canopy access tower or with static climbing ropes. Two to three adjacent branch sections approximately 1 m in length were collected from each tree, either from the upper (6 trees sampled for sun shoots) or lower (6 trees sampled for shade shoots) canopy layer. This sampling design was adopted to highlight differences in LMA and g_i among even-aged shoots in comparison to that among shoots of different age. Branch sections were collected during late afternoon on the day preceding the photosynthesis measurements. Upon cutting, the open branch end was immediately plunged in a water-filled plastic bag then re-cut. The collected branch sections were then transported to ground level where they were transferred to a holding container, re-cut under water, then left on the forest floor until placed under fluorescent lamps inside an instrumentation hut for at least 60 min before starting the photosynthesis measurements. A total of five shoots per tree, each representing a single current- to 4-year-old branch internode, were measured successively from the intact branch sections over a period of up to 12 hours. Preliminary experiments done on the scaffold tower established that gas exchange of shoots was unaffected by branch excision and remained so after overnight storage (data not shown).

Gas exchange measurements and integrating sphere apparatus

Shoot gas exchange rates were measured using an open gas exchange system with independent control of leaf chamber CO_2 and H_2O concentrations and air temperature (LI-6400, LI-COR,

Lincoln, NE). To eliminate shading among needles resulting from direct illumination, the instrument's standard 7.5 cm diameter clear cylindrical chamber designed for short needle conifers (model 6400-05, LI-COR) was enclosed in a 15.24 cm diameter integrating sphere (Fig. 3.1). The sphere's interior was coated with barium sulfate powder pressed onto titanium dioxide white epoxy to achieve a wall reflectance close to unity throughout the visible spectrum (Nonaka 1974). Additional reflective surface was provided by coating the shoot chamber's exposed metal parts with white epoxy and by replacing the chamber's black neoprene gaskets with white foam equivalents. The photosynthetic photon flux density (PPFD) incident on the needles (2-sided) was estimated from the readings of light sensors positioned on the sphere wall calibrated against angular PPFD measurements taken around the stem of representative sun & shade shoots (see Fig. 3.1a). These angular measurements showed that although the overall (hemispherically integrated) intensity of the upwelling light reflected from the lower hemisphere was 64% of that coming from above, when adding the fluxes coming from any two opposite directions, the angular 2-sided PPFD distribution measured around the shoot axis inside the clear chamber remained within 5% of the median value. Thus, this integrating sphere configuration, while preserving the uniformity of the 2-sided diffuse light field, retained some of the polar asymmetry of the shoot's natural light environment.

Needle temperature was estimated using an energy balance for which the amount of shortwave radiation (400–2600 nm) absorbed by Douglas-fir needles in the integrating sphere was determined. To this end, the integrating sphere light spectrum and Douglas-fir needle absorptance over the 400–1100 nm waveband were measured with a spectroradiometer (LI-1800, LI-COR) (Fig. 3.1b). A custom-made, matte black sensor head cover with open slits in which individual Douglas-fir needles were recessed then illuminated from above was used to measure needle transmittance. Foliar reflectance measurements were made according to Moran *et al.* (2000). Needle absorptance from 1100 to 2600 nm was approximated using the Douglas-fir needle reflectance curve of Woolley (1971) and general leaf transmittance *vs.* reflectance

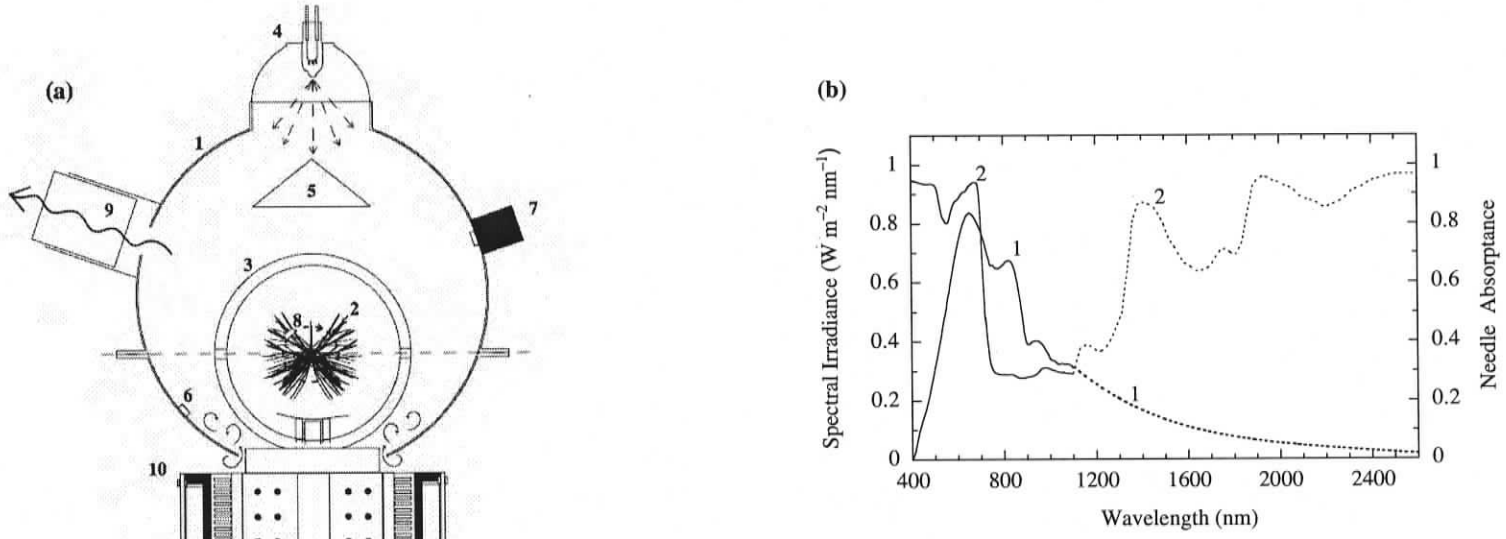

Figure 3.1 (a) Schematic diagram of the 15.24 cm integrating sphere (1) (drawn to scale) surrounding a Douglas-fir shoot (2) inside the clear conifer chamber (3). Light from the halogen lamp (4) (adjusted via a rheostat) is scattered onto the sphere's walls by a cone (5) and is monitored with a small gallium arsenide phosphide photodiode (6) and a quantum sensor (7). Also shown is the radial path (dotted circle) of the photodiode (8) used to determine the angular photosynthetic photon flux density (PPFD) distribution around the axis of representative shoots. A fan (9) continuously flushes air out of the sphere (air intake at the base) to dissipate the heat generated by the lamp (external fan blowing cold air onto the sphere surface from above not shown). (10) LI-6400 open-path infrared gas analyser sensor head. (b) Integrating sphere incident irradiance (I) (curve 1) and Douglas-fir needle absorptance (a) (curve 2) spectra. Solid lines represent measurements taken with a spectroradiometer while broken lines are approximations from literature data (see text for details). Total shortwave radiation absorbed by the needles is given as $\int_{400-2600} \frac{\alpha I}{I} = 0.59$. The ratio $I_{400-2600}/PPFD_{400-700}$ equals 0.67 Joules μmol^{-1}.

relationships derived from Gates *et al.* (1965). Correspondingly, the integrating sphere light spectrum beyond 1100 nm was approximated according to the known spectral output of quartz-halogen lamps adjusted so the calculated area under the whole spectral curve matched the total amount of shortwave radiation measured with a thermopile solarimeter (CM5, Kipp & Zonen, Delft, Holland). Radiation absorption coefficients derived from the above spectral curves (see Fig. 3.1b legend) were used in the instrument's energy balance algorithm to set the needle temperature to 22 ± 0.5 °C during measurements using the estimated median value for the 2-sided PPFD distribution around the shoot axis (corrected for the light attenuation caused by the shoot portion enclosed in the clear chamber) as initial input variable.

Following acclimation of a branch section under fluorescent lamps (PPFD ~ 400 μmol m^{-2} s^{-1}), the integrating sphere assembly was clamped onto a branch internode, taking care to enclose a single needle age class inside the shoot chamber. Light intensity inside the integrating sphere was then gradually increased to saturating levels (estimated median 2-sided PPFD ~ 1200 μmol m^{-2} s^{-1}) and the shoot chamber's CO_2 concentration and relative humidity eventually stabilised at 360 μmol mol^{-1} and above 70%, respectively. The shoot was left to acclimate to these conditions before its steady-state net CO_2 assimilation rate (A_n) was recorded. Measurements of A_n under saturating light were then repeated at various chamber CO_2 concentrations to obtain an A_n *vs.* intercellular CO_2 concentration (C_i) relationship. After recording the A-C_i curve end point, the CO_2 concentration of the chamber's incoming air stream was reduced to a constant 1100 μmol mol^{-1} and A_n measured at various light intensities (decreasing the estimated median 2-sided PPFD in steps from ~ 1600 μmol m^{-2} s^{-1} to full darkness) to obtain a light response curve for the shoot. Ambient CO_2 leakage inside the shoot chamber while being operated under low CO_2 was largely prevented by wrapping the chamber's foam gasket junction with Teflon tape and by keeping the air flow rate high enough to maintain sufficient positive pressure within the chamber to be applied against the under-pressurised air volume of the integrating sphere. Following gas exchange measurements, the shoot was excised from the branch section and immediately placed in liquid N for storage. Gas exchange

parameters were calculated on a projected area basis according to the equations of von Caemmerer & Farquhar (1981).

Leaf photosynthesis model and curve fitting procedure

Following the theory expounded in Chapter 1, A-C_i curves where fitted with a non-rectangular hyperbola version of the biochemical model of C_3 leaf photosynthesis of Farquhar *et al.* (1980) that accounts for g_i and whereby A_n is given as

$$A_n = \min\{A_c, A_j\} \tag{3.1}$$

$$\begin{aligned} A_c &= \frac{-b + \sqrt{b^2 - 4ac}}{2a} \\ a &= -1/g_i \\ b &= (V_{c\max} - R_d)/g_i + C_i + K_c(1 + O/K_o) \\ c &= R_d(C_i + K_c(1 + O/K_o)) - V_{c\max}(C_i - \Gamma^*) \end{aligned} \tag{3.2}$$

$$\begin{aligned} A_j &= \frac{-b + \sqrt{b^2 - 4ac}}{2a} \\ a &= -1/g_i \\ b &= (J/4 - R_d)/g_i + C_i + 2\Gamma^* \\ c &= R_d(C_i + 2\Gamma^*) - J/4(C_i - \Gamma^*) \end{aligned} \tag{3.3}$$

where A_c and A_j are the RuBP (ribulose-1,5-bisphosphate)-saturated and RuBP-limited net CO_2 assimilation rate, respectively, V_{cmax} is the maximal CO_2 carboxylation rate, J is the photochemical electron transport rate under RuBP-limited conditions, R_d is the mitochondrial respiration in the light, $\Gamma^*$is the chloroplastic CO_2 photocompensation point, K_c & K_o are Michaelis-Menten constants for RuBP carboxylation and oxygenation, respectively, and O is the oxygen concentration. Detailed derivations of Eqns 3.2 and 3.3, as well as a thorough evaluation of errors resulting from assuming an infinite g_i when fitting the Farquhar *et al.* (1980) model equations to A-C_i curves, are given in Chapter 1. Estimates of g_i, R_d, V_{cmax} and J

were obtained from non-linear least-squares fits (Levenberg-Marquardt algorithm) of Eqn 3.2 and 3.3 to the initial RuBP-saturated and remaining RuBP-limited A-C_i curve portion, respectively, taking care to exclude the end point(s) representing triose phosphates utilisation (*TPU*)-limited photosynthesis (Harley & Sharkey 1991), if observed. Contrary to established practice whereby the equation describing A_c is fitted to the data collected for C_i values below 200–250 μbar, I estimated that the transition from RuBP-saturated to RuBP-limited photosynthesis generally occurred around 400 μbar (see Appendix A) and therefore used that value as the C_i cut-off point for fitting Eqn 3.2. The continuation of RuBP-saturated photosynthesis at C_i values greater than 400 μbar has previously been observed at ambient O_2 concentration and high irradiance in Douglas-fir and other woody plant species with low g_i (Manter & Kerrigan 2004). Also, I noted in many cases that the curvature of the A-C_i relationship increased significantly when C_i approached the CO_2 compensation point (Γ) (e.g. Fig 3.2c). As discussed in Chapter 1, such an increase in the curvature of A-C_i curves at low CO_2 is likely indicative of Rubisco deactivation (von Caemmerer & Edmondson 1986; Sage, Sharkey & Seemann 1990) and of decreased re-fixation of respiratory CO_2 by the enzyme (Pinelli & Loreto 2003). These data were excluded from the curve fits to avoid a possible overestimation g_i. As with conventional A-C_i curve fitting methods, the non-rectangular hyperbola model requires that Γ^*, K_c and K_o be known *a priori* to estimate the remaining model parameters. The values used herein (Γ^* = 39.5 μbar; K_c = 234.6 μbar; K_o = 256.4 mbar) were derived from the original data of von Caemmerer *et al.* (1994) (see Chapter 2, Table 2.4) and adjusted to 22°C using the temperature responses published by Bernacchi *et al.* (2002). These are to my knowledge the only complete data sets from which the kinetic constants of Rubisco have been properly evaluated at C_c (chloroplastic CO_2 concentration) *in vivo*. With these Rubisco kinetic constants substituted in Eqns 3.2 and 3.3, it was then possible to estimate V_{cmax} and J concurrently by iterating the least-squares fits to the RuBP-saturated *vs.* RuBP-limited A-C_i curve portions described above until they produced converging solutions for g_i and R_d. A comparison of g_i values fitted by this method with alternative estimates of g_i derived solely from

the end points of the RuBP-limited A-C_i curve portion is presented in Appendix A. As shown therein, the agreement between the two methods is excellent, showing that the aforementioned choice of respective domain for the A_c and A_j functions is justified.

To evaluate the bias introduced by assuming g_i to be infinite when estimating V_{cmax}, the A-C_i curves' RuBP-saturated portion was refitted with the common rectangular hyperbola model equation

$$A_c = \frac{(C_i - \Gamma^*)V_{c\max}}{C_i + K_c(1 + O/K_o)} - R_d \tag{3.4}$$

(*c.f.* Eqn 1.14) using the aforementioned "chloroplastic" Rubisco kinetic constants.

Light response curves were fitted as a non-rectangular hyperbola model (von Caemmerer 2000) in which J is given as

$$J = \frac{I\alpha\beta\Phi + J_{\max} - \sqrt{(I\alpha\beta\Phi + J_{\max})^2 - 4\Theta I\alpha\beta\Phi J_{\max}}}{2\Theta} \tag{3.5}$$

where I is the incident irradiance (incident 2-sided PPFD around the shoot axis), α is the needle absorptance for the 400–700 nm waveband (0.9; determined from curve 2 in Fig. 3.1b), β is the fraction of absorbed light that reaches photosystem II (assumed to be 0.5), Φ is the quantum yield of photochemical electron flow to photosystem II, $J_{\max}$ is the maximal photochemical electron transport rate, and Θ is the convexity (curvature factor) of the rectangular hyperbola. Conversion from the original A_j measurements to J equivalents was done by rearranging Eqn 3.3 as

$$J = \frac{4(A_j + R_d)(C_i - A_j/g_i + 2\Gamma^*)}{(C_i - A_j/g_i - \Gamma^*)} \tag{3.6}$$

then solving Eqn 3.6 using the g_i and R_d values derived from the corresponding A-C_i curve fit.

Data collected at $I < 50$ μmol m^{-2} s^{-1} were excluded from the least-squares fits to avoid overestimation of Φ as a result of the "Kok effect" (Kirschbaum & Farquhar 1987). Transition from RuBP-limited to RuBP-saturated or *TPU*-limited photosynthesis at high irradiance which may occur when doing light response curves under ambient or saturating (e.g. 2000 μmol mol^{-1}) CO_2 concentrations, respectively, was avoided in our case by keeping the chamber CO_2 concentrations around 1000 μmol mol^{-1} (and C_i between 600 and 800 μbar, depending on the shoot) during the high irradiance measurements.

Determination of leaf N, protein, and pigment content

Needles from shoot samples stored in liquid N were weighed frozen and subsampled for determination of their projected area (measured by placing the needles between glass plates over a leaf area meter : LI-3100, LI-COR) to fresh weight ratio and LMA (oven-dried). The rest of the needles were broken into coarse fragments and subsampled for Rubisco and total proteins analysis (see below) or freeze-dried then ground in a ball mill (3110-3A Wig-L-Bug, Bratt Technologies LLC, East Orange, NJ) for measurement of total N with an elemental analyser (Flash EA 1112 Series, ThermoQuest, Rodano, Italy) or for extraction of chlorophylls and carotenoids using n, n-dimethylformamide. Pigment solutions were assayed spectrophotometrically (Genesys 10, GENEQ Inc., Montréal, Canada) using the equations of Wellburn (1994) (1–4 nm range).

Crude leaf preparations were obtained by first homogenising 50 mg of frozen fresh leaf tissue in 400 μL of ice cold buffer containing 133 mM TRIS pH 8.0, 25% (v/v) glycerol, 34 mM DL-dithiothreitol, 2% (w/v) polyvinylpolypyrolidone (PVPP), to which 100 μL of 10% (w/v) sodium dodecyl sulfate (SDS) were then added before vortexing for 4 min at 0–4°C followed by centrifugation at 15 000*g* for 5 min (4°C). After collecting the supernatant, the pellet was re-extracted three more times with the above buffer (without PVPP) diluted 4:1 with 10% SDS and the supernatants pooled for the assay. Preliminary analysis of the protein composition of individual supernatants (quantification of the large subunit of Rubisco (Lsu)

band on SDS-polyacrylimide gels by Coomassie brilliant blue R-250 staining) established the necessity of repeating the extraction 4-fold and of adding a detergent (SDS) to the extraction buffer to ensure a thorough extraction (data not shown). Following extraction of all leaf samples, five additional "combined" leaf extracts were prepared (to be used specifically for the preparation of Rubisco standards – see below) by taking an aliquot from each leaf extract and pooling these according to foliar age class then diluting 1:500 using carbonate buffer (50mM Na_2CO_3, 50mM $NaHCO_3$, 0.1mM $MgCl_2.6H_2O$, pH 9.4).

Rubisco from the leaf extracts diluted 1:1000 in carbonate buffer was quantified by enzyme-linked immunosorbtion assay (ELISA) as described in Warren *et al.* (2003b). The Rubisco standards used herein were made from purified wheat Rubisco stock diluted to a concentration range of 0.052 to 6.6 μg mL^{-1} with the above carbonate buffer. The standards were then made specific to the chemical environment of the leaf extracts and to the various foliar age classes of the samples by suspending them into the above combined leaf extracts (1:1 volumes). All twelve samples from each leaf age class were then assayed according to their corresponding Rubisco standards. This was necessary as previous sensitivity tests showed that the standard curve for the ELISA estimation was affected by the chemical composition of the protein solution (see also Metodiev & Demirevska-Kepova 1992).

Following from previous work (e.g. Warren *et al.* 2000; Niinemets *et al.* 2004, 2005), alternative estimates of Rubisco concentration were calculated from the quotient of $V_{c\max}/k_{cat}$ where k_{cat} is the assumed catalytic turnover rate of Rubisco. The value used herein (2.76 mol CO_2 mol Rubisco sites^{-1} s^{-1}) was determined *in vivo* by von Caemmerer *et al.* (1994) – the study on which the estimates of *in vivo* Rubisco kinetic constants chosen for this study are based – and adjusted to 22°C according to the temperature response of Makino, Mae & Ohira (1988).

The total protein content of the leaf extracts was determined from gel densitometry as described in Warren *et al.* (2003b). Proteins were first purified by precipitation according to the method of Wessel and Flügge (1984) and the resulting pellets re-suspended in 100 μl of 2%

(w/v) SDS.

Stable carbon isotope composition of leaf soluble sugars from field samples

In addition to the branch sections used for the photosynthesis measurements, several adjacent smaller twigs, each representing five years of incremental growth, were also collected at the same time to estimate the stable carbon isotope composition ($\delta^{13}C$) of recently fixed carbon from current- to 4-year-old shoots at each sampling location. The samples (pooled by age class) were stored in liquid N immediately after collection. Leaf soluble sugars were subsequently extracted from freeze-dried ground sub-samples following the method of Brugnoli *et al.* (1988). The $\delta^{13}C$ value of the dry sugar extracts was measured with a continuous flow isotope ratio mass spectrometer (Integra, Europa Scientific, Crewe, U.K.) at the Stable Isotope Facility of UC Davis. Carbon isotope discrimination (Δ) was calculated as

$$\Delta = \frac{\delta^{13}C_a - \delta^{13}C_p}{1 + \delta^{13}C_p} \tag{3.7}$$

where $\delta^{13}C_a$ and $\delta^{13}C_p$ are the isotope compositions of the ambient canopy air (determined as –10‰ during daytime; Whiticar, personal communication) and plant sugar extract, respectively, relative to the PDB (Pee Dee Belemnite) standard.

For Douglas-fir shoots whose gas exchange characteristics were determined in the integrating sphere, according to the model of Farquhar, O'Leary & Berry (1982), isotope discrimination during photosynthesis is given by (ignoring respiration terms – see von Caemmerer & Evans 1991)

$$\Delta = a_b \frac{C_a - C_s}{C_a} + a \frac{C_s - C_i}{C_a} + a_i \frac{C_i - C_c}{C_a} + b \frac{C_c}{C_a} \tag{3.8}$$

where C_a and C_s are the CO_2 concentrations of the ambient air and leaf surface, respectively,

a_b and a are the fractionations due to diffusion through the boundary layer (2.9‰) and through stomata (4.4‰), respectively, a_i is the combined fractionation due to the dissolution and diffusion of CO_2 in water (1.8‰), and b is the net fractionation caused by Rubisco and phosphoenolpyruvate (PEP) carboxylation (30‰).

RESULTS

Photosynthetic capacity and CO_2 diffusion

Gradual loss of photosynthetic capacity with age was observed in both sun and shade shoots, the decline being equally apparent in the CO_2 and light response of the shoots (e.g. Fig. 3.2). In some cases, the loss of photosynthetic capacity was eventually large enough to keep photosynthesis Rubisco-limited even at up to four times the normal daytime canopy air space CO_2 concentrations (e.g. Fig. 3.2c). Strong linear relationships between g_i and V_{cmax} were observed in individual foliar age classes (Fig. 3.3a), although the overall relationship for all age classes appeared to be slightly curvilinear. The slope of the relationships did not differ significantly among age classes ($P > 0.5$, analysis of covariance), suggesting that the sensitivity of carboxylation capacity to g_i – or vice-versa – does not change considerably with age. Yet, the $V_{c\max}/g_i$ ratio increased significantly with age (Table 3.1), hence reflecting an important age-related diminution of the internal CO_2 supply to the chloroplasts relative to their collective carboxylation capacity. Within each foliar age class, the $V_{c\max}/g_i$ ratio remained conserved between sun and shade shoots ($P > 0.1$, unpaired *t*-tests). Carboxylation capacity (V_{cmax}) was consistently matched by the potential for photochemical electron transport (J_{max}) throughout the range of g_i values fitted by non-rectangular hyperbola model and across all age classes (Fig. 3.3b). Similar to photosynthetic capacity, the stomatal conductance to CO_2 (g_{sc}) was correlated with g_i in all foliar age classes (Fig. 3.3c) and the slope of the relationship did not change significantly among the age classes ($P > 0.5$, analysis of covariance). However, unlike V_{cmax} and J_{max}, the magnitude of g_{sc} relative to g_i decreased with age, essentially cancelling out the positive

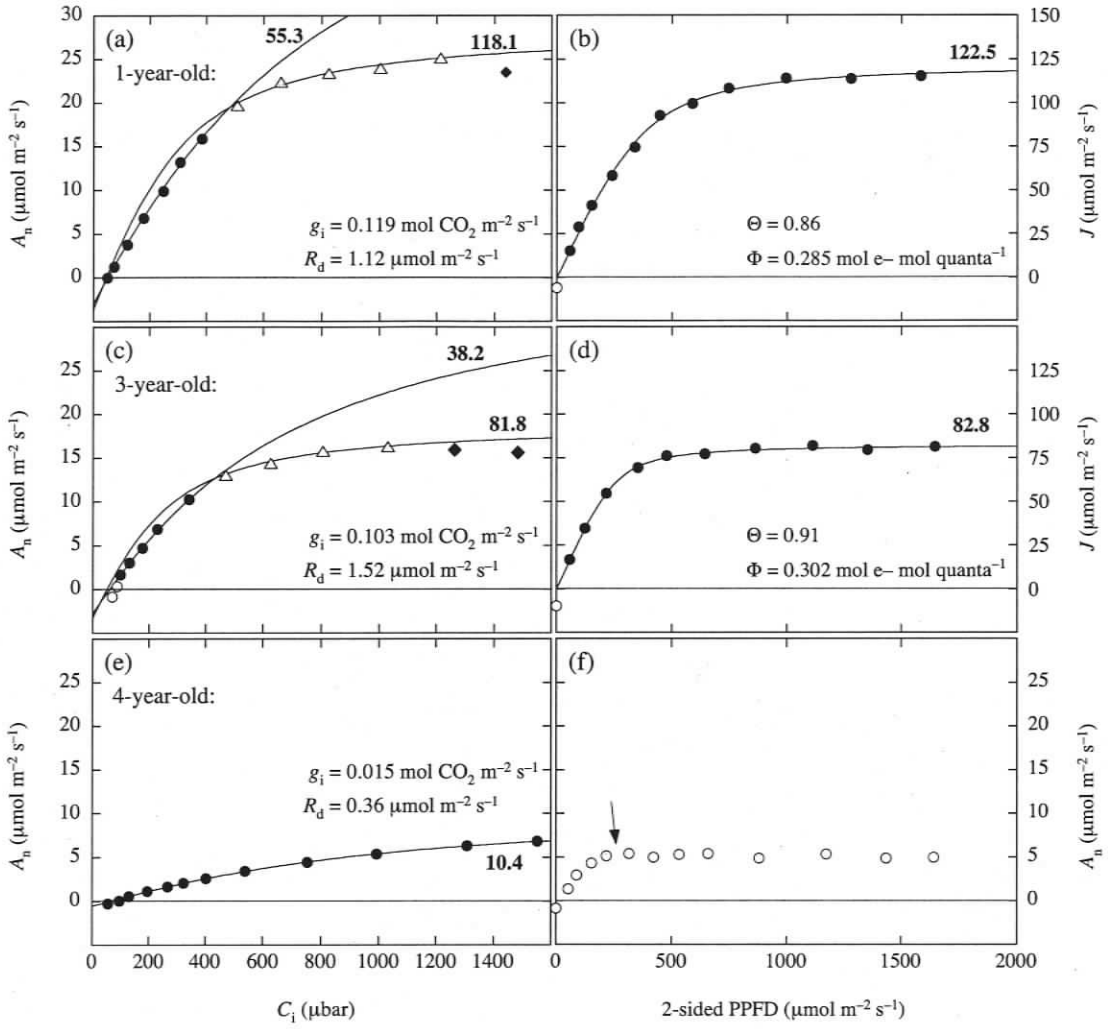

Figure 3.2 Examples of least-squares regression fits to A-C_i curves (left panels) and corresponding light response curves (right panels) of 1-, 3-, and 4-year old Douglas-fir shade shoots from a common branch section. For the A-C_i curves, the RuBP-saturated (solid circles) and RuBP-limited (open triangles) curve portions were fitted with Eqns 3.2 and 3.3, respectively; the corresponding estimated maximal carboxylation rate (V_{cmax}) and photochemical electron transport rate (J) are indicated beside the curve fits. Solid diamonds represent the remaining *TPU*-limited A-C_i curve portion. Light response curves from the 1- and 3-year-old shoots were fitted with Eqn 3.5 (solid circles); the maximal photochemical electron transport rate (J_{max}) is indicated beside the curve fit; for the 4-year-old shoot, the original light response curve data is shown – the arrow indicates the transition from RuBP-limited to RuBP-saturated photosynthesis at higher irradiance. Open circles indicate data excluded from the curve fits (see text for details).

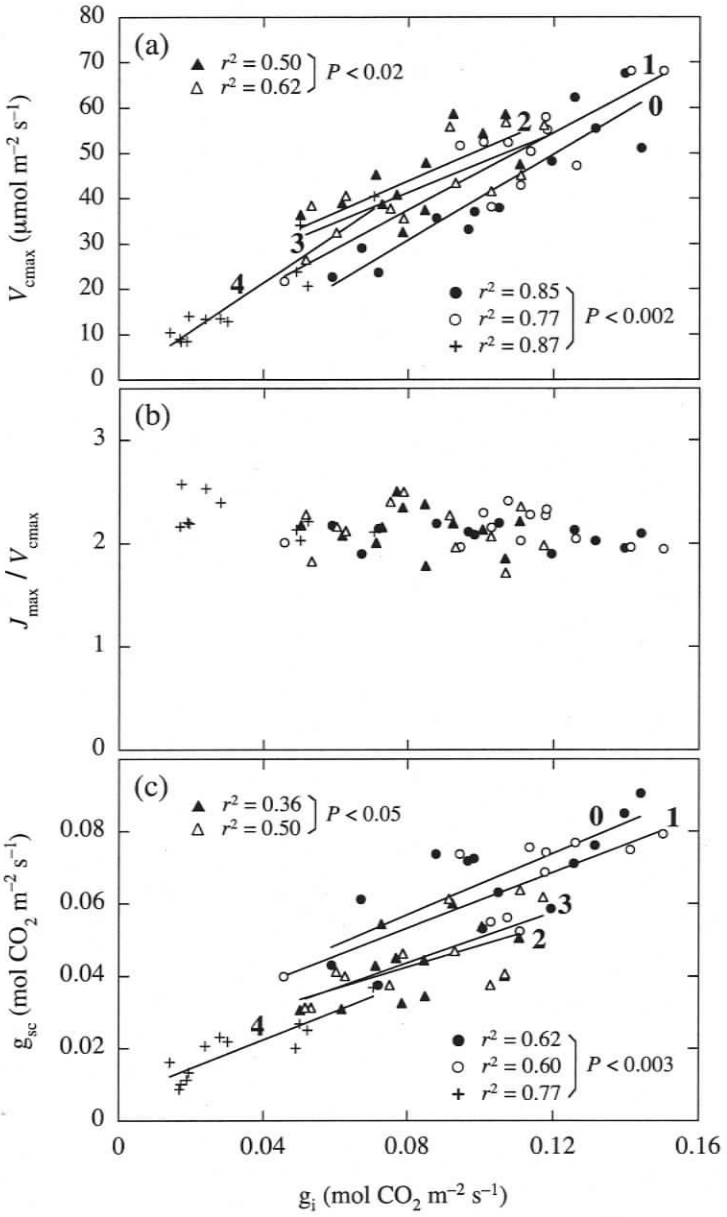

Figure 3.3 Relationship between the CO_2 transfer conductance (g_i) and (a) the maximal carboxylation rate (V_{cmax}), (b) the maximal photochemical electron transport rate (J_{max}) to V_{cmax} ratio, and (c) the stomatal conductance to CO_2 (g_{sc}) of current-year (●), 1-year-old (○), 2-year-old (▲), 3-year-old (△), and 4-year-old (+) Douglas-fir shoots. Simple linear regression lines in panels (a) and (c) are numbered according to needle age.

Table 3.1 Effect of needle age on the maximal carboxylation capacity (V_{cmax}) to CO_2 transfer conductance (g_i) ratio of Douglas-fir shoots

Needle age	$V_{c\max}/g_i$ (μmol mol^{-1})
Current-year	401 (15)[a]
1-year-old	460 (16)[ab]
2-year-old	553 (27)[c]
3-year-old	523 (28)[bc]
4-year-old	544 (33)[c]
P	< 0.0001

Values given are the mean (standard error) of 12 shoots. The significance of differences among age-classes (P) was assessed by one-way ANOVA (repeated measures). Where differences were significant ($P < 0.05$), Tukey HSD test was used to explore pair-wise comparisons among age-classes. Means followed by different letters are significantly different.

age effect of $V_{c\max}/g_i$ on the CO_2 drawdown from the sub-stomatal cavities to the carboxylation sites ($C_i - C_c$) (Fig. 3.4a).

Area-based estimates of g_i were consistently higher in sun shoots (Fig. 3.4b), although the difference was significant only in 4-year-old shoots ($P < 0.05$, unpaired *t*-tests). When LMA was factored in, the g_i difference between sun and shade shoots disappeared (Fig. 3.4b-d), showing that, within each foliar age class, the response of g_i to the shoot's light environment is determined by changes in leaf anatomy. Over time, however, the courses of LMA and g_i were mismatched – LMA increased steadily through successive years while g_i decreased in steps after the second and fourth growing seasons (Fig. 3.4b-d). Variations in LMA were closely associated with parallel changes in both needle thickness ($r^2 = 0.67$, $P < 0.0001$), needle dry to fresh weight ratio ($r^2 = 0.57$, $P < 0.0001$), or tissue density ($r^2 = 0.56$, $P < 0.0001$), and the slope of the relationships were conserved in sun and shade shoots ($P > 0.5$, analysis of covariance) whether evaluated among foliar age classes or within even-aged cohorts (data not shown). Yet, within each age class and over a similar range of values observed in sun or in shade shoots through time, mass-based estimates of g_i did not correlate with LMA or the other anatomical traits ($P > 0.3$, data not shown).

Strong linear relationships between A_n and g_{sc} evaluated at 360 μmol mol^{-1} ambient CO_2 concentration were observed in all foliar age classes (Fig. 3.5a). The differences among slopes were small but significant in some cases owing to the close coupling of A_n and g_{sc} in each age class. Consistent with the age differences in carboxylation capacity *vs.* internal CO_2 supply inferred from the A-C_i curve analyses, the slopes of the A_n *vs.* g_{sc} relationships scaled according to the ranking of the $V_{c\max}/g_i$ ratios fitted by the non-rectangular hyperbola model. Since g_i was closely coordinated with g_{sc} and A_n across the measured CO_2 assimilation range, both C_i and C_c remained largely conserved among foliar age classes (Fig. 3.5b) and the corresponding $\Delta_{\text{gas exchange}}$ values calculated from Eqn 3.8 agreed well with the Δ value of sugars extracted from neighbouring field samples (Fig. 3.6). In fact, the isotopic composition of the field samples indicated an even greater conservativeness of C_i and C_c among age classes (Fig. 3.6b).

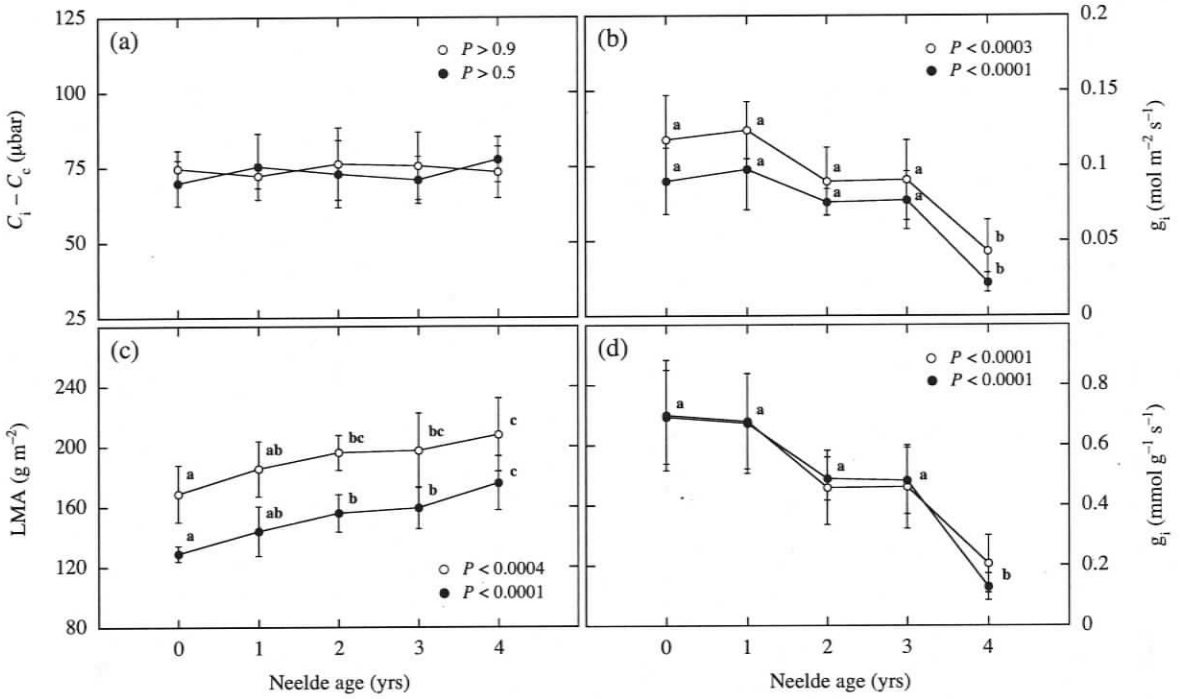

Figure 3.4 Effect of needle age on (a) the CO_2 drawdown between the sub-stomatal cavities and the stromal carboxylation sites ($C_i - C_c$) evaluated at an ambient CO_2 concentration of 360 μmol mol^{-1}, (b) the CO_2 transfer conductance (g_i) calculated on an area basis, (c) the leaf mass per area (LMA), and (d) g_i calculated on a mass basis. Data are means (± SD) of 6 sun (○) and 6 shade (●) Douglas-fir shoots. The significance of differences among age-classes (P) was assessed as outlined in Table 3.1. Means followed by different letters are significantly different.

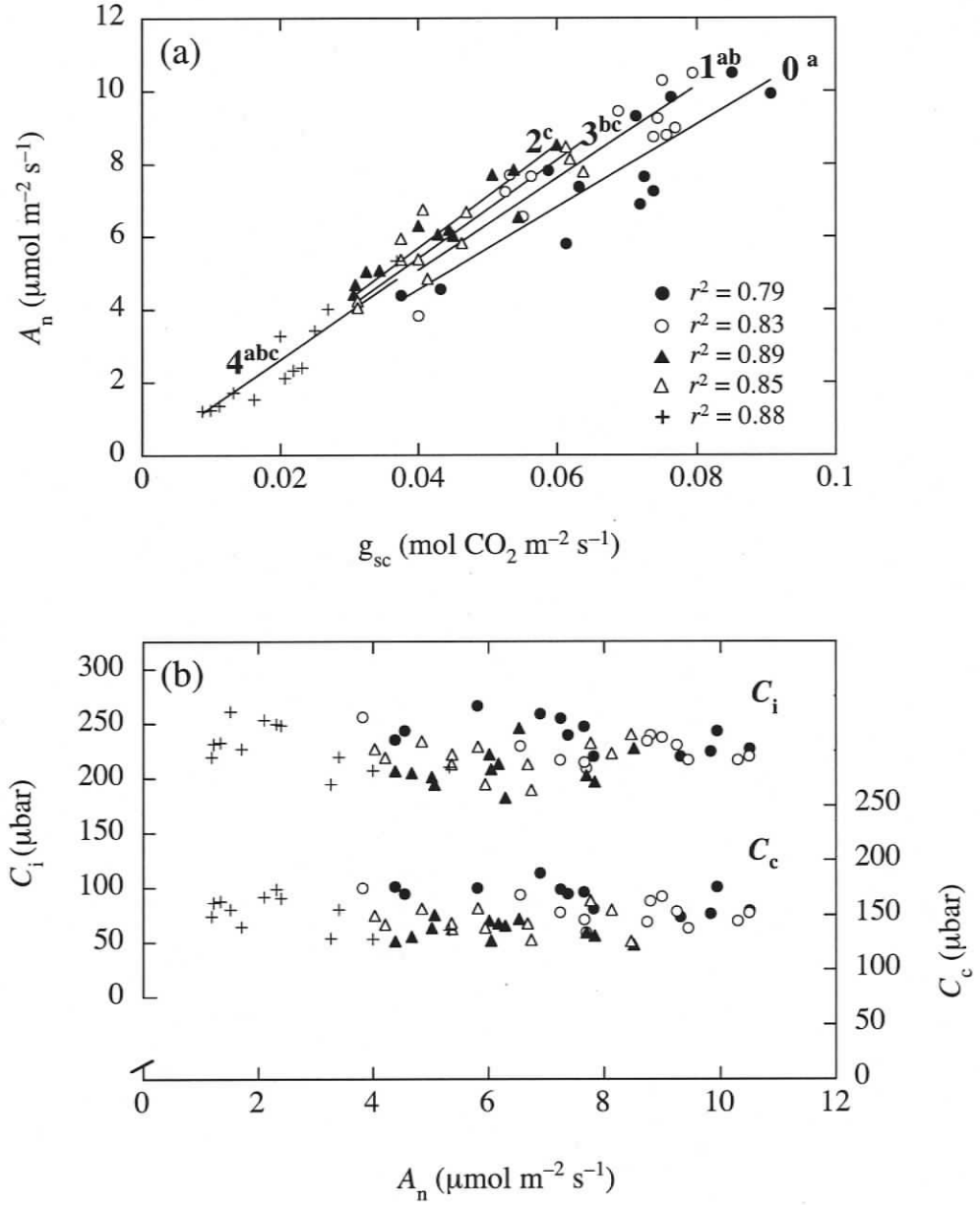

Figure 3.5 Relationship between the net CO_2 assimilation rate (A_n) and (a) the stomatal conductance to CO_2 (g_{sc}), and (b) the intercellular (C_i) and chloroplastic (C_c) CO_2 concentrations of Douglas-fir shoots, evaluated at an ambient CO_2 concentration of 360 μmol mol^{-1}. Symbols denoting the different foliar age classes are as in Fig. 3.3. Simple linear regression lines (intercepts constrained to zero; $P < 0.0001$ in all cases) in panel (a) are numbered according to needle age; significant differences ($P < 0.05$, analysis of covariance with *post hoc* Tukey HSD test) among slopes are indicated by different letter superscripts.

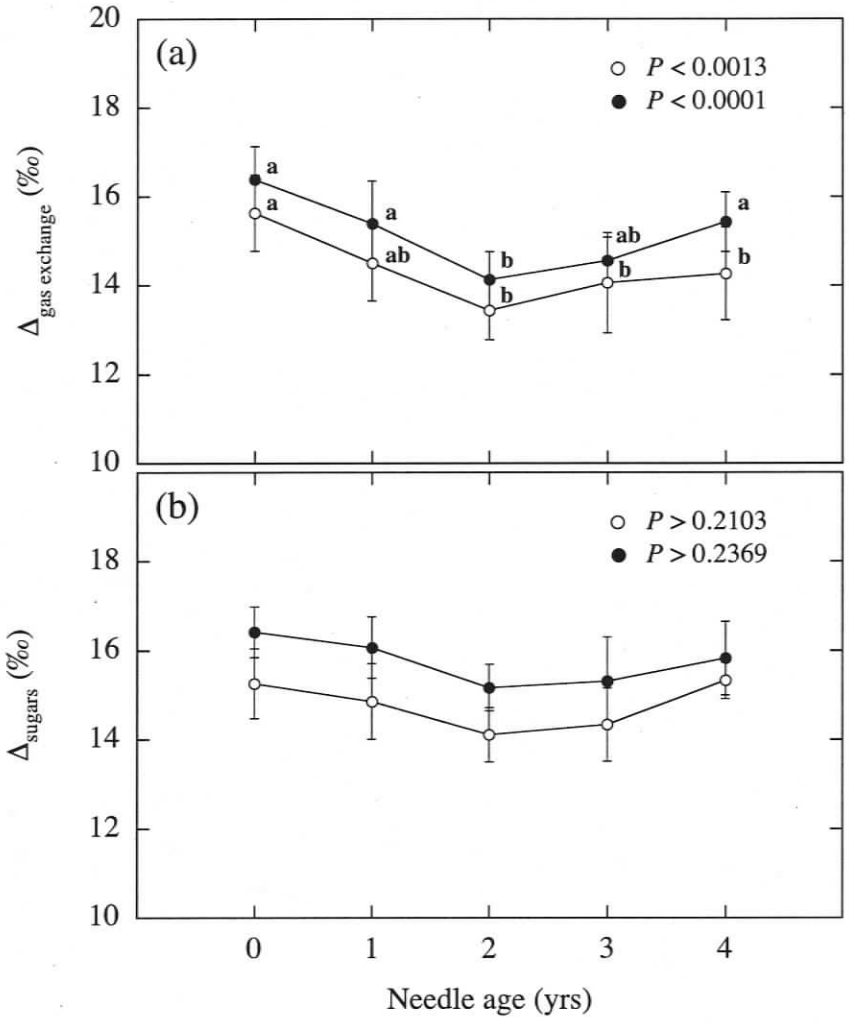

Figure 3.6 Effect of needle age on the carbon isotope discrimination (Δ) of Douglas-fir shoots calculated from (a) the gas exchange characteristics of shoots evaluated at 22 °C and 360 μmol mol^{-1} ambient CO_2 concentration under saturating diffuse irradiance, and (b) the isotopic composition of leaf soluble sugars extracted from representative field samples. Data are means (± SD) of 6 sun (○) and 6 shade (●) shoots in (a) or pooled shoot samples in (b). The significance of differences among age-classes (*P*) was assessed as outlined in Table 3.1. Means followed by different letters are significantly different.

Considering the shift of microclimate going from the field to the integrating sphere, this constancy of Δ is remarkable, especially for lower canopy shoots which went from mostly full shade to sustained saturating diffuse irradiance.

Nitrogen allocation, Rubisco and leaf pigments

Nitrogen per unit leaf area increased significantly with age in both sun and shade shoots (Table 3.2). In both cases, the accumulation of N was brought about by increases in mass concentration (Table 3.2) and by the steady rise of LMA (Fig. 3.4c). The fraction of needle N allocated to Rubisco was generally higher in sun shoots, the difference being significant in current-year shoots only ($P < 0.05$, unpaired *t*-tests), but did not differ significantly among foliar age classes (Table 3.2). Nitrogen allocation to other SDS-soluble proteins increased slightly with age and, although the differences were not significant, they were sufficient (assuming 50 mol thylakoid N per mol chlorophyll – Evans 1989) to account for the observed increases in N allocation to chlorophyll-protein complexes (Table 3.2).

Despite their accumulating relatively high amounts of nitrogen, older shoots (≥ 2-year-old) had significantly lower V_{cmax} per unit Rubisco than younger foliage and, as a result, had lower (up to 80% lower) PNUE values (Table 3.2). The loss of catalytic turnover rate of Rubisco (k_{cat}) was considerable in 2–3-year-old shoots (25%), but particularly acute in 4-year-old shoots (68%), relative to the average k_{cat} value of current- and 1-year-old shoots (2.81 ± 0.28 mol CO_2 mol^{-1} Rubisco sites s^{-1}) (Fig. 3.7a). Since the latter k_{cat} value differs by less than 2% from our originally assumed value, the Rubisco concentrations determined from V_{cmax} and the k_{cat} value of von Caemmerer *et al.* (1994) were essentially the same as those determined by ELISA for current- and 1-year-old shoots, but underestimated Rubisco in older shoots (Fig. 3.7b). By comparison, Rubisco concentrations calculated from V_{cmax} values estimated without considering g_i (Eqn 3.4) underestimated the ELISA values in all foliar age classes (45–80% in older shoots – Fig. 3.7b).

Table 3.2 Effect of needle age on the photosynthetic nitrogen use efficiency (PNUE) of Douglas-fir shoots and the allocation of total nitrogen (N_{mass}, N_{area}) to Rubisco, other SDS-soluble proteins, and chlorophylls (Chl)

Needle age	PNUE (μmol CO_2 mol^{-1} N s^{-1})	N_{mass} (mg g^{-1})	N_{area} (g m^{-2})	Rubisco (% of total N)†	Other proteins (% of total N)†	Chl/N (mmol mol^{-1})
Sun shoots:						
Current-year	62.4 (2.0)^{a}	11.7 (0.8)^{ab}	1.98 (0.14)^{a}	11.6 (0.5)	26.0 (2.7)	2.91 (0.17)^{a}
1-year-old	53.1 (3.8)^{a}	13.1 (0.3)^{a}	2.42 (0.09)^{b}	10.2 (0.6)	29.5 (1.7)	3.67 (0.19)^{b}
2-year-old	37.4 (2.9)^{b}	12.9 (0.3)^{a}	2.53 (0.06)^{b}	10.1 (0.8)	31.0 (2.0)	3.82 (0.21)^{b}
3-year-old	39.0 (3.6)^{b}	12.3 (0.3)^{a}	2.43 (0.09)^{b}	11.5 (0.7)	31.1 (1.5)	3.76 (0.20)^{b}
4-year-old	20.8 (4.1)^{c}	10.4 (0.4)^{b}	2.15 (0.09)^{ab}	11.3 (1.1)	32.5 (2.4)	3.72 (0.27)^{b}
P	< 0.0001	0.0005	0.0033	0.4011	0.2203	0.0043
Shade shoots:						
Current-year	62.8 (2.8)^{a}	10.9 (0.8)^{a}	1.42 (0.12)^{a}	8.3 (0.8)	25.4 (3.6)	3.72 (0.13)
1-year-old	54.8 (2.2)^{a}	12.9 (0.8)^{ab}	1.87 (0.18)^{b}	8.8 (1.2)	27.5 (2.1)	4.13 (0.15)
2-year-old	38.3 (3.0)^{b}	13.2 (0.2)^{b}	2.06 (0.05)^{b}	9.8 (0.4)	28.4 (1.7)	4.18 (0.04)
3-year-old	36.7 (1.9)^{b}	13.0 (0.1)^{ab}	2.07 (0.07)^{b}	9.7 (0.6)	29.8 (2.9)	4.43 (0.15)
4-year-old	12.6 (1.6)^{c}	11.7 (0.3)^{ab}	2.05 (0.07)^{b}	9.9 (0.6)	29.1 (3.3)	4.21 (0.30)
P	< 0.0001	0.0168	< 0.0001	0.5434	0.8448	0.0855

Values given are the mean (standard error) of 6 shoots. The significance of differences among age-classes (*P*) was assessed as described in Table 3.1. Means followed by different letters are significantly different.

†Assuming proteins are 16% N (Takashima *et al.* 2004).

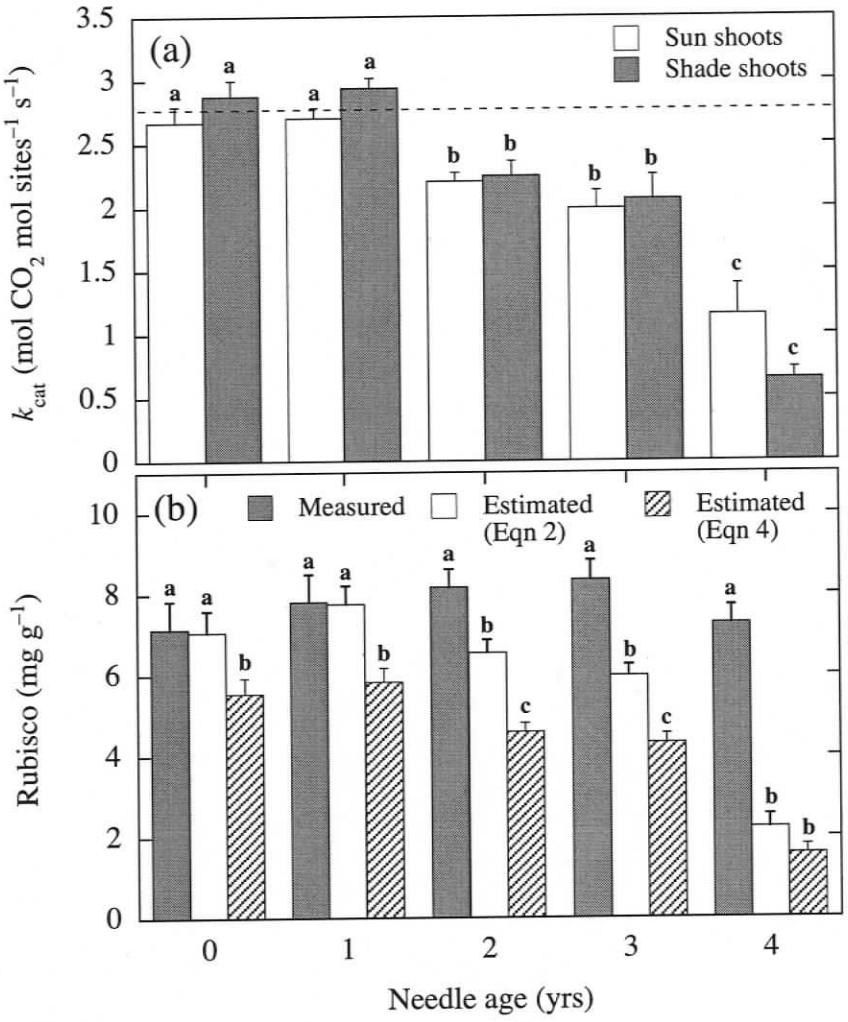

Figure. 3.7 (a) Catalytic turnover rate of Rubisco (k_{cat} – quotient of the shoot's maximal carboxylation rate (V_{cmax}) divided by its Rubisco site content) from Douglas-fir needles. The dashed line indicates the Rubisco k_{cat} value determined *in vivo* by von Caemmerer *et al.* (1994) adjusted to 22°C. (b) Comparison of needle Rubisco content determined by enzyme-linked immunosorbtion assay with the calculated amount of Rubisco required to achieve the corresponding shoot V_{cmax} (estimated from Eqn 3.2 *vs.* Eqn 3.4 – see text for details) assuming a k_{cat} value of 2.76 mol CO_2 mol Rubisco sites^{-1} s^{-1} (dashed line in panel a). Values indicated in panel (a) and (b) are the mean (+ standard error) of 6 and 12 shoots, respectively; significant differences ($P < 0.05$, one-way analysis of variance (repeated measures) with *post hoc* Tukey HSD test) among age classes in panel (a) and Rubisco estimates in panel (b) are indicated by different letters.

There were significant correlations between k_{cat} and the overall conductance to CO_2 from the leaf surface to the stromal carboxylation sites $(1.6/g_s + 1/g_i)^{-1}$ in ≥ 2-year-old shoots, whereas saturation of k_{cat} was observed in younger foliage (mass-based relationships shown in Fig. 3.8). Both the slope and the regression coefficient of the relationships increased with needle age, suggesting an increasing degree of coupling between Rubisco activation and CO_2 supply.

Loss of Rubisco activity in older foliage was matched by a proportional down-regulation of electron transport towards the photosynthetic carbon reduction (PCR) and photorespiratory (PCO) cycles (Fig. 3.9a) and by a corresponding increase in the carotenoid to chlorophyll ratio of needles (Fig. 3.9b). The correlations of k_{cat} with J and the needle carotenoid to chlorophyll ratio were significant among foliar age classes for both sun and shade shoots (Fig. 3.9).

DISCUSSION

Leaf photosynthesis model curve fitting and estimation of g_i

The non-rectangular hyperbola version of the model of Farquhar *et al.* (1980) contains an additional parameter (g_i) used to quantify departures from the curvature of the original Michaelis-Menten kinetics rectangular hyberbola function valid at C_c (see Chapter 1). Because 1) the addition of one more degree of freedom in the model introduces greater interaction among the fitted parameters and 2) the evaluation of the curvature of the RuBP-saturated and RuBP-limited A-C_i curve portions is usually done over a limited C_i range and is sensitive to experimental errors and/or significant changes in Rubisco activity, I recommend the use of a higher degree of measurement resolution (e.g. 25 μbar steps) over the domains of interest to increase the robustness of the corresponding least-squares fits. The A-C_i curves presented in this study were originally intended for use with the standard A-C_i curve fitting procedure and, therefore, do not meet the above requirement. Thus, rather than treating the least-square fits of the RuBP-saturated and RuBP-limited A-C_i curve portions independently, I iterated the curve fits concurrently to obtain a unique solution for g_i and thereby increase the number of

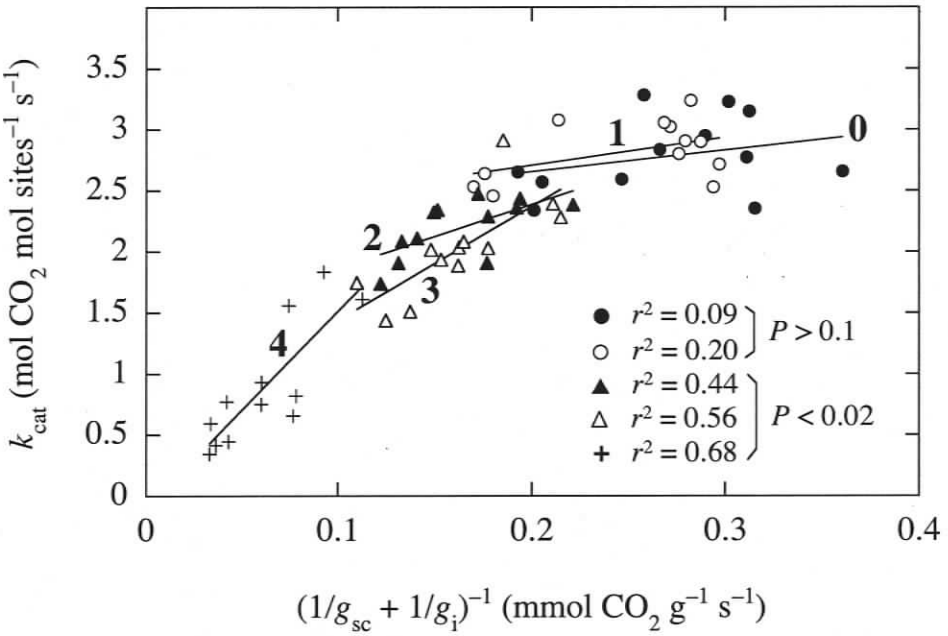

Figure 3.8 Relationship between the catalytic turnover rate of Rubisco (k_{cat}) and the overall conductance to CO_2 from the leaf surface to the stromal carboxylation sites $(1/g_{sc} + 1/g_i)^{-1}$ (mass basis) in Douglas-fir. Symbols denoting the different foliar age classes and corresponding numbering of simple linear regression lines are as in Fig. 3.3.

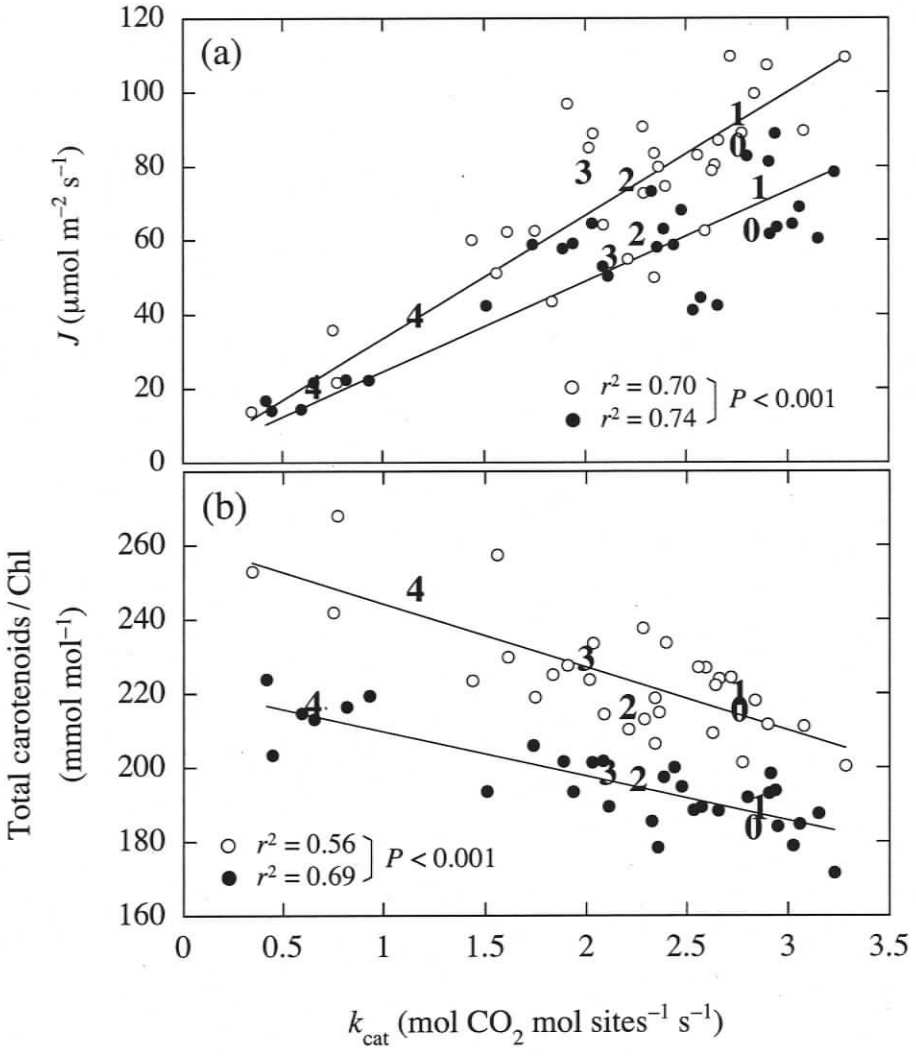

Figure 3.9 Relationship between the catalytic turnover rate of Rubisco (k_{cat}) and (a) the photochemical electron transport rate (J) of Douglas-fir shoots evaluated at saturating light and 360 μmol mol^{-1} ambient CO_2 concentration (calculated from Eqn 3.6, substituting A_j for the measured A_n), and (b) the total carotenoid to chlorophyll ratio of needles. Simple linear regression lines (intercepts constrained to zero in panel a) are for sun (○) and shade (●) shoots; the numbers along each line are positioned at (x, y) representing the sample mean (n = 6) of the corresponding foliar age class.

measurements upon which the estimate is based. I assumed a constant g_i throughout the measurement range; this has been partially confirmed (von Caemmerer & Evans 1991; Harley *et al.* 1992), but remains to be fully validated. This parameterisation depends on my choice of 1) C_i transition region between RuBP-saturated and RuBP-limited A-C_i curve portions (see Appendix A), 2) stoichiometry of the equation describing RuBP-limited photosynthesis (Eqn 3.3), and 3) Rubisco kinetic constants. Given these assumptions, the aforementioned A-C_i curve fitting method produced g_i estimates that ranged from 0.059 to 0.144 mol m^{-2} s^{-1} for current-year shoots. This is on average 30% lower than the values obtained by Warren *et al.* (2003b) for the same study trees using a different method. I doubt that this is due to my choice of Rubisco kinetic constants as the values of Bernacchi *et al.* (2002) increased the g_i estimates by only 7% while the commonly used *in vitro* values of Jordan & Ogren (1984) decreased them by 15%. Comparatively, changing the stoichiometry of Eqn 3 for the formulation which assumes that O_2 is required as an additional electron acceptor to $NADP^+$ via the Mehler reaction (i.e. $A_j + R_d = J\,(C_c + \Gamma^*)/(4.5C_c + 10.5\Gamma^*)$ — see von Caemmerer 2000) increased the g_i estimates by 13%, but resulted in greater initial disparity between the g_i estimates of the RuBP-saturated *vs.* RuBP-limited A-C_i curve portions to be iterated. The photocompensation point method of Warren *et al.* (2003b) is based on the intersection point of two A-C_i curves (high *vs.* low irradiance), which occurs below Γ. As noted earlier, I found that, in many cases, the curvature of the A_n *vs.* C_i relationship increases markedly in that region, which could influence the determination of the intercellular CO_2 photocompensation point (C_i^*) and R_d from which g_i was estimated. Indeed, given the high relative sensitivity of the photocompensation point method to potential errors in R_d (i.e. potentially up to a 1:1 correspondence), the relative difference between g_i values obtained in this study and those of Warren *et al.* (2003b) is easily explained by the larger R_d values derived in the latter study (data not shown). Furthermore, Niinemets *et al.* (2005, 2006) recently established that the novel A-C_i curve fitting method outlined in Chapter 1 produced essentially the same estimates of g_i as the chlorophyll fluorescence method.

Factors contributing to the PNUE decline of aging Douglas-fir foliage

In Douglas-fir, the age-related PNUE decline of leaves begins after two years of growth and becomes severe after four years (Table 3.2). Because the proportion of leaf N allocated to Rubisco and other SDS-soluble proteins did not change appreciably throughout this period (or else increased in the case of chlorophyll-associated thylakoid proteins – Table 3.2), I reject the hypothesis that the PNUE decline resulted from a decrease in fractional investment of leaf N in photosynthetic machinery. Although I did not measure the amount of residual SDS-insoluble (presumably cell wall) proteins left in the final extraction pellet, I doubt that this protein fraction would have increased significantly with leaf age since Takashima *et al.* (2004) indicated that such an increase would be associated with a decrease in fractional investment of N to Rubisco and proteins involved in bioenergetics and light harvesting. According to an extensive foliage sampling at the study site in the year preceding my measurements, significant N resorption from senescing needles does not occur until the seventh growing season (data not shown). This surprisingly contrasts with my observation that the down-regulation of Rubisco began during the third growing season (Fig. 3.7a) when the foliar N concentration was at its highest (Table 3.2) and continued thereafter. A similar pattern was found in *P. pinaster* (Warren 2006), hence confirming the role of Rubisco as a N storage protein in evergreen species (Warren *et al.* 2000, 2003a). Similarly, the age-related accumulation of chlorophyll-associated thylakoid proteins in spite of significant down-regulation of Rubisco and electron transport towards the PCR and PCO cycles (Fig. 3.9a) may reflect their role as potential N stores. Still, the concomitant increase of the carotenoid to chlorophyll ratio of needles (Fig. 3.9b) could instead indicate a shift in the function of protein-pigment complexes towards non-radiative dissipation of excess light energy via the xanthophyll cycle. For example, Ebbert *et al.* (2005) showed that overwintering sun- and shade-adapted Douglas-fir needles have the ability to down-regulate their photosynthetic capacity and up-regulate their capacity for xanthophyll cycle-dependent photoprotection. On the other hand, the work of Brooks, Hinckley & Sprugel (1994) and Brooks *et al.* (1996) on temperate conifers suggests that the age-related increase in N allocation

to chlorophylls-protein complexes could be a consequence of acclimation to gradual shading. However, in these cases, shade acclimation was also indicated by a significant shift in pigment stoichiometry favoring chlorophyll *b* over chlorophyll *a*. By comparison, I found no significant age effect on the chlorophyll *a/b* ratio of Douglas-fir needles, whether collected from the upper ($P = 0.2871$) or lower ($P = 0.6128$) canopy layers (data not shown).

In this study, I found a 3-fold variation of Rubisco k_{cat} values which affected V_{cmax} (Fig. 3.7) and to which J_{max} and g_i were correlated (Figs. 3.3a, b). In light of such results, I do not recommend the sole use of gas exchange parameters (i.e. V_{cmax} and J_{max}) determined without considering the activation state of Rubisco (e.g. Niinemets *et al.* 2005, 2006), or Rubisco and g_i (e.g. Ripullone *et al.* 2003; Niinemets *et al.* 2004), to explain age- or leaf life span-related differences in PNUE in terms of N allocation to Rubisco *vs.* proteins involved in bioenergetics or light harvesting. Moreover, since g_{sc} and g_i both remained tightly coupled to the carboxylation efficiency of Rubisco over the years (Figs. 3.3a, c & 3.8), I cannot exclude them as the primary cause of the age-related decline of PNUE (see below).

Age-related decline of g_i *vs.* LMA and light acclimation

In Douglas-fir, LMA increases with irradiance during the first growing season (Aussenac 1973; Warren *et al.* 2003b), and then increases with needle age regardless of light in subsequent years (Ishii *et al.* 2002; this study). In both cases, the increase in LMA is modulated through changes in both needle thickness and tissue density, although in developing needles the changes mostly take place in the palisade mesophyll layer (Aussenac 1973), whereas in aging needles, they are more likely to occur in the hypodermal layer and other lignified tissues (Apple *et al.* 2002). According to Niinemets *et al.* (2005, 2006) who discussed the possible effect of light acclimation *vs.* leaf aging on LMA and g_i in Mediterranean broadleaf evergreens, the initial positive effect of light on LMA and g_i (area basis) is a consequence of the greater chloroplast to total leaf surface area ratio of the "sun leaf type" palisade tissue (see references given therein), whereas the subsequent negative effect of LMA on g_i (mass or area basis) reflects the

accumulation of cell wall compounds which would impede the diffusion of CO_2 in the liquid phase. I agree that the positive effect of light on LMA and g_i (area) in current-year foliage (Fig. 3.4b, c) is likely related to the development of a greater relative chloroplastic surface area. However, because the courses of LMA and g_i were mismatched though time (Fig. 3.4b-d), I doubt that the overall negative correlation between LMA and g_i (mass) I observed among foliar age classes reflects a direct causal link.

Coordination between Rubisco activity and CO_2 conductances: a "chicken *vs.* egg" question

Over 20 years ago, Wong, Cowan & Farquhar (1979) were the first to propose that stomatal aperture is determined by the collective photosynthetic capacity of the chloroplasts such that g_{sc} remains proportional to A_n, and C_i is kept nearly constant in the face of changing growth conditions that affect mesophyll photosynthesis directly (e.g. light, ambient CO_2, N nutrition – Wong, Cowan & Farquhar 1985). My results (Figs. 3.5 & 3.6) confirm that A_n and g_{sc} remain coordinated through successive growing seasons in evergreen leaves (Field & Money 1983; Yoshie 1986) which, according to Wong *et al.* (1979, 1985), would be the consequence of guard cells responding to the declining photosynthetic capacity of the mesophyll by reducing their aperture. Several photosynthetic metabolites have been proposed as possible mediators of the response, including ATP, NADPH, and RuBP (Wong *et al.* 1979; Farquhar & Wong 1984), but many researchers have argued that C_i itself is the signal to which guard cells respond directly (Mott 1988; Lawson *et al.* 2002). If so, Rubisco deactivation would come first in the chain of events that leads to stomatal closure in aging Douglas-fir leaves, the homeostatic response being mediated by a transient rise in C_i. Recently, however, von Caemmerer *et al.* (2004) challenged the theory of Wong *et al.* (1979) by showing that transgenic plants with reduced amounts of Rubisco and decreased photosynthetic capacity and g_i (Evans *et al.* 1994) retain normal, wild-type guard cell characteristics including rate of stomatal opening, steady-state g_{sc}, and g_{sc} sensitivity to ambient CO_2, but do not appear to perceive changes in C_i. Such

results are difficult to reconcile with the view that g_{sc} responds to changes in mesophyll photosynthetic capacity by sensing fluctuations in C_i. If loss of photosynthetic capacity due to Rubisco deactivation did not cause the g_{sc} decline in aging Douglas-fir leaves, what did?

Lately, the coordination between leaf photosynthetic capacity and xylem hydraulic conductance has been established at multiple scales including large tree trunks (e.g. Hubbard, Bond & Ryan 1999), branches (e.g. Brodribb, Holbrook & Gutiérrez 2002), whole seedlings (Hubbard *et al.* 2001), and leaf lamina or short-needle conifer shoots (Brodribb *et al.* 2005). Considering the serial positioning of stomata in the flow path of water and CO_2 through leaves and the necessary dynamic coordination of the vapour and liquid phase resistances to water transport in plants (reviewed in Meinzer 2002), it is tempting to propose that the age-related stomatal and photosynthetic decline of Douglas-fir shoots is originally caused by a loss of hydraulic conductivity in aging xylem pathways. In Douglas-fir stems, the hydraulic conductivity of xylem decreases with the age of annual wood rings (Spicer & Gartner 2001); this trait has been associated with a loss of hydraulic connection to leaves in aging annual rings of maple tree branches (Melcher, Zwieniecki & Holbrook 2003) and with the formation of "hydraulic bottlenecks" that become shoot abscission zones on older, pedunculate oak branches (Rust & Roloff 2002). In analogy to this, the addition of successive growth rings on older Douglas-fir branch internodes to supply the distal growth of younger foliage is likely to be associated with a loss hydraulic conductivity in the aging, recessed vascular traces connected to old needles. My observation that the diameter of the vascular connection of needles (determined from leaf scars examined under a dissecting microscope) gradually decreases with age could be a consequence of such hydraulic bottlenecking. More detailed microscopy studies are needed to verify this hypothesis.

CO_2 supply *vs.* the chloroplastic CO_2 operating point

If we take the conservativeness of the N allocation to Rubisco and associated soluble proteins in the face of a declining hydraulic-stomatal capacity as an indication of the limited post-ontogenic

phenotypic plasticity of the "evergreen" carbon fixation machinery of aging Douglas-fir needles, it becomes easier to appreciate the importance of Rubisco down-regulation to prevent the exhaustion of CO_2 in the chloroplasts and ensuing impairment of the cycling of photosynthetic metabolites. For example, according to my calculations, had the Rubisco from 2–3-year-old needles remained fully activated, the operating C_c would have fallen close to Γ^* at the measured g_{sc} and g_i values. In 4-year-old shoots, C_c would have been completely exhausted if the Rubisco activation state had increased to only 50% of its potential. Judging from the limited range of C_c values observed both in the field and in the controlled environment of the integrating sphere (Figs. 3.5b & 3.6), it would appear that the homeostatic constraints of Douglas-fir photosynthetic metabolism set the lower operational limit for C_c (at least in non-droughted conditions) above 100 μbar. Because CO_2 itself is involved in the regulation of the Rubisco activation state (via the reversible carbamylation of a lysine residue within the Rubisco's catalytic site prior to the binding of Mg^{2+} – Andrews & Lorimer 1987), the C_c decrease resulting from a significant loss of conductance to CO_2 may indeed provide a simple feedforward mechanism by which the activation of Rubisco is reduced in proportion to the diminishing supply of CO_2 (see Fig. 3.8). Interestingly, in transgenic plants with reduced Rubisco activity due to decreased expression of Rubisco activase, the senescence-related degradation of Rubisco is delayed relative to chlorophyll and other soluble proteins (He *et al.* 1997). Presumably, the persistence of large amounts of Rubisco late into leaf development is a consequence of the reduced carbamylation of the Rubisco pool (He *et al.* 1997); a similar mechanism may be involved in the age-related accumulation of Rubisco in evergreen leaves.

CONCLUSION

I have shown that, in Douglas-fir, the age-related PNUE decline of non-senescing leaves is not a consequence of decreased allocation of N towards Rubisco and other proteins involved in bioenergetics and light harvesting. Rather, loss of photosynthetic capacity was the result of the decreased activation state of Rubisco and proportional down-regulation of electron transport

towards the PCR and PCO cycles in response to a reduction of CO_2 supply to the carboxylation sites. This study emphasises the dynamic character of g_i, as well as the regulatory potential and conservative nature of C_c – rather than photosynthetic metabolites or C_i – in relation to the previously observed coordination between photosynthesis and stomatal conductance (Wong *et al.* 1979, 1985). My results are consistent with the recent proposal that the integration of guard cell and mesophyll physiological responses could be the result of co-evolution rather than direct mechanistic linkage (von Caemmerer *et al.* 2004).

REFERENCES

Andrews T.J. & Lorimer G.H. (1987) Rubisco: Structure, mechanisms, and prospects for improvement. In *The Biochemistry of Plants: Photosynthesis* (eds M.D. Hatch & N.K. Boardman) Vol. 10, pp. 131–218. Academic Press, San Diego, CA, USA.

Apple M., Tiekotter K., Snow M., Young J., Soeldner A., Tingey D. & Bond B.J. (2002) Needle anatomy changes with increasing tree age in Douglas-fir. *Tree Physiology* **22,** 129–136.

Aussenac G. (1973) Effets de conditions microclimatiques différentes sur la morphologie et la structure anatomique des aiguilles de quelques résineux. *Annales des Sciences Forestieres* **30**, 375–392.

Bernacchi C.J., Portis A.R., Nakano H., von Caemmerer S. & Long S.P. (2002) Temperature response of mesophyll conductance. Implications for the determination of Rubisco enzyme kinetics and for limitations to photosynthesis in Vivo. *Plant Physiology* **130,** 1–7.

Brodribb T.J., Holbrook N.M. & Gutiérrez M.V. (2002) Hydraulic and photosynthetic co-ordination in seasonally dry tropical forest trees. *Plant, Cell and Environment* **25,** 1435–1444.

Brodribb T.J., Holbrook N.M., Zwieniecki M.A. & Palma B. (2005) Leaf hydraulic capacity in ferns, conifers and angiosperms: impacts on photosynthetic maxima. *New Phytologist* **165,** 839–846.

Brooks J.R., Hinckley T.M. & Sprugel D.G. (1994) Acclimation responses of mature *Abies amabilis* sun foliage to shading. *Oecologia* **100,** 316–324.

Brooks J.R., Sprugel D.G. & Hinckley T.M. (1996) The effect of light acclimation during and after foliage expansion on photosynthesis of *Abies amabilis* foliage within the canopy. *Oecologia* **107,** 21–32.

Brugnoli E, Hubick K.T., von Caemmerer S., Wong S.C. & Farquhar G.D. (1988) Correlation between the carbon isotope discrimination in leaf starch and sugars of C_3 plants and the ratio of intercellular and atmospheric partial pressures of carbon dioxide. *Plant Physiology* **88,** 1418–1424.

Cheng L. & Fuchigami L.H. (2000) Rubisco activation state decreases with increasing nitrogen content in apple leaves. *Journal of Experimental Botany* **51,** 1687–1694.

Chiba A., Ishida H., Nishizawa N.K., Makino A. & Mae T. (2003) Exclusion of ribulose-1,5-bisphosphate carboxylase/oxygenase from chloroplasts by specific bodies in naturally senescing leaves of wheat. *Plant and Cell Physiology* **44,** 914–921.

Delfine S., Alvino A., Villani M.C. & Loreto F. (1999) Restrictions to carbon dioxide conductance and photosynthesis in spinach leaves recovering from salt stress. *Plant Physiology* **119,** 1101–1106.

Ebbert V., Adams III W.W., Mattoo A.K., Sokolenko A. & Demmig-Adams B. (2005) Up-regulation of a photosystem II core protein phosphatase inhibitor and sustained D1 phosphorylation in zeaxanthin-retaining, photoinhibited needles of overwintering Douglas fir. *Plant, Cell and Environment* **28,** 232–240.

Eichelmann H. & Laisk A. (1999) Ribulose-1,5-bisphosphate carboxylase/oxygenase content, assimilatory charge, and mesophyll conductance in leaves. *Plant Physiology* **119,** 179–189.

Escudero A. & Mediavilla S. (2003) Decline in photosynthetic nitrogen use efficiency with leaf age and nitrogen resorption as determinants of leaf life span. *Journal of Ecology* **91,** 880–889.

Evans J.R. (1989) Photosynthesis and nitrogen relationships in leaves of C_3 plants. *Oecologia*

78, 9-19.

Evans J.R., von Caemmerer S., Setchell B.A. & Hudson G.S. (1994) The relationship between CO_2 transfer conductance and leaf anatomy in transgenic tobacco with a reduced content of Rubisco. *Australian Journal of Plant Physiology* **21,** 475–495.

Farquhar G.D., O'Leary M.H. & Berry J.A. (1982) On the relationship between carbon isotope discrimination and the intercellular carbon dioxide concentration in leaves. *Australian Journal of Plant Physiology* **9,** 121–137.

Farquhar G.D., von Caemmerer S. & Berry J.A. (1980) A biochemical model of photosynthetic CO_2 assimilation in leaves of C_3 species. *Planta* **149,** 78–90.

Farquhar G.D. & Wong S.C. (1984) An empirical model of stomatal conductance. *Australian Journal of Plant Physiology* **11,** 191–210.

Field C. & Mooney H.A. (1983) Leaf age and seasonal effects on light, water, and nitrogen use efficiency in a California shrub. *Oecologia* **56,** 348–355.

Friedrich J.W. & Huffaker R.C. (1980) Photosynthesis, leaf resistances, and ribulose-1,5-bisphosphate carboxylase degradation in senescing barley leaves. *Plant Physiology* **65,** 1103–1107.

Gates D.M., Keegan H.J., Schleter J.C. & Weidner V.R. (1965) Spectral properties of plants. *Applied Optics* **4,** 11–20.

Grassi G. & Magnani F. (2005) Stomatal, mesophyll conductance and biochemical limitations to photosynthesis as affected by drought and leaf ontogeny in ash and oak trees. *Plant, Cell and Environment* **28,** 834–849.

Hanba Y.T., Miyazawa S.-I. & Terashima I. (1999) The influence of leaf thickness on the CO_2 transfer conductance and leaf stable carbon isotope ratio for some evergreen tree species in Japanese warm-temperate forests. *Functional Ecology* **13,** 632–639.

Harley P.C., Loreto F., Di Marco G. & Sharkey T.D. (1992) Theoretical considerations when estimating the mesophyll conductance to CO_2 flux by analysis of the response of photosynthesis to CO_2. *Plant Physiology* **98,** 1429–1436.

Harley P.C. & Sharkey T.D. (1991) An improved model of C_3 photosynthesis at high CO_2: reversed O_2 sensitivity explained by lack of glycerate reentry into the chloroplast. *Photosynthesis Research* **27,** 169–178.

He Z., von Caemmerer S., Hudson G.S., Price G.D., Badger M.R. & Andrews T.J. (1997) Ribulose-1,5-bisphosphate carboxylase/oxygenase activase deficiency delays senescence of ribulose-1,5-bisphosphate carboxylase/oxygenase but progressively impairs its catalysis during tobacco leaf development. *Plant Physiology* **115,** 1569–1580.

Hörtensteiner S. & Feller U. (2002) Nitrogen metabolism and remobilization during senescence. *Journal of Experimental Botany* **53,** 927–937.

Hubbard R.M., Bond B.J. & Ryan M.G. (1999) Evidence that hydraulic conductance limits photosynthesis in old *Pinus ponderosa* trees. *Tree Physiology* **19,** 165–172.

Hubbard R.M., Ryan M.G., Stiller V. & Sperry J.S. (2001) Stomatal conductance and photosynthesis vary linearly with plant hydraulic conductance in ponderosa pine. *Plant, Cell and Environment* **24,** 113–121.

Humphreys E.R., Black T.A., Ethier G.J., Drewitt G.B., Spittlehouse D.L., Jork E.M., Nesic Z., Livingston N.J. (2003) Annual and seasonal variability of sensible and latent heat fluxes above a coastal Douglas-fir forest, British Columbia, Canada. *Agricultural and Forest Meteorology* **115,** 109–125.

Ishii H., Ford E.D., Boscolo M.E., Manriquez A.C., Wilson M.E. & Hinckley T.M. (2002) Variation in specific needle area of old-growth Douglas-fir in relation to needle age, within-crown position and epicormic shoot production. *Tree Physiology* **22,** 31–40.

Jordan D.B. & Ogren W.L. (1984) The CO_2/O_2 specificity of ribulose 1,5-bisphosphate carboxylase/oxygenase. Dependence on ribulose bisphosphate concentration, pH and temperature. *Planta* **161,** 308–313.

Jurik T.W. (1986) Seasonal patterns of leaf photosynthetic capacity in successional northern hardwood tree species. *American Journal of Botany* **73,** 131–138.

Kang S.M. & Titus J.S. (1980) Qualitative and quantitative changes in nitrogen compounds in

senescing leaf and bark tissue of the apple. *Physiologia Plantarum* **50,** 285–290.

Kayama M., Sasa K. & Koike T. (2002) Needle life span, photosynthetic rate and nutrient concentration of *Picea glehnii*, *P. jezoensis* and *P. abies* planted on serpentine soil in northern Japan. *Tree Physiology* **22,** 707–716.

Kirschbaum M.U.F. & Farquhar G.D. (1987) Investigation of the CO_2 dependence of quantum yield and respiration in *Eucalyptus pauciflora*. *Plant Physiology* **83,** 1032-1036.

Lawson T., Oxborough K., Morison J.I.L. & Baker N.R. (2002) Responses of photosynthetic electron transport in stomatal guard cells and mesophyll cells in intact leaves to light, CO_2, and humidity. *Plant Physiology* **128,** 52–62.

Loreto F., Di Marco G., Tricoli D. & Sharkey T.D. (1994) Measurements of mesophyll conductance, photosynthetic electron transport and alternative electron sinks of field grown wheat leaves. *Photosynthesis Research* **41,** 397–403.

Loreto F., Harley P.C., Di Marco G. & Sharkey T.D. (1992) Estimation of mesophyll conductance to CO_2 flux by three different methods. *Plant Physiology* **98,** 1437–1443.

Makino A., Mae T. & Ohira K. (1988) Differences between wheat and rice in the enzymic properties of ribulose-1,5-bisphosphate carboxylase/oxygenase and the relationship to photosynthetic gas exchange. *Planta* **174,** 30–38.

Manter D.K. & Kerrigan J.A. (2004) *A*/*C*i curve analysis across a range of woody plant species: influence of regression analysis parameters and mesophyll conductance. *Journal of Experimental Botany* **55,** 2581–2588.

Meinzer F.C. (2002) Co-ordination of vapour and liquid phase water transport properties in plants. *Plant, Cell and Environment* **25,** 265–274.

Melcher P.J., Zwieniecki M.A. & Holbrook N.M.(2003) Vulnerability of xylem vessels to cavitation in sugar maple. Scaling from individual vessels to whole branches. *Plant Physiology* **131,** 1775–1780.

Metodiev M. & Demirevska-Kepova K. (1992) Rubisco quantitation in leaves of different barley varieties by enzyme-linked immunosorbent assay. *Journal of Experimental Botany*

43, 155–158.

Moran J.A., Mitchell A.K., Goodmanson G. & Stockburger K.A. (2000) Differentiation among effects of nitrogen fertilization treatments on conifer seedlings by foliar reflectance: a comparison of methods. *Tree Physiology* **20,** 1113–1120.

Morgenstern K., Black T.A., Humphreys E.R., Griffis T.J., Drewitt G.B., Cai T., Nesic Z., Spittlehouse D.L., Livingston N.J. (2004) Sensitivity and uncertainty of the carbon balance of a Pacific Northwest Douglas-fir during an EI Niño/La Niña cycle. *Agricultural and Forest Meteorology* **123,** 201–219.

Mott K.A. (1988) Do stomata respond to CO_2 concentrations other than intercellular? *Plant Physiology* **86,** 200–203.

Niinemets Ü., Cescatti A., Rodeghiero M. & Tosens T. (2005) Leaf internal diffusion conductance limits photosynthesis more strongly in older leaves of Mediterranean evergreen broad-leaved species. *Plant, Cell and Environment* **28,** 1552–1566.

Niinemets Ü., Cescatti A., Rodeghiero M. & Tosens T. (2006) Complex adjustments of photosynthetic potentials and internal diffusion conductance to current and previous light availabilities and leaf age in Mediterranean evergreen species *Quercus ilex. Plant, Cell and Environment* **29,** 1159–1178.

Niinemets Ü., Tenhunen J.D. & Beyschlag W. (2004) Spatial and age-dependent modifications of photosynthetic capacity in four Mediterranean oak species. *Functional Plant Biology* **31,** 1179–1193.

Nonaka M. (1974) Improved paint coating for photometric integrators. *Lighting Research and Technology* **6,** 30–31.

Oleksyn J., Tjoelker M.G., Lorenc-Plucinska G., Konwinska A., Zytkowiak R., Karolewski P. & Reich P.B. (1997) Needle CO_2 exchange, structure and defense traits in relation to needle age in *Pinus heldreichii* Christ – a relict of Tertiary flora. *Trees* **12,** 82–89.

Pinelli P. & Loreto F. (2003) ^{12}CO2 emission from different metabolic pathways measured in illuminated and darkened C_3 and C_4 leaves at low, atmospheric and elevated CO_2

concentration. *Journal of Experimental Botany* **54,** 1761–1769.

Ripullone F., Grassi G., Lauteri M. & Borghetti J. (2003) Photosynthesis–nitrogen relationships: interpretation of different patterns between *Pseudotsuga menziesii* and *Populus* x *euroamericana* in a mini-stand experiment. *Tree Physiology* **23,** 137–144.

Rust S. & Roloff A. (2002) Reduced photosynthesis in old oak (*Quercus robur*): the impact of crown and hydraulic architecture. *Tree Physiology* **22,** 597–601.

Sage R.F., Sharkey T.D. & Seemann J.R. (1990) Regulation of ribulose-1,5-bisphosphate carboxylase activity in response to light intensity and CO_2 in the C_3 annuals *Chenopodium album* L. and *Phaseolus vulgaris* L. *Plant Physiology* **94,** 1735–1742.

Spicer R. & Gartner B.L. (2001) The effects of cambial age and position within the stem on specific conductivity in Douglas-fir (*Pseudotsuga menziesii*) sapwood. *Trees* **15,** 222–229.

Standish J.T., Manning G.H. & Demaerschalk J.P. (1985) *Development of biomass equations for British Columbia tree species*. Canadian Forestry Service, Victoria, B.C. Inf. Rep. BC-X-264.

Takashima T., Hikosaka K. & Hirose T. (2004) Photosynthesis or persistence: nitrogen allocation in leaves of evergreen and deciduous *Quercus* species. *Plant, Cell and Environment* **27,** 1047–1054.

Turner D.P., Steven A.A., Means J.E. & Garman S.L. (2000) Assessing alternative allometric algorithms for estimating leaf area og Douglas-fir trees and stands. *Forest Ecology and Management* **126,** 61–76.

von Caemmerer S. (2000) *Biochemical models of leaf photosynthesis*. Techniques in Plant Sciences N0. 2. CSIRO Publishing, Collingwood, Victoria, Australia.

von Caemmerer S. & Edmondson D.L. (1986) Relationship between steady-state gas exchange, *in vivo* ribulose bisphosphate carboxylase activity and some carbon reduction cycle intermediates in *Raphanus sativus*. *Australian Journal of Plant Physiology* **13,** 669–688.

von Caemmerer S. & Evans J.R. (1991) Determination of the average partial pressure of CO_2 in chloroplasts from leaves of several C_3 plants. *Australian Journal of Plant Physiology* **18,**

287–305.

von Caemmerer S., Evans J.R., Hudson G.S. & Andrews T.J. (1994) The kinetics of ribulose-1,5-bisphosphate carboxylase/oxygenase in vivo inferred from measurements of photosynthesis in leaves of transgenic tobacco. *Planta* **195,** 88–97.

von Caemmerer S. & Farquhar G.D. (1981) Some relationships between the biochemistry of photosynthesis and the gas exchange of leaves. *Planta* **153,** 376–387.

von Caemmerer S., Lawson T., Oxborough K., Baker N.R., Andrews T.J. & Raines C.A. (2004) Stomatal conductance does not correlate with photosynthetic capacity in transgenic tobacco with reduced amounts of Rubisco. *Journal of Experimental Botany* **55,** 1157–1166.

Warren C.R. (2006) Why does photosynthesis decrease with needle age in *Pinus pinaster*? *Trees* **20,** 157–164.

Warren C.R. & Adams M.A. (2000) Trade-offs between the persistence of foliage and productivity in two *Pinus* species. *Oecologia* **124,** 487–494.

Warren C.R., Adams M.A. & Chen Z.L. (2000) Is photosynthesis related to concentrations of nitrogen and Rubisco in leaves of Australian native plants? *Australian Journal of Plant Physiology* **27,** 407–416.

Warren C.R., Dreyer E. & Adams M.A. (2003a) Photosynthesis-Rubisco relationships in foliage of *Pinus sylvestris* in response to nitrogen supply and the proposed role of Rubisco and amino acids as nitrogen stores. *Trees* **17,** 359–366.

Warren C.R., Ethier G.J., Livingston N.J., Grant N.J., Turpin D.H., Harrison D.L. & Black T.A. (2003b) Transfer conductance in second growth Douglas-fir (*Pseudotsuga menziesii* (Mirb.)Franco) canopies. *Plant, Cell and Environment* **26,** 1215–1227.

Wellburn A.R. (1994) The spectral determination of chlorophylls *a* and *b*, as well as total carotenoids, using various solvents with spectrophotometers of different resolution. *Journal of Plant Physiology* **144,** 307-313.

Wendler R., Carvalho P.O., Pereira J.S. & Millard P. (1995) Role of nitrogen remobilization from old leaves for new leaf growth of *Eucalyptus globulus* seedlings. *Tree Physiology* **15,**

679–683.

Wessel D. & Flügge U.I. (1984) A simple method for the quantitative recovery of protein in dilute solution in the presence of detergent and lipids. *Analytical Biochemistry* **138,** 141–143.

Woolley J.T. (1971) Reflectance and transmittance of light by leaves. *Plant Physiology* **47,** 656–662.

Wong S.C., Cowan I.R. & Farquhar G.D. (1979) Stomatal conductance correlates with photosynthetic capacity. *Nature* **282,** 424–426.

Wong S.C., Cowan I.R. & Farquhar G.D. (1985) Leaf conductance in relation to rate of CO_2 assimilation. I. Influence of nitrogen nutrition, phosphorus nutrition, photon flux density, and ambient partial pressure of CO_2 during ontogeny. *Plant Physiology* **78,** 821–825.

Yoshie F. (1986) Intercellular CO_2 concentration and water-use efficiency of temperate plants with different life-forms and from different microhabitats. *Oecologia* **68,** 370–374.

Appendix A

Determination of C_i cut-off point

Recalling that in the non-rectangular hyperbola version of the biochemical model of C_3 leaf photosynthesis of Farquhar *et al.* (1980), the net CO_2 assimilation rate of a leaf (A_n) is given by

$$A_n = \min\{A_c, A_j\} \tag{A.1}$$

$$\begin{aligned} A_c &= \frac{-b + \sqrt{b^2 - 4ac}}{2a} \\ a &= -1/g_i \\ b &= (V_{c\max} - R_d)/g_i + C_i + K_c(1 + O/K_o) \\ c &= R_d(C_i + K_c(1 + O/K_o)) - V_{c\max}(C_i - \Gamma^*) \end{aligned} \tag{A.2}$$

$$\begin{aligned} A_j &= \frac{-b + \sqrt{b^2 - 4ac}}{2a} \\ a &= -1/g_i \\ b &= (J/4 - R_d)/g_i + C_i + 2\Gamma^* \\ c &= R_d(C_i + 2\Gamma^*) - J/4(C_i - \Gamma^*) \end{aligned} \tag{A.3}$$

(*c.f.* Eqns 3.1 to 3.3) where A_c and A_j are the RuBP (ribulose-1,5-bisphosphate)-saturated and RuBP-limited net CO_2 assimilation rate, respectively, V_{cmax} is the maximal CO_2 carboxylation rate, J is the photochemical electron transport rate under RuBP-limited conditions, R_d is the mitochondrial respiration in the light, Γ^* is the chloroplastic CO_2 photocompensation point, C_i is the substomatal intercellular CO_2 concentration, $K_c(1+O/K_o)$ is the *effective* Michaelis-Menten constant for CO_2, and g_i is the CO_2 transfer conductance from the substomatal air spaces to the carboxylation sites.

I will use an idealised representation of the A-C_i curve shown in Fig. 3.2a to illustrate

the theoretical principle upon which I based my determination of the C_i cut-off point where the transition from RuBP-saturated (Eqn A.2) to RuBP-limited (Eqn A.3) photosynthesis is expected to take place at 22 °C for Douglas-fir shoots exposed to a saturating diffuse irradiance. In this example (Fig. A.1), the transition takes place at around 480 μbar, between data points 6 & 7, after which the difference between the measured RuBP-limited A_n and that predicted from Eqn A.2 increases with C_i. Hence, when moving the C_i cut-off point to higher values into the RuBP-limited portion of the A-C_i curve, the curvature of the remaining lower curve section is increased accordingly, and, consequently, the g_i value estimated from Eqn A.2 rises proportionally (see theory expounded in Chapter 1). Conversely, if the C_i cut-off point is lowered into the RuBP-saturated A-C_i curve portion, the curvature of the remaining higher curve section is reduced and the g_i value estimated from Eqn A.3 decreases proportionally.

Table A.1 gives the summary of model parameters fitted by Eqns A.2 and A.3 using the C_i cut-off points numbered 3 to 9 in Fig. A.1a (see table footnote for details). As shown in Fig. A.1b, the correct C_i cut-off point is found where the two g_i values fitted by Eqns A.2 and A.3 converge. Thus, in non-ideal cases, provided that g_i is sufficiently conserved over the respective domain of the RuBP-saturated and RuBP-limited A-C_i curve portions, the correct C_i cut-off point is expected to be found where the difference between the two g_i values fitted by Eqns A.2 and A.3 is minimised.

In this study, in the majority of cases, the difference between the two g_i estimates was minimised when the C_i cut-off point was set around 400 μbar. Corresponding model parameters derived as described in this appendix were then used as starting values for the subsequent concurrent iteration of Eqns A.2 & A.3 (see Chapter 3 for details).

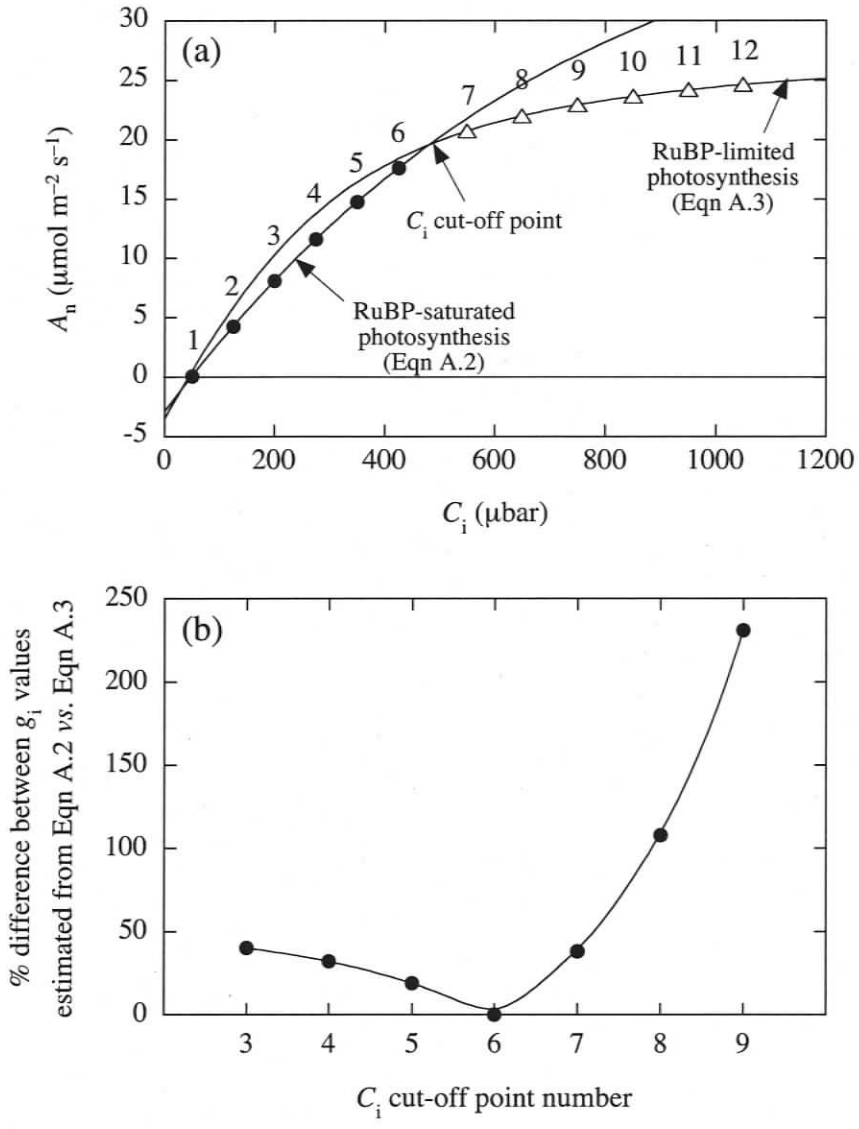

Figure A.1 (a) Idealised representation of the net CO_2 assimilation rate (A_n) *vs.* intercellular CO_2 concentration (C_i) relationship shown in Fig. 3.2a; the RuBP-saturated (solid circles numbered 1 to 6) and RuBP-limited (open triangles numbered 7 to 12) A_n values were calculated from Eqns A.2 and A.3, respectively, with g_i = 0.119 mol m^{-2} s^{-1}, R_d = 1.12 μmol m^{-2} s^{-1}, V_{cmax} = 55.3 μmol m^{-2} s^{-1}, and J = 118.1 μmol m^{-2} s^{-1}. (b) Difference between g_i estimates obtained from least-squares regression fits of Eqn A.2 *vs.* Eqn A.3 to the ideal A-C_i curve shown in panel (a) resulting from potential errors in the determination of the C_i cut-off point marking the transition between RuBP-saturted and RuBP-limited photosynthesis (see Table A.1 for details).

Table A.1 Sensitivity of non-rectangular hyperbola model parameters (true values indicated in bold characters) to errors in the determination of the intercellular CO_2 concentration (C_i) marking the transition between RuBP-saturated and RuBP-limited photosynthesis for the ideal A-C_i curve shown in Fig. A.1a

C_i cut-off point†	R_d (μmol m^{-2} s^{-1})	g_i (Eqn A.2) (mol m^{-2} s^{-1})	g_i (Eqn A.3) (mol m^{-2} s^{-1})	V_{cmax} (μmol m^{-2} s^{-1})	J (μmol e^- m^{-2} s^{-1})
3	1.12	0.119	0.085	55.3	121.6
4	1.12	0.119	0.090	55.3	120.7
5	1.12	0.119	0.100	55.3	119.5
6	**1.12**	**0.119**	**0.119**	**55.3**	**118.1**
7	1.18	0.166	0.120	48.9	118.4
8	1.25	0.249	0.120	45.1	118.7
9	1.31	0.401	0.121	42.8	118.9
9	1.68	–	0.125	–	120.5
9	0.56	–	0.114	–	115.7

The first estimate of the CO_2 transfer conductance (g_i) as well as the maximal carboxylation rate (V_{cmax}) and the mitochondrial respiration in the light (R_d) values were obtained by fitting Eqn A.2 to the data including and falling below the indicated C_i cut-off point, after which the second estimate of g_i and the value for the photochemical electron transport rate (J) were obtained by fitting Eqn A.3 to the remainder of the data. The last two rows of the table show the effect of a ± 50% deviation of R_d from its true value on the estimates of g_i and J obtained from Eqn A.3.

†See successive numbering of data points in Fig. A.1a.

Alternative estimate of g_i not requiring prior determination of a C_i cut-off point

Recently, Niinemets *et al.* (2006) showed that the overall effect of large errors in R_d (e.g. ± 50%) on g_i estimation based on Eqn A.3 (more specifically Eqn 3.6 solved for g_i) is minor for leaves that have inherently low g_i (e.g. < 0.2 mol m^{-2} s^{-1}). This was also demonstrated above for a Douglas-fir shoot with an estimated g_i of 0.119 mol m^{-2} s^{-1}, showing less than 5% variation in g_i for ± 50% deviation of R_d from its "true" value (see Table A.1). To obtain alternative estimates of g_i requiring no *a priori* determination of a C_i cut-off point for the present study, I first derived a second set of R_d estimates for the shoots by fitting the original light response curve data ($I \geq 50$ μmol m^{-2} s^{-1}) as

$$A_j = \frac{I\alpha\Phi_{CO_2} + A_{max} - \sqrt{(I\alpha\Phi_{CO_2} + A_{max})^2 - 4\Theta I\alpha\Phi_{CO_2}A_{max}}}{2\Theta} - R_d \qquad (A.4)$$

where A_{max} is the maximal, RuBP-limited gross CO_2 assimilation rate, Φ_{CO2} is the quantum yield of CO_2 assimilation, I is the incident photosynthetic photon flux density, α is the needle absorptance, and Θ is the convexity of the rectangular hyperbola. I then refitted Eqn A.3 to the end points of the A-C_i curves' RuBP-limited portion using the new estimates of R_d. Since the measured A_j from the light response curves approached CO_2 saturation at low irradiance, I assumed that the R_d values fitted by Eqn A.4 were little affected by differences in C_c. As predicted from the aforementioned sensitivity analyses, since the alternative estimates of R_d differed from the initial values by ± 20% at most (13% higher in average), I found excellent agreement between the initial g_i estimates derived from concurrent fitting of Eqn A.2 & A.3 and the alternative g_i estimates based on the end points of the RuBP-limited A-C_i curve portion (Fig. A.2). Taken together, these results suggest that my choice of C_i cut-off point for the CO_2 response curve of Douglas-fir shoots is realistic, as are my estimates of g_i and other model parameters.

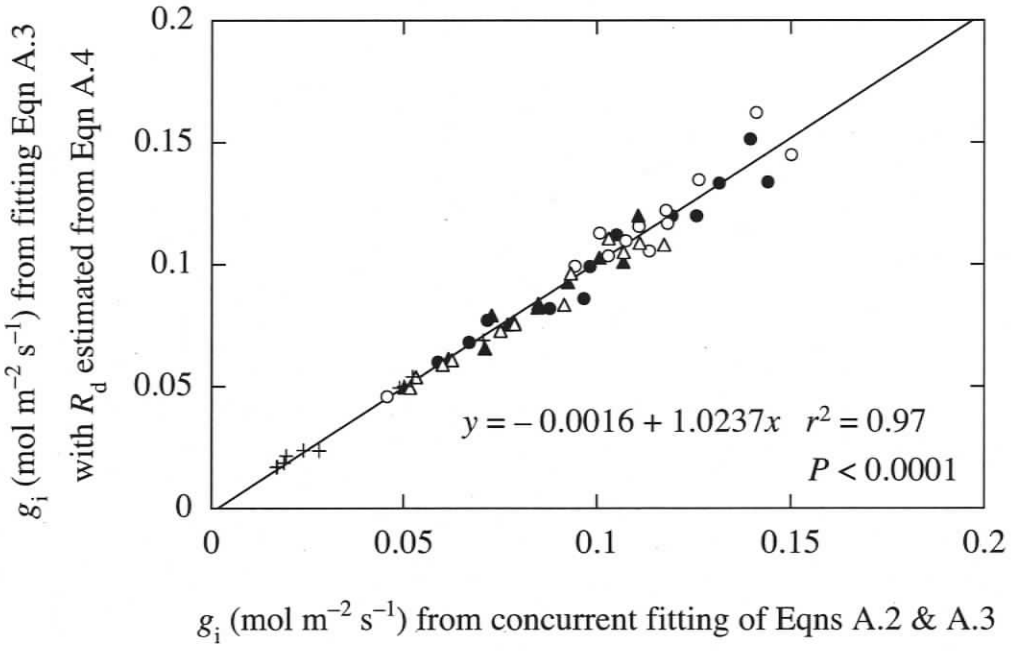

Figure A.2 Comparison between the CO_2 transfer conductance (g_i) of Douglas-fir shoots estimated from concurrent fitting of Eqns A.2 & A.3 to the RuBP-saturated and RuBP-limited A-C_i curve portions and that estimated from fitting Eqn A.3 to the end points of the A-C_i curves' RuBP-limited portion using alternative estimates of the rate of mitochondrial respiration in the light (R_d) based on Eqn A.4 (see text for details).

REFERENCES

Farquhar G.D., von Caemmerer S. & Berry J.A. (1980) A biochemical model of photosynthetic CO_2 assimilation in leaves of C_3 species. *Planta* **149,** 78–90.

Niinemets Ü., Cescatti A., Rodeghiero M. & Tosens T. (2006) Complex adjustments of photosynthetic potentials and internal diffusion conductance to current and previous light availabilities and leaf age in Mediterranean evergreen species *Quercus ilex*. *Plant, Cell and Environment* **29,** 1159–1178.

Appendix B

Transfer conductance in second growth Douglas-fir (*Pseudotsuga menziesii* (Mirb.) Franco) canopies

Plant, Cell and Environment (2003) **26**, 1215–1227

Transfer conductance in second growth Douglas-fir (*Pseudotsuga menziesii* (Mirb.)Franco) canopies

C. R. WARREN[1,*], G. J. ETHIER[1], N. J. LIVINGSTON[1], N. J. GRANT[1], D. H. TURPIN[2], D. L. HARRISON[1] & T. A. BLACK[3]

[1]*Centre for Forest Biology, Department of Biology, Uni ersity of Victoria, PO Box 3020 Stn Csc, Victoria BC V8N 3 N5, Canada,* [2]*Department of Biology, Uni ersity of Victoria, PO Box 3020 Stn Csc, Victoria BC V8N 3 N5, Canada and* [3]*Faculty of Agricultural Sciences, 135–2357 Main Mall, Uni ersity of British Columbia, Vancou er BC V6T 1Z, Canada*

ABSTRACT

The internal conductance from intercellular spaces to the sites of carboxylation (g_i) has only been measured in a few tree species and not in conifers, despite the fact it may impose a large limitation on photosynthesis. The present study provides the first estimates of g_i for a coniferous species, and examines variation in g_i with height and its relationships to anatomical, biochemical and physiological traits. Measurements were made on upper and lower canopy current-year needles of 50-year-old Douglas-fir (*Pseudotsuga menziesii* (Mirb.) Franco). Needle thickness and specific leaf area decreased by 30% from the top to bottom of the canopy. These anatomical/morphological changes were accompanied by modest variation in allocation of N to chlorophyll and the chlorophyll *a*/*b* ratio. Allocation of N to Rubisco did not vary with height, but the ratio of Rubisco to chlorophyll did owing to the aforementioned changes in allocation to chlorophyll. The value of g_i was estimated in one tree from concurrent measurements of carbon isotope discrimination and net photosynthesis. To examine the variation in g_i among trees a second independent method based on day respiration and the difference between the chloroplastic and intercellular photocompensation points (photocompensation point method) was used. Estimates of g_i obtained by the two methods agreed well with values varying between 0.14 and 0.20 mol m^{-2} s^{-1}. It is estimated that g_i limits photosynthesis by approximately 20% as compared to an approximately 30% stomatal limitation (under well-watered conditions). The value of g_i scaled approximately with maximum rates of photosynthesis, which were significantly greater in upper canopy needles. Nevertheless, g_i did not vary significantly with canopy height, owing to greater variability in g_i than photosynthesis.

Key-words: carbon isotope discrimination; chlorophyll; internal resistance; needle anatomy; needle morphology; photocompensation point; photosynthesis; Rubisco.

Correspondence C, R, Warren. Fax: +61 3 5321 4277; e-mail: crwarren@unimelb.edu.au

**Present address: Forest Science Centre, Water Street, Creswick VIC 3363, Australia.*

Abbre iations: A, rate of photosynthesis; a_i, carbon isotope fractionation during diffusion/hydration into water; A_n, rate of light-saturated photosynthesis measured at C_a = 360 μmol mol^{-1}; A_{pn}, rate of photosynthesis assuming g_i and g_s are infinite (i.e. at a C_c of 360 μmol mol^{-1}); A_{on}, rate of photosynthesis assuming infinite g_i and g_s as measured (i.e. at a $C_c = C_i$); b, carbon isotope fraction due to Rubisco and PEP carboxylation; C_a, ambient CO_2 concentration; C_e, CO_2 concentration of air entering chamber; C_i, intercellular CO_2 concentration; C_i*, intercellular CO_2 concentration at which the chloroplastic CO_2 concentration = Γ*; C_c, chloroplastic CO_2 concentration; Δ_{obs}, observed carbon isotope discrimination; Δ_i, carbon isotope discrimination estimated for a shoot with infinite transfer conductance; δ_o, carbon isotope discrimination of air leaving chamber without a shoot enclosed; δ_e, carbon isotope discrimination of air leaving chamber with a shoot enclosed; f, carbon isotope fractionation due to photorespiration; Γ*, CO_2 compensation concentration in the absence of mitochondrial respiration (photocompensation point); G, CO_2 compensation concentration; K_c and K_o, Michaelis–Menten constants for RuBP carboxylation and oxygenation, respectively; PAR, photosynthetically active radiation; R_d, mitochondrial respiration in the light (day respiration); g_i, transfer conductance; g_m, mesophyll conductance (the initial slope of the A versus C_i curve); g_s, stomatal conductance; L_i, relative limitation to photosynthesis due to transfer conductance; L_s, relative limitation of photosynthesis due to stomatal conductance; O_c, O_2 concentration in chloroplasts; RSD, relative standard deviation (SD/mean); s, projected leaf area; SLA, specific leaf area – projected area per unit dry mass; u, molar flow rate through chamber; V_{cmax}, maximum rate of carboxylation.

INTRODUCTION

For photosynthesis to occur, CO_2 must diffuse from the atmosphere to the sites of carboxylation. The concentration of CO_2 at the sites of carboxylation (C_c) is less than atmospheric (C_a) owing to a series of gas-phase (air) and liquid-phase (mesophyll cell) resistances. In the gaseous phase, CO_2 must diffuse across a boundary layer in the air above the foliage surface, through a stomatal opening, and across intercellular air spaces in the substomatal cavity. In the

liquid phase there are resistances as CO_2 enters the liquid phase at the surface of mesophyll cells (Henry's law), as CO_2 diffuses within the cell to the chloroplast membrane, and from there to the sites of carboxylation (Aalto & Juurola 2002). It has been assumed that the concentration of CO_2 in the substomatal cavities (C_i, e.g. as measured by gas exchange) is uniform throughout the leaf and thus the same as C_c. There is mounting evidence that this assumption is invalid and C_c may be significantly less than C_i (Evans *et al.* 1986; Parkhurst & Mott 1990; Lloyd *et al.* 1992; Epron *et al.* 1995). In a silver birch leaf, for example, 61.4% of the modelled total resistance to CO_2 diffusion was from the intercellular air spaces to the centre of chloroplasts, whereas stomatal and boundary layer resistances only accounted for 38.6% of the total resistance (Aalto & Juurola 2002). Transfer conductance (g_i) describes this drawdown in CO_2 concentration between C_i and C_c. Low g_i may impose a significant limitation on photosynthesis (Epron *et al.* 1995), yet it has only been measured in a few tree species and not in any conifers.

Leaf morphology and anatomy are often correlated with g_i (e.g. Vitousek, Field & Matson 1990; Evans *et al.* 1994; Kogami *et al.* 2001), although this correlation may be weak (e.g. Hanba, Kogami & Terashima 2002). The potential for CO_2 diffusion in the liquid phase is a function of cell wall thickness (Nobel 1991) and the surface area of mesophyll cells or chloroplasts exposed to the intercellular air spaces (Laisk, Oja & Rahi 1970; Nobel, Zaragoza & Smith 1975; Nobel 1991; Evans *et al.* 1994). In 'typical' mesophytic leaves that are relatively thin, porous and with stomata on both surfaces, these liquid phase resistances are the principal determinants of g_i (Evans *et al.* 1994). If mesophyll porosity is small and foliage is hypostomatous, gas phase conductance is correspondingly small and may be a significant component of g_i (Parkhurst & Mott 1990; Syvertsen *et al.* 1995). In *Citrus* and *Macadamia*, for example, Syvertsen *et al.* (1995) concluded that low mesophyll porosity and a relatively long path from the stomatal cavity to mesophyll cell surface resulted in a low gas phase conductance and this accounted for about half of g_i.

In closed canopies of Douglas-fir (*Pseudotsuga menziesii* [Mirb.] Franco) there is a large decrease in light intensity with depth in the canopy (e.g. Bond *et al.* 1999; Lewis *et al.* 2000; Parker, Davis & Chapotin 2002). Needles and shoots acclimate to this light environment anatomically, morphologically and physiologically (e.g. Aussenac 1973; Bond *et al.* 1999; Lewis *et al.* 2000). In one study with Douglas-fir, for example, the specific leaf area (SLA, leaf area per unit dry mass) of needles increased by 86% from the top of the canopy to the bottom (Bond *et al.* 1999). We might expect therefore that g_i would vary through the canopy of Douglas-fir given the relationships among g_i, anatomy and morphology, yet this hypothesis has not been tested.

Two separate objectives were considered in this study. Firstly, we used an established method (estimation of g_i from carbon isotope fractionation during photosynthesis – Evans *et al.* 1986) to determine the variation in g_i of upper and lower canopy current-year needles from a dominant 50-year-old Douglas-fir tree (i.e. within-tree variation). As potential determinants of g_i, we examined variation in needle anatomy and morphology. The concentrations of nitrogen, Rubisco and chlorophylls (Chls) were also measured to explore acclimation to the light environment and explain any differences in rates of photosynthesis. With these data we tested two hypotheses: (1) g_i is less in sunlit needles than in shaded needles owing to differences in thickness and the pathlength for CO_2 diffusion; (2) variation in photosynthetic rates are related to g_i (e.g. Lloyd *et al.* 1992; Evans *et al.* 1994) and concentrations of N and Rubisco (e.g. Field & Mooney 1986). Lastly, we used a new method (estimation of g_i from the difference between the chloroplastic and intercellular photocompensation points – Γ^* and C_i^*, respectively, – Peisker & Apel 2001) to obtain estimates of g_i for upper and lower canopy needles from many trees and thereby determine variation in g_i at the canopy level.

MATERIALS AND METHODS

Study site

Measurements were made on an even-aged 50-year-old stand of 33 m tall Douglas-fir located approximately 10 km south-west of Campbell River, on the east coast of Vancouver Island, British Columbia, Canada (49°52′ N, 125°20′ W, 300 m above sea level). The site is described in detail elsewhere (Humphreys *et al.* 2002). Briefly, the stand is about 80% second growth coastal Douglas-fir and 20% western red-cedar (*Thuja plicata* Donn) and western hemlock [*Tsuga heterophylla* (Raf.) Sarg.] with a sparse understorey dominated by salal (*Gaultheria shallon* Pursh), Oregon-grape (*Bereris ner osa* Pursh), vanilla-leaf deer foot [*Achyls triphylla* (Smith) DC].

Sampling protocol

Shoot collection and photosynthesis measurements were made on three separate occasions from late-September to mid-October shoots collected for estimation of g_i by the isotopic method were taken from the lower canopy (whorls 17–20, as numbered from top) and the upper canopy (whorls 4–8 from top) of a 34 m dominant tree adjacent to a canopy access scaffold tower. The mean photosynthetically active radiation (PAR) for lower canopy whorls was approximately 10% of full sunlight. A total of eight upper and eight lower canopy current-year shoots were measured over two field trips. For estimation of g_i by the photocompensation point method, a total of six upper and six lower canopy current-year shoots were collected from 12 different trees accessed with static climbing ropes. *in situ* gas exchange measurements were impractical owing to the technical difficulties in accessing the shoots, and thus all measurements were made on excised shoots. Branches, approximately 1 m in length, were cut from the trees,

wrapped in a plastic bag to reduce transpiration and transported to ground level where they were re-cut under water twice. This procedure usually took less than 15 min, and preliminary experiments done on the scaffold tower established that gas exchange of shoots was unaffected by excision (data not shown).

Photosynthesis measurement system and gas collection apparatus

Gas exchange measurements were made with an open gas exchange system (LI-6400; Li-Cor, Lincoln, NE, USA) and a clear cylindrical chamber (6400–05 conifer chamber, Li-Cor) nested into a 15-cm diameter integrating sphere to minimize mutual shading among needles (Fig. 1). The integrating sphere, similar in design to that of Serrano, Gamon & Berry (1997), was illuminated by a single halogen globe (JCR12V-100 W; Ushio Inc., Tokyo, Japan) and cooled by blowing cold air over its outer and inner surfaces. Light intensity was controlled with a rheostat. The angular two-sided PAR distribution measured around the shoot axis inside the clear chamber was within 5% of the measured average (i.e. a nearly isotropic diffuse light field). All gas exchange measurements were done at 22 ± 1 °C and 50–70% relative humidity.

For concurrent measurements of photosynthesis and instantaneous carbon isotope discrimination, reference gas was supplied from a cylinder containing a certified mixture of 443 μmol mol^{-1} CO_2 in air (Praxair, Mississauga, Ontario, Canada). To minimize problems with low humidity of the reference gas causing stomatal closure it was at times necessary to humidify this gas using a portable dew point generator (LI-610; Li-Cor). This did not affect the carbon isotope composition of gas entering the chamber (data not shown). The lines from the cylinder to LI-610 and from the LI-610 to LI-6400 were vented to the atmosphere through a T-piece and flowmeter (F1 and F2 in Fig. 1). The flow rate of air from the cylinder, controlled by a throttle, was always at least 400 mL min^{-1} in excess of that required by the LI-610 pump to avoid back diffusion of gases. In a similar fashion, the air pump of the LI-610 was manipulated so as to maintain flow rates at least 400 mL min^{-1} in excess of that required by the LI-6400 pump. The molar flow rate through the chamber was varied between 250 and 750 μmol s^{-1} depending on the rate of photosynthesis of the shoot. Sample gas was collected in-between the chamber exhaust and the match valve of the LI-6400 chamber head. The sample gas was collected in 2 L glass gas-sampling flasks previously purged with pure nitrogen gas. The flasks were fitted with Teflon stopcocks (V3 and V4) and ground glass joints and were connected to the chamber exhaust by Tygon tubing (Saint–Gobain, Akron, OH, USA) and Swagelok fittings (Swagelok Co., Cleveland, OH, USA). Two three-way valves (V1 and V2) directed gas either directly to the match valve, or to the match valve via the 2 L glass flask and a flowmeter (F3). When gas was not being collected the sampling flask was bypassed. Gas samples were collected when measured gas exchange was stable, this was achieved by opening the stopcocks (V3 and V4) and manipulating the three-way valves (V1 and V2) to direct gas through the sampling flask. The flowmeter F3 was used to check for leaks in the system. Upon collecting a gas sample, the sampling flask was bypassed, stopcocks (V3 and V4) were closed and the flask was set aside for later analysis. Refer-

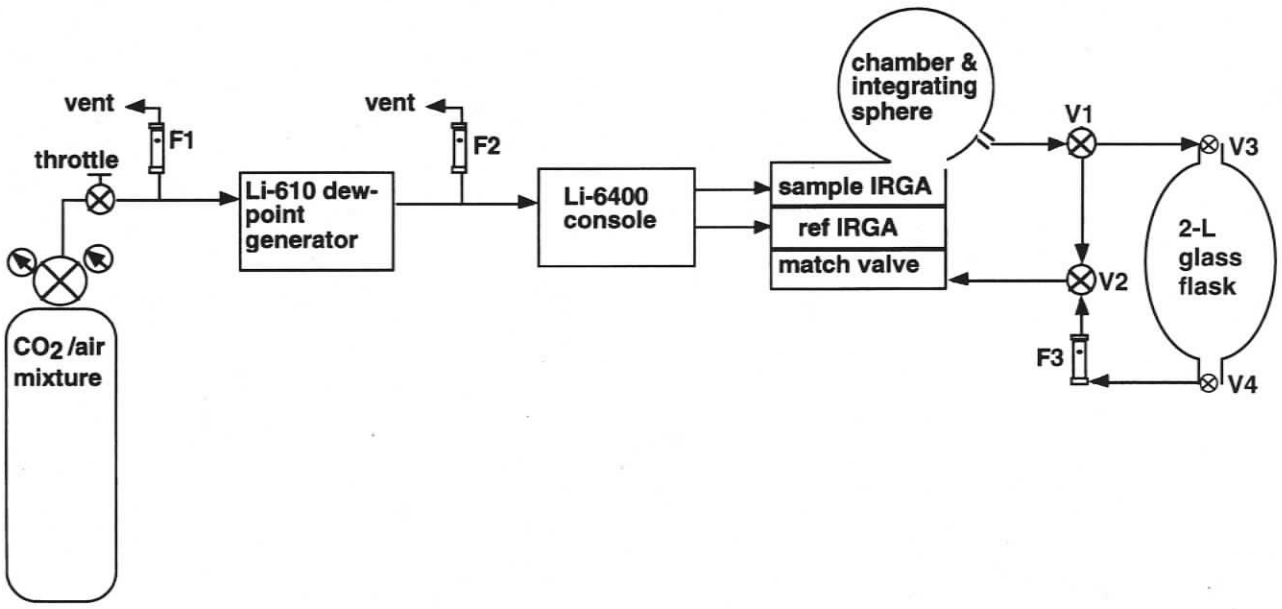

Figure 1. Schematic diagram of the gas exchange system used for measurement of photosynthesis and collection of gas samples for carbon isotope measurement. F1, F2 and F3 are flowmeters. V1 and V2 are three-way valves. V3 and V4 are Teflon stopcocks.

ence gas samples were collected without a shoot in the chamber. At least four reference samples were collected each day, the $\delta^{13}C$ of replicate reference samples differed by less than 0.2‰. Preliminary experiments established that the flasks were airtight and $\delta^{13}C$ of air samples did not change significantly between their collection and analysis (data not shown).

Experimental protocol

A section of the shoot containing only current year needles was enclosed in the shoot chamber and acclimated at a light-saturating PAR (approx. 1500 μmol m^{-2} s^{-1}) until rates of photosynthesis and transpiration were steady, at which time the light-saturated rate of photosynthesis (A_n) was recorded. Following this, measurements of gas exchange proceeded according to the method used to estimate g_i. For the isotopic method, continuous photosynthesis measurements were made and sample gas collected over a period of 8–15 min, to ensure that the flasks were flushed of N_2 and equilibrated with the sample gas. For each shoot we measured photosynthesis and collected gas samples at three different light intensities. For the photocompensation point method, CO_2-response curves were generated at saturating and limiting irradiance, respectively (approx. 1500 and 150 μmol m^{-2} s^{-1} PAR). These light intensities were chosen following preliminary trials to ensure maximum separation of the response curves while maintaining a similar degree of inhibition of dark respiration in the light (data not shown). Following gas exchange measurements, needles were removed from shoots and placed in liquid N. The total mass of each sample was measured and a subsample taken for determination of projected area (Li-3100 leaf area meter; Li-Cor). Gas exchange parameters were calculated on a projected area basis with the equations of von Caemmerer & Farquhar (1981).

Data were not corrected for diffusion of CO_2 into and out of the leaf chamber because this was insignificant with our experimental set-up. Preliminary experiments established that with a molar flow rate of 250 μmol s^{-1} (the lowest flow rate used in our experiments) there was never more than 2 μmol mol^{-1} diffusion of CO_2 into an empty chamber maintained at 50 μmol m^{-1} CO_2.

Analysis of stable carbon isotope composition

The set-up was similar to other $\delta^{13}C$-CO_2 analysis techniques using continuous flow, isotope ratio mass spectrometry (CF-IRMS; e.g. Miller *et al.* 1999) with a Valco six-port valve (Valco Instruments Co., Houston, TX, USA) used to alternately load and flush sample loop with an air sample. A separate pump down/expansion system consisting of a one-quarter inch outside diameter glass 'T' tube connected to one of the sample flask stopcocks via a 14/35 female ground glass joint, a rotary vacuum pump, and a Cajon Ultra-Torr union (Swagelok Co.) fitted with a butyl rubber septa, respectively, allowed the syringe removal of an aliquot of air from the 2 L glass sample flask and the loading of the sample loop prior to injection to a CF-IRMS system (Finnigan MAT 252; ThermoFinnigan, Bremen, Germany). The glass T was pumped down with the rotary pump, the system was isolated from the pump via a bellows valve and the valve to the sample flask opened. A helium-flushed syringe was used to draw and mix gas from the flask back and forth via a sample loop to the syringe barrel. The gas was then allowed to equilibrate for 1 min. The 1 mL sample was flushed from the loop by helium carrier gas and cryofocused in liquid nitrogen before its release into the gas chromatograph column (0.32 mm × 30 m GS-Q). The Ni/NiO combustion reactor normally used for the IRMS analysis of organics was bypassed; instead the gas stream was directed via a four-way switching valve (backflush valve) and Nafion® water trap (DuPont, Fayetteville, NC, USA) directly to the ion source. The backflush valve was used to divert N_2O (a contaminant at mass 44) to waste before the elution of CO_2. This technique routinely yields 95% confidence limits about the mean of 0.1‰ for $n = 20$ expansions and injections from the same flask (N. Grant & M. Eek, unpublished results).

Estimation of g_i by the isotopic method

Carbon isotope discrimination by the shoot (Δ_{obs}) was calculated as described in equation A15 of Evans *et al.* 1986):

$$(\Delta_{obs}) = \xi(\delta_o - \delta_e)/(1 + \delta_o - \xi[\delta_o - \delta_e]) \quad (1)$$

where δ_o and δ_e are the carbon isotope composition ($^{13}C/^{12}C$) of air leaving the chamber with (δ_o) or without (δ_e) a shoot enclosed. Carbon isotope composition of sample air was expressed against the carbon isotopic composition of the Pee Dee Belemnite formation (PDB), where $\delta = 1000\ [(({}^{13}C_{sample}/{}^{12}C_{sample})/({}^{13}C_{PDB}/{}^{12}C_{PDB})) - 1]$. $\xi = uC_e/(sA)$ where u is the molar flow rate through the chamber, C_e is the concentration of CO_2 entering the chamber, A is the rate of photosynthesis and s the projected leaf area.

The value of g_i was estimated from the equation:

$$\Delta_i - \Delta_{obs} = A/C_a\,(b - a_i)/g_i \quad (2)$$

where Δ_i is the expected carbon isotope discrimination when g_i is infinite and fractionations due to photorespiration and dark respiration are zero (see below), C_a is the CO_2 concentration in the ambient air, a_i is the carbon isotope discrimination during CO_2 diffusion/hydration into water (1.8‰), and b is the carbon isotope discrimination caused by Rubisco and PEP carboxylase (30‰). The value of g_i was calculated from Eqn 2 for each measurement and a mean was calculated for each shoot (Evans *et al.* 1994).

In our simplified equation for carbon isotope discrimination we ignored the effects of photorespiration and dark respiration. This is unlikely to bias our results because the effect of fractionations due to photorespiration on Δ are governed by Γ^*/C_c. This term will be near constant across a wide range of assimilation rates because temperature (and thus Γ^*) was held constant. Similarly, the effect of dark

respiration on Δ is given by R_d/V_c and because dark respiration rates are low, dark respiratory inputs would only become significant when rates of CO_2 assimilation were very low (Gillon & Griffiths 1997).

To obtain gas exchange parameters for calculation of g_i, 30 s gas exchange measurements were averaged over the duration that gas was being collected. Gas exchange parameters were not significantly different when calculated by integrating photosynthesis-weighted values because the measured gas exchange parameters varied by less than 5% between the beginning and end of the period during which gas was collected.

Estimation of g_i by the photocompensation point method

We estimated C_i^* and R_d from the intersection of the initial linear portion of the two CO_2-response curves generated at different light intensities (Laisk 1977). The original formulation of Laisk (1977) assumes the drawdown in CO_2 concentration between substomatal cavities and the chloroplast is negligible (i.e. g_i is infinite). If one considers finite g_i, then the Laisk method measures the intercellular compensation point (C_i^*) which is related to Γ^* by R_d and g_i (von Caemmerer & Evans 1991; Peisker & Apel 2001):

$$C_i^* = \Gamma^* - R_d/g_i \quad (3)$$

Following Eqn 3, a mean Γ^* was determined from the y-intercept of a C_i^* versus R_d plot. Having determined Γ^*, g_i was calculated for individual shoots as:

$$g_i = R_d/(\Gamma^* - C_i^*) \quad (4)$$

Estimation of V_{cmax} from the CO_2 response of photosynthesis

According to the photosynthesis model of Farquhar, von Caemmerer & Berry (1980), the light-saturated and CO_2-limited rate of net CO_2 assimilation is expressed as:

$$A = \{V_{cmax}(C_c - \Gamma^*)/[C_c + K_c(1 + O_c/K_o)]\} - R_d \quad (5)$$

where V_{cmax} is the maximum rate of carboxylation, K_c and K_o are the Michaelis–Menten constants for RuBP carboxylation and oxygenation, respectively, R_d is the rate of daytime (non-photorespiratory) respiration, O_c and C_c are the chloroplastic O_2 and CO_2 concentrations, respectively. O_c was assumed to be 210 mmol mol^{-1}. Differentiating Eqn 5 and evaluating at $C_c = \Gamma^*$ yields:

$$dA/dC_c = V_{cmax}/[\Gamma^* + K_c(1 + O_c/K_o)] \quad (6)$$

Replacing dA/dC_c by $g_m/(1 - g_m/g_i)$ and solving for V_{cmax} gives:

$$V_{cmax} = g_m[\Gamma^* + K_c(1 + O_c/K_o)]/(1 - g_m/g_i) \quad (7)$$

where g_m is the initial slope of the A versus C_i curve, usually termed the mesophyll conductance. Under the assumption of infinite transfer conductance, dA/dC_c equals g_m and Eqn 7 reduces to:

$$V_{cmax} = g_m[\Gamma^* + K_c(1 + O_c/K_o)] \quad (8)$$

Values for the kinetic constants K_c and K_o at 25 °C were taken from the *in itro* values of freshly ruptured spinach chloroplasts in Farquhar *et al.* (1980) and were adjusted to 22 °C according to the temperature response functions of Badger & Collatz (1977).

Estimation of C_c and relative limitation on photosynthesis imposed by g_i and g_s

Using estimated g_i and measured A and C_i, C_c was calculated as:

$$C_c = C_i - (A/g_i) \quad (9)$$

The value of C_c was calculated for each A and C_i. The limitation of A imposed by finite g_i and g_s was based on estimates of the potential rate of photosynthesis assuming these conductances were either infinite or as measured (Farquhar & Sharkey 1982). Estimates of A were made using light-saturated CO_2-response curves and measured g_i and g_s. Rates of net photosynthesis were estimated assuming g_i and g_s were as measured (A_n, the light-saturated rate of photosynthesis at $C_a = 360$ μmol mol^{-1}), assuming g_i was infinite and g_s as measured (A_{il}, the light-saturated rate of photosynthesis at $C_c = C_i$), or assuming g_i as measured and g_s was infinite (A_{sl}, the light-saturated rate of photosynthesis at $C_i = 360$ μmol mol^{-1}) (see Fig. 3). The relative limitations due to internal resistances (L_i) and stomatal resistances (L_s) were estimated as:

$$L_i = (A_{il} - A_n)/A_{il} \quad (10)$$

$$L_s = (A_{sl} - A_n)/A_{sl} \quad (11)$$

Measurement of N, chlorophylls, soluble proteins and Rubisco

Total N of freeze-dried and ground samples was measured by Dumas combustion with an elemental analyser (Flash EA 1112 Series; ThermoQuest, Rodano, Italy). The Chls were extracted with *N*,*N*-dimethylformamide and analysed spectrophotometrically using the extinction coefficients of Wellburn (1994).

Soluble proteins were extracted at 0–4 °C by grinding 50 mg (fresh mass) of frozen leaf tissue in 400 μL of grinding buffer [133 mM Tris pH 8.0, 25% (v/v) glycerol, 34 mM DL-dithiothreitol, 2% (w/v) polyvinylpolypyrolidone (PVPP) using a Tissue Tearor® Homogenizer (BioSpec Products, Bartlesville, OK, USA]. The homogenate was mixed with 100 μL of 10% (w/v) sodiom dodecyl sulphate (SDS), and vortexed for 4 min at 0–4 °C before being centrifuged at 10 000 *g* for 5 min (4 °C). The pellet was re-extracted three times with modified grinding buffer (as above but without PVPP and diluted 4 : 1 with 10% SDS). The supernatants were pooled and used for protein analysis.

The total content of soluble proteins was determined on extracts purified by precipitation with trichloroacetic acid

(TCA) in the presence of KCl (Carraro *et al.* 1994). Protein pellets were re-suspended in 1 volume of 2% SDS in 0.06 N NaOH. This procedure co-extracted substances that adversely affected both the Bicinchoninic acid protein assay (No. B-9643; Sigma-Aldrich Ltd, Oakville, ON, Canada) and the Lowry RC DC protein assay (No. 500–0120; Bio-Rad Laboratories, Philadelphia, PA, USA). Owing to these problems, the concentration of soluble proteins was determined by SDS-polyacrylamide gel electrophoresis with bovine albumen standards (No. A-7906; Sigma-Aldrich) and Coomassie blue stain [0.1% Coomassie Blue R-250 in 40% (v/v) methanol, 10% (v/v) acetic acid]. The protein content of each lane was determined densitometrically with NIH image analysis software (NIH, Bethesda, MD, USA).

Rubisco was quantified by enzyme-linked immunosorbent assaay, essentially as described by Catt & Millard (1988) but with minor modifications. Re-suspended protein pellets were diluted 1 : 1000 with carbonate buffer (50 mM Na_2CO_3, 50 mM $NaHCO_3$, 0.1 mM $MgCl_2$. $6H_2O$, pH 9.4), triplicate100-μL aliquots were applied to a Costar high binding microtitre plate (Costar 9018; Corning Costar Corp., Corning, NY, USA) and left to incubate in darkness for 18 h at 4 °C. Plates were rinsed three times with Tris/NaCl (10 mM Tris-HCl, pH 7.2, 150 mM NaCl), blocked for 1 h with Tris/NaCl containing 1% BSA (w/v) (Sigma-Aldrich), and then washed with the blocking solution containing 0.01% (v/v) Tween 20 (Sigma-Aldrich). Wells were incubated for 2 h with polyclonal antibodies prepared from sheep injected with purified wheat Rubisco, diluted 1 : 1000 (v/v) in blocking solution containing 0.01% Tween 20. Following three more washes, the plates were incubated for 1 h with the secondary antibody (donkey antirabbit IgG linked with alkaline phosphatase conjugate, A-5187; Sigma-Aldrich) diluted 1 : 300 (v/v) with wash buffer. After three more washes, colour development of the antibody complexes proceeded with the addition of 0.1% (w/v) *p*-nitrophenylphosphate (in carbonate buffer) and was stopped with the addition of 15 μL of 3 M NaOH. Plate absorbance was measured at 405 nm on a UVMax microplate reader (Molecular Devices Corporation, Sunnyvale, CA, USA) and the amount of Rubisco was calculated from the linear portion of the calibration curve. Our laboratory standard was partially purified spinach Rubisco (Sigma-Aldrich), which was standardized against pure wheat Rubisco.

Light microscopy

Eight shoots from the September sampling (four upper canopy, four lower canopy) were used for anatomical measurements. One needle per shoot was fixed in formalin/acetic acid/alcohol fixative and embedded in paraffin using Johansen's series dehydration schedule (Johansen 1940). Paraffin blocks were softened for 3–4 weeks with Gifford's softener and sectioned at 8 mm with a microtome. Transverse-sections were mounted on slides with Haupts, stained with Toluidine Blue CI 52040 (0.1% Toluidine blue in 2.5% sodium carbonate) (after Berlyn & Miksche 1976; modified by using Hemo-D to remove the wax instead of xylene) and the cover slip was mounted with Entellan. Needle width, needle thickness and area of the main tissue types were measured on five transverse-sections from the middle of each needle using a Zeiss Universal light microscope (Zeiss, Jena, Germany) with a Cohu video camera (Cohu, San Diego, CA, USA) and Optimas software (Optimas Corp., Bothell, WA, USA) or a Leitz Laborlux S light microscope (Leitz, Stuttgart, Germany). For each transverse-section we estimated the percentage of the total area occupied by the vascular bundle, epidermal tissue, hypodermal tissue and mesophyll tissue. Mesophyll porosity is the percentage of the mesophyll area that is air spaces, whereas whole-section porosity is the percentage of the whole section that is air spaces.

RESULTS

Foliage anatomy, morphology and biochemistry

In general there were few anatomical differences between upper and lower canopy needles. The primary difference being that needles from the upper canopy were approximately 30% thicker than those from the lower canopy (Table 1). There were small differences in the proportion of needle area occupied by vascular bundle, epidermal and mesophyll tissue.

Specific leaf area was approximately 30% less in upper canopy needles in comparison with lower canopy needles (Table 2). Needle contents of N, Chls, total soluble proteins and Rubisco were significantly greater in the upper canopy in comparison with the lower canopy when expressed on an area basis, but not per unit mass. The Chl *a*/*b* ratio was significantly greater in the upper canopy than the lower canopy, whereas the ratio of total Chls to N was greater in needles from the lower canopy compared with the upper

Table 1. Comparison of the anatomy of current-year needles from the lower and upper canopy of a single dominant Douglas-fir tree

Characteristic	Lower canopy	Upper canopy
Needle width (mm)	1.37 (0.06)	1.38 (0.02)
Needle thickness (mm)	0.45 (0.01)	0.59 (0.02)[a]
Vascular bundle area (%)	7.3 (0.4)	8.3 (0.2)[a]
Epidermis area (%)	7.2 (0.2)	5.9 (0.1)[a]
Hypodermis area (%)	4.3 (0.3)	4.5 (0.2)
Mesophyll area (%)	79.8 (0.2)	81.1 (0.1)[a]
Mesophyll porosity (%)	21.3 (0.7)	20.6 (1.2)
Whole-section porosity (%)	17.2 (0.5)	16.6 (1.0)

Transverse sections were obtained from the middle of needles. For each transverse section we estimated the percentage of the total area occupied by the vascular bundle, epidermal tissue, hypodermal tissue and mesophyll tissue. Mesophyll porosity is the percentage of the mesophyll area that is air spaces, while whole-section porosity is the percentage of the whole section that is air spaces. Data are means (1 SE) of four needles (five transverse sections per needle). [a]Significant differences ($P < 0.05$, Fisher's PLSD) between lower and upper canopy.

Table 2. Comparison of morphology and biochemistry of current-year needles from the lower and upper canopy of a single dominant Douglas-fir tree

Characteristic	Lower canopy	Upper canopy
Specific leaf area ($cm^2\ g^{-1}$)	72 (3)	50 (1)[a]
N ($g\ m^{-2}$)	1.7 (0.6)	2.56 (0.10)[a]
N ($mg\ g^{-1}$)	12.1 (0.3)	12.6 (0.3)
Chl $a+b$ ($g\ m^{-2}$)	0.44 (0.01)	0.49 (0.02)[a]
Chl $a+b$ ($mg\ g^{-1}$)	1.40 (0.07)	1.28 (0.05)
Chl a/b ($mol\ mol^{-1}$)	1.88 (0.02)	2.02 (0.03)[a]
Chl/N ($g\ g^{-1}$)	0.259 (0.008)	0.191 (0.004)[a]
Protein ($g\ m^{-2}$)	3.3 (0.1)	5.4 (0.5)[a]
Protein ($mg\ g^{-1}$)	23 (1)	26 (2)
Rubisco ($g\ m^{-2}$)	1.6 (0.2)	2.6 (0.1)[a]
Rubisco ($mg\ g^{-1}$)	12 (1)	12.8 (0.5)
Rubisco/protein (%)	51 (6)	51 (5)
Rubisco/Chl ($g\ g^{-1}$)	3.7 (0.4)	5.3 (0.3)[a]
Protein-N (% of total N)	32 (2)	35 (2)
Rubisco-N (% of total N)	16.1 (1.9)	16.9 (0.6)

Characteristics of needles collected in September were not significantly different from the October sampling ($P > 0.05$, Fisher's PLSD) and thus data from the two dates were combined. Data are means (1 SE, $n = 8$). [a]Significant differences ($P < 0.05$, Fisher's PLSD) between lower and upper canopy.

Table 3. Mean photosynthetic characteristics of current-year needles from the upper and lower canopy of a single dominant Douglas-fir tree

Characteristic	Lower canopy	Upper canopy
Isotopic method (one tree, $n = 8$)		
A_n ($\mu mol\ m^{-2}\ s^{-1}$)	8.4 (0.3)	10.6 (0.4)[a]
g_s ($mol\ m^{-2}\ s^{-1}$)	0.093 (0.004)	0.126 (0.005)[a]
g_i ($mol\ m^{-2}\ s^{-1}$)	0.16 (0.01)	0.20 (0.03)
C_c/C_i	0.75 (0.01)	0.73 (0.03)

Transfer conductance (g_i) was estimated from simultaneous measurement of carbon isotope discrimination and photosynthesis. Also indicated are light-saturated photosynthesis at $C_a = 360\ \mu mol\ mol^{-1}$ (A_n) and stomatal conductance (g_s). Owing to the fixed 443 $\mu mol\ mol^{-1}$ CO_2 supply used, C_a varied (384 ± 11 $\mu mol\ mol^{-1}$; mean ± SD, $n = 16$) among shoots and thus A_n was normalized to $C_a = 360\ \mu mol\ mol^{-1}$ based on the A/C_a responses of the 12 shoots used for the photocompensation point method (see Table 4). All data are means (SE) of eight replicate shoots. [a]Significant differences ($P < 0.05$, Fisher's PLSD) between lower and upper canopy.

canopy. The percentage of total N as soluble proteins (32–35%) and Rubisco (16–17%) did not vary with canopy height; however, the content of Rubisco per Chl was greater in the upper canopy compared with the lower canopy.

Within-tree variation of g_i – isotopic method

In the tree used for g_i determination by the isotopic method, the rate of photosynthesis at $C_a = 360\ \mu mol\ mol^{-1}$ (A_n) was significantly less in lower canopy needles ($8.3 \pm 0.3\ \mu mol\ m^{-2}\ s^{-1}$; mean ± SE, $n = 4$) compared with upper canopy needles ($10.7 \pm 0.4\ \mu mol\ m^{-2}\ s^{-1}$) (Table 3). Carbon isotope discrimination during photosynthesis (Δ_{obs}) and C_i/C_a were positively and significantly related (Fig. 2). The value of Δ_{obs} was in all cases less than predicted from theory ($\Delta_i = [4.4‰ + (30‰ - 4.4‰)C_i/C_a]$, with this difference being greater at lower values of C_i/C_a. Using these data, g_i was 0.16 $mol\ m^{-2}\ s^{-1}$ in lower canopy needles and 0.20 $mol\ m^{-2}\ s^{-1}$ in upper canopy needles; however, this difference was not statistically significant (Table 3). These values of g_i were 1.6–1.7 times greater than stomatal conductance (g_s). The mean ratio of C_c to C_i was 0.75 and 0.73 in lower and upper canopy needles, respectively.

Variation of g_i among trees – photocompensation method

C_i* was strongly negatively correlated to R_d (Fig. 3), and this relationship was virtually identical to that reported by Peisker & Apel (2001) with *Nicotiana tobacum*. From the regression equation (see Eqn 3) the mean Γ* was estimated as 39.4 $\mu mol\ mol^{-1}$ and g_i as 0.15 $mol\ m^{-2}\ s^{-1}$. Because Γ* is conservative, we used the mean Γ* (39.4 $\mu mol\ mol^{-1}$) and measured C_i* and Rd to calculate g_i for individual shoots (Eqn 4). Using this method, g_i was 0.14 $mol\ m^{-2}\ s^{-1}$ in lower canopy needles and 0.17 $mol\ m^{-2}\ s^{-1}$ in upper canopy needles; however, this differences was not statistically significant (Table 4). These values of g_i were 1.4–1.6 times greater

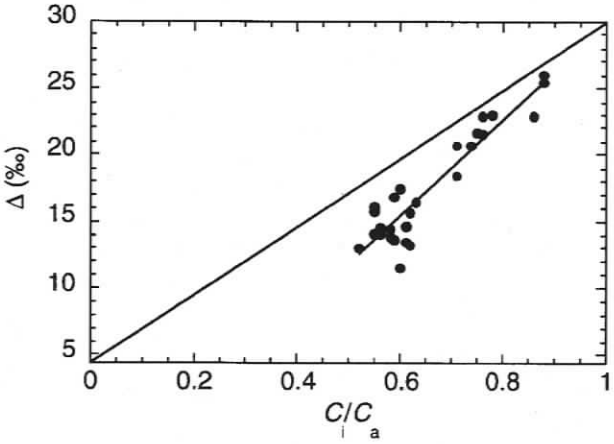

Figure 2. Relationship between the ratio of intercellular to ambient CO_2 concentrations (C_i/C_a) and discrimination against C^{13} during photosynthesis (Δ) for a single dominant Douglas-fir tree. The straight line (with $x = 0$ intercept) indicates the discrimination expected if transfer conductance were infinite (i.e. $\Delta = 4.4 + (30 - 4.4)\ C_i/C_a$). Each data point is a single simultaneous measurement of carbon isotope discrimination and gas exchange. A significant linear regression related Δ to C_i/C_a: $\Delta = -6.1 + 35.9 * C_i/C_a$, $r^2 = 0.86$).

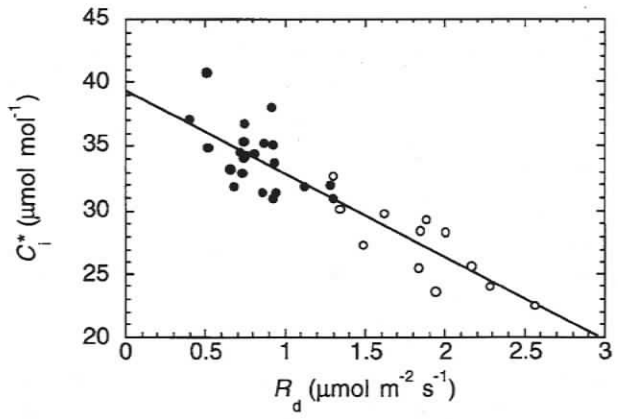

Figure 3. Relationship between the intercellular photocompensation point (C_i^*) and respiration in the light (R_d) in Douglas-fir (hollow circles). The straight line is a linear regression fitted to the Douglas-fir data: $C_i^* = 39.4 - 6.5 * R_d$, $r^2 = 0.67$. Also shown are data from Peisker & Apel (2001) for *Nicotiana tabacum* measured at 21.7 ± 0.1 °C (filled circles). Their regression equation is $C_i^* = 39.4 - 7.0 * R_d$, $r^2 = 0.34$.

than stomatal conductance (g_s). The mean ratio of C_c to C_i was 0.81 and 0.77 in lower and upper canopy needles, respectively.

Effects of g_i on photosynthesis

V_{cmax} was determined from the initial slope of A/C_i or A/C_c curves and our estimate of Γ^* (Fig. 4). When calculated from C_i, V_{cmax} values were 68–71% of estimates based on C_c (Table 4). At an ambient C_a of 360 μmol mol^{-1} internal limitations (L_i) constrained photosynthesis by 19–21%, somewhat less than that imposed by stomata (L_s of 30–31%)(Table 4).

Relationship of g_i to anatomy, morphology and physiology

It was not possible to examine relationships between g_i and anatomical/morphological traits because of the absence of significant differences in g_i and the small range in anatomical/morphological traits.

A compilation of data from 14 studies with our own data for Douglas-fir showed a positive relationship between A_n and g_i, and this relationship did not vary between measure-

Table 4. Variation in photosynthetic characteristics among Douglas-fir trees

Characteristic	Lower canopy	Upper canopy
Photocompensation point method ($n = 6$)		
A_n(μmol m^{-2} s^{-1})	6.5 (0.6)	9.0 (0.8)[a]
g_s(mol m^{-2} s^{-1})	0.09 (0.01)	0.12 (0.01)[a]
g_i (mol m^{-2} s^{-1})	0.14 (0.01)	0.17 (0.01)
C_c/C_i	0.81 (0.01)	0.77 (0.02)
V_{cmax}* (μmol m^{-2} s^{-1}) from A/C_i curves	27.8 (2.6)	36.9 (3.8)
V_{cmax} (μmol m^{-2} s^{-1}) from A/C_c curves	39.6 (4.6)	55.9 (7.5)
L_s (%)	30 (3)	31 (3)
L_i (%)	19 (1)	21 (2)

The maximum rate of light-saturated photosynthesis (A_n) and stomatal conductance (g_s) were determined at a C_a of 360 μmol mol^{-1}. Transfer conductance (g_i) was determined by the photocompensation point method (see methods). Maximal rates of carboxylation (V_{cmax}) were determined from A/C_i (*) or A/C_c curves at 22 °C, 210 mmol mol^{-1} O_2 and 1000 μmol m^{-2} s^{-1} PAR. The relative limitations of the net photosynthetic rate (at $C_a = 360$ μmol mol^{-1}) by stomatal (L_s) and internal (L_i) resistances were calculated as described in the text. Data are means (SE) of six replicates. [a]Significant differences ($P < 0.05$, Fisher's PLSD) between lower and upper canopy.

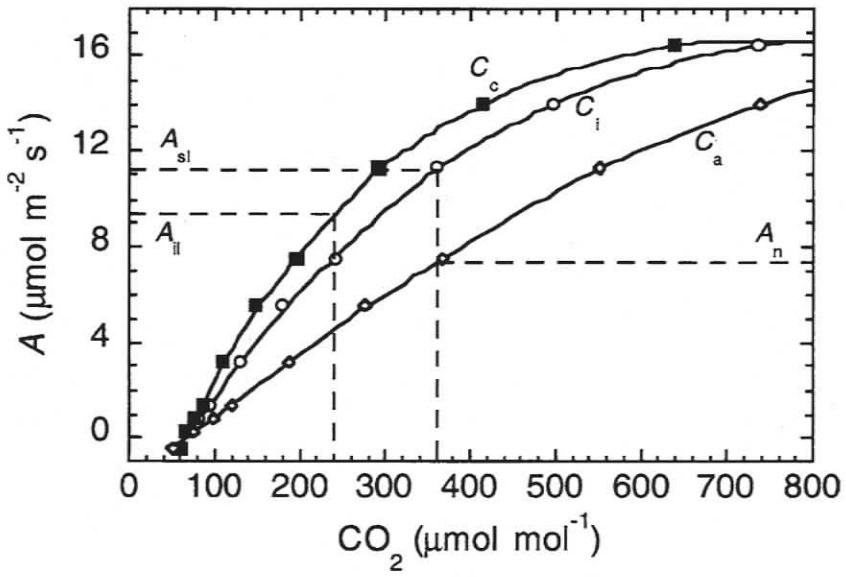

Figure 4. The response of net CO_2 assimilation (A) to CO_2 concentration in current-year foliage of Douglas-fir. The concentration of CO_2 was estimated in the chloroplast (filled squares), intercellular spaces (hollow circles), and ambient (hollow diamonds). Rates of net photosynthesis were estimated assuming g_i and g_s were as measured (A_n, the light-saturated rate of photosynthesis at $C_a = 360$ μmol mol^{-1}), assuming g_i was infinite and g_s as measured (A_{il}, the light-saturated rate of photosynthesis at $C_c = C_i$), or assuming g_i was as measured and g_s was infinite (A_{sl}, the light-saturated rate of photosynthesis at $C_i = 360$ μmol mol^{-1}). Data are for a typical lower canopy shoot.

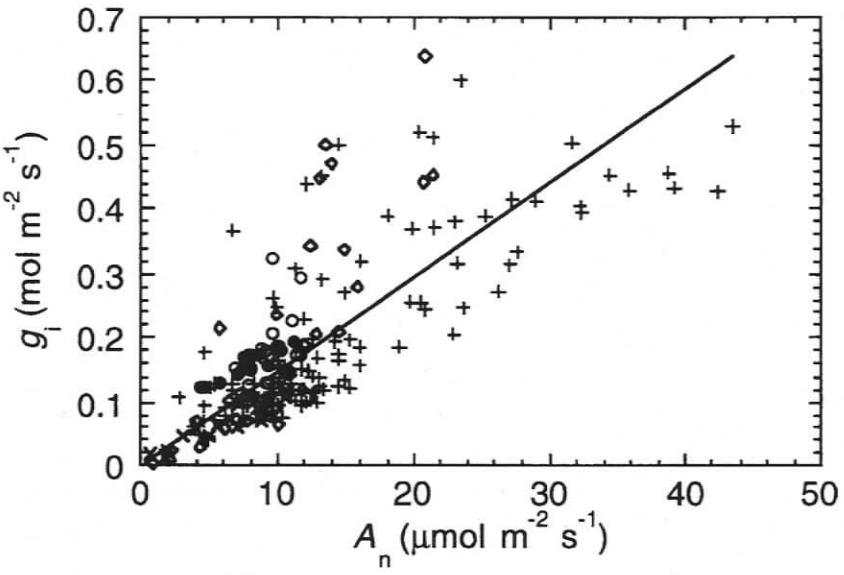

Figure 5. The relationship between the light-saturated rate of net CO_2 assimilation at $C_a = 360$ μmol mol^{-1} (A_n) and transfer conductance (g_i) from our own data and 14 published studies. Data were obtained from simultaneous gas exchange and carbon isotope discrimination (+)(von Caemmerer & Evans 1991; Lloyd *et al.* 1992; Loreto *et al.* 1992; Evans *et al.* 1994; Lauteri *et al.* 1997; Hanba, Miyazawa & Terashima 1999; Gillon & Yakir 2000; Hanba *et al.* 2001; Kogami *et al.* 2001), simultaneous gas exchange and chlorophyll fluorescence (✧)(Loreto *et al.* 1992; Loreto *et al.* 1994; Epron *et al.* 1995; Roupsard *et al.* 1996; Flexas *et al.* 2002), Rubisco content versus g_m (×)(Miyazawa & Terashima 2001). Douglas-fir data were derived from simultaneous gas exchange and carbon isotope discrimination (○), or the photocompensation point method (●). The straight line is the linear least-squares relationship between A_n and g_i for all data: $g_i = 0.0147 \times A_n$, $r^2 = 0.59$, $P < 0.0001$, $n = 209$.

ment techniques (Fig. 5). Among all studies and species, g_i was, on average, 0.0147 times A_n. In Douglas-fir, g_i was 0.019 times A_n when estimated with either the isotopic or photocompensation methods.

DISCUSSION

G_i and its effect on photosynthesis of Douglas-fir

Transfer conductance in current-year needles of 50-year-old Douglas-fir trees, determined by two independent methods, varied between 0.14 and 0.20 mol m^{-2} s^{-1} (Tables 3 & 4). There are no other measurements of g_i for conifers and few generally for evergreen trees. Our values of g_i for Douglas-fir are less than reported for herbaceous species (e.g. *Triticum* spp. $g_i = 0.4$–0.6 mol m^{-2} s^{-1}, von Caemmerer & Evans 1991; Loreto *et al.* 1992) and woody *Populus* sp. (0.50 mol m^{-2} s^{-1}, Roupsard, Gross & Dreyer 1996), but close to those reported for *Quercus* spp., *Eucalyptus* spp., *Fagus syl atica*, *Castanea sati a* (0.10–0.19 mol m^{-2} s^{-1}, von Caemmerer & Evans 1991; Loreto *et al.* 1992; Epron *et al.* 1995). In general, g_i of Douglas-fir is similar to plants with similar rates of photosynthesis (Fig. 5).

In contrast to our hypothesis, there was no statistically significant difference in g_i between upper and lower canopy needles even though g_i scaled approximately with A_n and g_s, both of which differed significantly between upper and lower canopy needles. Differences in g_i were not significant because of their greater variability compared to A_n and g_s. Nonetheless, the variability in our study (12% RSD, photocompensation method; 14% RSD, isotopic method) is somewhat less than studies with Chl fluorescence (e.g. 19–22% RSD, Harley *et al.* 1992; 34–38% RSD, Epron *et al.* 1995), but within the range of RSDs reported for studies using the isotopic method (6–13%, Lloyd *et al.* 1992; 19–24%, Loreto *et al.* 1992; 11–50%, Lauteri *et al.* 1997; 7–34%, Kogami *et al.* 2001). Hence, estimates of g_i are inherently variable irrespective of which method is used. This variability could be a serious problem for studies in which treatment differences are probably small. In our study, with a mean difference in g_i of 0.026 between upper and lower canopy needles we would have needed 17 replicates to have an equal probability of type I and type II errors at the 0.05 level (i.e. α and $\beta = 0.05$) (calculated after Cohen 1977).

In our study the range in g_i and anatomical traits was too small to discern relationships among them. Nevertheless, g_i did scale with A_n and g_s, as has been observed in other studies (e.g. von Caemmerer & Evans 1991; Loreto *et al.* 1992; Lloyd *et al.* 1992; Epron *et al.* 1995; Roupsard *et al.* 1996; Hanba *et al.* 2001). The strength of this relationship improves when the range in A_n and g_i increases, hence among species this relationship is strong with g_i being, on average, 0.0147 times A_n (Fig. 5). Nevertheless, there is large variation in g_i at a given A_n; for example at an A_n of 10 μmol m^{-2} s^{-1}, g_i varies between 0.06 and 0.31 mol m^{-2} s^{-1}. Therefore, a large proportion of variation in g_i is not explained by A_n, and relationships vary between species (e.g. Hanba *et al.* 2001). In many respects, these trends in the g_i–A_n relationships are analogous to those in A_n–N relationships (Field & Mooney 1986).

A small transfer conductance in Douglas-fir causes a large drawdown from C_i to C_c and imposes a large limitation on photosynthesis (Tables 3 & 4). Under light-saturated photosynthesis C_c was, on average, 73–81% of C_i. We estimated the relative limitations imposed on photosynthesis by internal (L_i) and stomatal (L_s) resistances (Table 4). Internal resistance imposed a limitation of approximately 20% on photosynthesis of Douglas-fir and is thus an important factor in the carbon balance of this species. To put this in perspective, the internal limitation is somewhat less than that imposed by stomata (30%) under well-watered conditions. Whereas the methods used for calculating limitations vary between studies, the limitations found here are similar to those reported for other evergreens (e.g. Epron *et al.* 1995). Transfer conductance affects estimates of V_{cmax} from the CO_2 response of photosynthesis (Table 4). Most published estimates of V_{cmax} under-estimate the true values by not considering the drawdown from C_i to C_c. In the case of Douglas-fir, C_i-based V_{cmax} estimates were 68–71% of estimates based on C_c. Hence, reports of apparently low V_{cmax} in woody species are, at least in part, a function of small transfer conductances (Epron *et al.* 1995). Small transfer conductances may also partly explain an apparent over-investment in Rubisco by woody species (e.g. Warren & Adams 2001) and poor photosynthetic nitrogen-use efficiency (Lloyd *et al.* 1992).

Anatomy, morphology, biochemistry, physiology and the light gradient

Acclimation of foliage within conifer canopies begins as foliage develops from buds and continues as leaves age and become more distal from shoot tips and more shaded over time (Schoettle & Smith 1991; Brooks, Sprugel & Hinckley 1996). Changes in needle thickness were the primary mechanism by which Douglas-fir acclimated to the light environment (Table 1, see also Aussenac 1973). Differences in needle thickness were largely responsible for the difference in SLA between upper and lower canopy foliage. Variation in most other anatomical traits was small or not significant, consistent with a recent report of modest developmental changes in the anatomy of Douglas-fir needle (Apple *et al.* 2002). This contrasts with broad-leaved species such as *Acer* spp. in which traits such as porosity and cell wall thickness respond to growth PAR (Hanba *et al.* 2002).

Variation in morphological or physiological traits was only evident when expressed on an area basis, as reported previously for Douglas-fir and other species (DeJong, Day & Johnson 1989; Bond *et al.* 1999). Hence, differences in the content per unit area of N, soluble proteins, and Rubisco were solely a function of differences in needle thickness and SLA. These data argue against any optimization of N allocation to leaves within the canopy, as also reported for *Pinus radiata* D. Don (Livingston *et al.* 1998). Instead, 'acclimation' in N content is simply a function of differences in SLA.

Nevertheless, there was some evidence of within-leaf acclimation of Douglas-fir needles to the light environment (Table 2). That is, needles from the lower canopy allocated more N to light harvesting (i.e. Chl/N greater) and had a lower Chl *a*/*b* ratio than needles from the upper canopy. Allocation of N to Rubisco did not vary with canopy height; however, Rubisco/Chl was less in lower canopy needles owing to their greater Chl/N. There are few comparative data on Rubisco and Rubisco/Chl ratios for conifers. Most studies have gone no further than measuring nitrogen, photosynthetic pigments (sometimes) and estimating nitrogen allocation from gas exchange data (e.g. V_{cmax} and J_{max} derived from the CO_2-response together with kinetic 'constants'). Such indirect estimation of nitrogen allocation may be misleading if inappropriate kinetic constants are used or the activation state of Rubisco varies (Warren & Adams 2001). In one of the few studies to directly measure the concentration of Rubisco, Warren & Adams (2001) reported an almost five-fold variation in Rubisco/Chl from the top to the bottom of a *Pinus pinaster* Ait. canopy. In Douglas-fir, Rubisco/Chl decreased from 8.6 to 6.0 mmol mol^{-1}, and thus the photosynthetic apparatus is much less plastic than *P. pinaster*.

Methodological considerations

Two independent methods of estimating g_i yielded similar results (compare Tables 3 & 4) despite having different theoretical bases and assumptions. Confidence in both methods is strengthened by Fig. 5 which shows that g_i values conform well to a 'universal' A_n–g_i relationship. g_i is typically estimated from concurrent measurements of photosynthesis and either carbon isotope discrimination or Chl fluorescence. Estimating g_i from the difference between chloroplastic and intercellular compensation points is appealing because of the reduced measurement and equipment demands. However, this method rests on a number of assumptions:

1 The Laisk (1977) method of determining C_i^* and R_d requires that neither R_d nor the specificity of Rubisco vary with the PAR used for measurement (Brooks & Farquhar 1985). Violation of this assumption introduces uncertainties in estimates of Γ^* and thus g_i. Our preliminary measurements indicated complete light inhibition of mitochondrial respiration occurs at light intensities of 150 μmol m^{-2} s^{-1} and above, as is supported by many studies (e.g. Brooks & Farquhar 1985; Atkin, Evans & Siebke 1998; Peisker & Apel 2001), but not all (e.g. Villar, Held & Merino 1994; Atkin *et al.* 2000).
2 Estimating g_i as $g_i = R_d/(\Gamma^* - C_i^*)$ (e.g. Table 4) permits estimates for individual shoots, but these estimates are highly sensitive to Γ^* and C_i^*. For example, in our study if Γ^* were 2 μmol mol^{-1} less, then g_i would increase by an average of 0.066 mol m^{-2} s^{-1}; whereas if Γ^* were 2 μmol mol^{-1} greater, g_i would decrease by an average of 0.026 mol m^{-2} s^{-1}. This sensitivity (of g_i to Γ^*) is very similar to that reported for estimates of g_i from Chl fluorescence (Harley *et al.* 1992).

3 Determining Γ^* (after Peisker & Apel 2001) from a linear regression of C_i^* versus R_d (Fig. 4) is reliant upon both Γ^* and g_i being invariant. Γ^* is a fundamental property of Rubisco and should, in theory, vary little among C_3 species (von Caemmerer 2000), and we note our Γ^* estimate for Douglas-fir is identical to the value found by Peisker & Apel (2001) for tobacco (Fig. 4) and to the value determined *in itro* by Jordan & Ogren (1984) for spinach. In our study R_d and g_i were unrelated (data not shown), and thus we could calculate Γ^* from a linear regression of C_i^* versus R_d. However, in studies in which the range in photosynthesis is greater, this assumption will most likely be violated owing to positive relationships between photosynthesis and R_d (e.g. Le Roux *et al.* 1999; Meir *et al.* 2002) and A_n and g_i (Fig. 5).

CONCLUSIONS

Our study has provided the first estimates of g_i for a coniferous species. In current-year needles of Douglas-fir, g_i limited photosynthesis by approximately 20% as compared to approximately 30% stomatal limitation (under well-watered conditions). Our data demonstrate that gas exchange estimates of V_{cmax} may seriously underestimate Rubisco activity if g_i and the drawdown from C_i to C_c are ignored. Variation in g_i with height was shown to be comparatively small. The absence of significant differences in g_i is, at least in part, a reflection of the inherently high variability of such estimates. Nevertheless, we cannot exclude the possibility that g_i does not vary with canopy height. This latter possibility is consistent with the relatively fixed needle anatomy of Douglas-fir, and reports that one or other anatomical traits are strong determinants of g_i.

ACKNOWLEDGMENTS

This research was supported by grants from the Natural Sciences and Engineering Research Council of Canada, the Canadian Foundation for Innovation, Forest Renewal British Columbia, BC Science Council. Michael Whiticar is thanked for providing access to mass spectrometer facilities. The $\delta^{13}C$ analysis methodology was developed in collaboration with Magnus Eek. Gas sampling flasks were kindly provided by C.S. Wong at the Institute of Ocean Sciences, Victoria. We gratefully acknowledge A.J. Keys (IACR-Rothamsted) for providing pure wheat Rubisco, and P. Millard (Macauley Land Research Institute) for supplying polyclonal antibodies. Matthew Mitchell, Samantha Robbins, and Lindsay White are warmly thanked for technical assistance. Timberwest Forest Co. and Weyerhaeuser Canada Ltd. generously provided access to and logistical support at the research site.

REFERENCES

Aalto T. & Juurola E. (2002) A three-dimensional model of CO_2 transport in airspaces and mesophyll cells of a silver birch leaf. *Plant, Cell and En ironment* **25,** 1399–1409.

Apple M., Tiekotter K., Snow M., Young J., Soeldner A., Phillips D., Tingey D. & Bond B.J. (2002) Needle anatomy changes with increasing tree age in Douglas-fir. *Tree Physiology* **22,** 129–136.

Atkin O.K., Evans J.R., Ball M.C., Lambers H. & Pons T.L. (2000) Leaf respiration of snow gum in the light and dark. Interactions between temperature and irradiance. *Plant Physiology* **122,** 915–923.

Atkin O.K., Evans J.R. & Siebke K. (1998) Relationship between the inhibition of leaf respiration by light and enhancement of leaf dark respiration following light treatment. *Australian Journal of Plant Physiology* **25,** 437–443.

Aussenac G. (1973) Effets de conditions microclimatiques différentes sur la morphologie et la structure anatomique des aiguilles de quelques résineux. *Annales Des Sciences Forestieres* **30,** 375–392.

Badger M.R. & Collatz G.J. (1977) Studies on the kinetic mechanism of ribulose-1,5-bisphosphate carboxylase and oxygenase reactions, with particular reference to the effect of temperature on kinetic parameters. *Carnegie Institution of Washington Year Book* **76,** 355–361.

Berlyn G. & Miksche J. (1976) *Botanical Microtechnique and Cytochemistry.* The Iowa State University Press, Ames, IA, USA.

Bond B.J., Farnsworth B.T., Coulombe R.A. & Winner W.E. (1999) Foliage physiology and biochemistry in response to light gradients in conifers with varying shade tolerance. *Oecologia* **120,** 183–192.

Brooks A. & Farquhar G.D. (1985) Effects of temperature on the CO_2/O_2 specificity of ribulose-1,5-bisphosphate carboxylase/oxygenase and the rate of respiration in the light. Estimates from gas exchange measurements on spinach. *Planta* **165,** 397–406.

Brooks J.R., Sprugel D.G. & Hinckley T.M. (1996) The effect of light acclimation during and after foliage expansion on photosynthesis of *Abies amabilis* foliage within the canopy. *Oecologia* **107,** 21–32.

von Caemmerer S. (2000) Biochemical models of leaf photosynthesis. *Techniques in Plant Sciences No. 2,* 165 pp. CSIRO Publishing, Collingwood, Victoria, Australia.

von Caemmerer S. & Evans J.R. (1991) Determination of the average partial pressure of CO_2 in chloroplasts from leaves of several C_3 plants. *Australian Journal of Plant Physiology* **18,** 287–305.

von Caemmerer S. & Farquhar G.D. (1981) Some relationships between the biochemistry of photosynthesis and the gas exchange of leaves. *Planta* **153,** 376–387.

Carraro U., Doria D., Rizzi C. & Sandri M. (1994) A new two-step precipitation method removes free SDS and thiol reagents from diluted solutions, and then allows recovery and quantitation of proteins. *Biochemical and Biophysical Research Communications* **200,** 916–924.

Catt J.W. & Millard P. (1988) The measurement of ribulose 1,5-bisphosphate carboxylase/oxygenase concentration in the leaves of potato plants by enzyme linked immunosorbtion assays. *Journal of Experimental Botany* **39,** 157–164.

Cohen J. (1977) *Statistical Power Analysis for the Beha ioural Sciences.* Academic Press, New York, USA.

DeJong T.M., Day K.R. & Johnson R.S. (1989) Partitioning of leaf nitrogen with respect to within canopy light exposure and nitrogen availability in peach (*Prunus persica*). *Trees* **3,** 89–95.

Epron D., Godard D., Cornic G. & Genty B. (1995) Limitation of net CO_2 assimilation rate by internal resistance to CO_2 transfer in the leaves of two tree species (*Fagus syl atica* L. & *Castanea sati a* Mill.). *Plant, Cell and En ironment* **18,** 43–51.

Evans J.R., Sharkey T.D., Berry J.A. & Farquhar G.D. (1986) Carbon isotope discrimination measured concurrently with gas

exchange to investigate CO_2 diffusion in leaves of higher plants. *Australian Journal of Plant Physiology* **13,** 281–292.

Evans J.R., von Caemmerer S., Setchell B.A. & Hudson G.S. (1994) The relationship between CO_2 transfer conductance and leaf anatomy in transgenic tobacco with a reduced content of Rubisco. *Australian Journal of Plant Physiology* **21,** 475–495.

Farquhar G.D. & Sharkey T.D. (1982) Stomatal conductance and photosynthesis. *Annual Re iew of Plant Physiology* **33,** 317–345.

Farquhar G.D., von Caemmerer S. & Berry J.A. (1980) A biochemical model of photosynthetic CO_2 assimilation in leaves of C_3 species. *Planta* **149,** 78–90.

Field C. & Mooney H.A. (1986) The photosynthesis-nitrogen relationship in wild plants. In: *On the Economy of Form and Function* (ed. T.J. Givnish) pp. 25–55. Cambridge University Press, Cambridge, UK.

Flexas J., Bota J., Escalona J.M., Sampol B. & Medrano H. (2002) Effects of drought on photosynthesis in grapevines under field conditions: an evaluation of stomatal and mesophyll limitations. *Functional Plant Biology* **29,** 461–471.

Gillon J.S. & Griffiths H. (1997) The influence of (photo) respiration on carbon isotope discrimination in plants. *Plant, Cell and En ironment* **20,** 1217–1230.

Gillon J.S. & Yakir D. (2000) Internal conductance to CO_2 diffusion and (COO) -O-18 discrimination in C-3 leaves. *Plant Physiology* **123,** 201–213.

Hanba Y.T., Kogami H. & Terashima I. (2002) The effect of growth irradiance on leaf anatomy and photosynthesis in *Acer* species differing in light demand. *Plant, Cell and En ironment* **25,** 1021–1030.

Hanba Y.T., Miyazawa S.-I., Kogami H. & Terashima I. (2001) Effects of leaf age on internal CO_2 transfer conductance and photosynthesis in tree species having different types of shoot phenology. *Australian Journal of Plant Physiology* **28,** 1075–1084.

Hanba Y.T., Miyazawa S.-I. & Terashima I. (1999) The influence of leaf thickness on the CO_2 transfer conductance and leaf stable carbon isotope ratio for some evergreen tree species in Japanese warm-temperate forests. *Functional Ecology* **13,** 632–639.

Harley P.C., Loreto F., Di Marco G. & Sharkey T.D. (1992) Theoretical considerations when estimating the mesophyll conductance to CO_2 flux by analysis of the response of photosynthesis to CO_2. *Plant Physiology* **98,** 1429–1436.

Humphreys E.R., Black T.A., Ethier G.J., Drewitt G.B., Spittlehouse D.L., Jork E.-M., Nesic Z. & Livingston N.J. (2002) Annual and seasonal variability of sensible and latent heat fluxes above a coastal Douglas-fir forest, British Columbia, Canada. *Agricultural and Forest Meteorology* **3084,** 1–17.

Johansen D.A. (1940) *Plant Microtechnique*. McGraw-Hill Co., Inc, New York, USA.

Jordan D.B. & Ogren W.L. (1984) The CO_2/O_2 specificity of ribulose 1,5-bisphosphate carboxylase/oxygenase. Dependence on ribulosebisphosphate concentration, pH and temperature. *Planta* **161,** 308–313.

Kogami H., Hanba Y.T., Kibe T., Terashima I. & Masuzawa T. (2001) CO_2 transfer conductance, leaf structure and carbon isotope composition of *Polygonum cuspidatum* leaves from low and high altitudes. *Plant, Cell and En ironment* **24,** 529–538.

Laisk A.K. (1977) *Kinetics of Photosynthesis and Photorespiration in C_3-Plants*. Nauka, Moscow, Russia.

Laisk A., Oja V. & Rahi M. (1970) Diffusion resistance of leaves in connection with their anatomy. *Fiziologiya Rastenii* **47,** 40–48.

Lauteri M., Scartazza A., Guido M.C. & Brugnoli E. (1997) Genetic variation in photosynthetic capacity, carbon isotope discrimination ands mesophyll conductance in provenances of *Castanea sati a* adapted to different environments. *Functional Ecology* **11,** 675–683.

Le Roux X., Grand S., Dreyer E. & Daudet F.-A. (1999) Parameterization and testing of a biochemically based photosynthesis model for walnut (*Juglans regia*) trees and seedlings. *Tree Physiology* **19,** 481–492.

Lewis J.D., McKane R.B., Tingey D.T. & Beedlow P.A. (2000) Vertical gradients in photosynthetic light response within an old-growth Douglas-fir and western hemlock canopy. *Tree Physiology* **20,** 447–456.

Livingston N.J., Whitehead D., Kelliher F.M., Wang Y.-P., Grace J.C., Walcroft A.S., Byers J.N., Mcseveny T.M. & Millard P. (1998) Nitrogen allocation and carbon isotope fractionation in relation to intercepted and position in a young *Pinus radiata* D.Don tree. *Plant, Cell and En ironment* **21,** 795–803.

Lloyd J., Syvertsen J.P., Kriedemann P.E. & Farquhar G.D. (1992) Low conductances for CO_2 diffusion from stomata to the sites of carboxylation in leaves of woody species. *Plant, Cell and En ironment* **15,** 873–899.

Loreto F., Di Marco G., Tricoli D. & Sharkey T.D. (1994) Measurements of mesophyll conductance, photosynthetic electron transport and alternative electron sinks of field grown wheat leaves. *Photosynthesis Research* **41,** 397–403.

Loreto F., Harley P.C., Di Marco G. & Sharkey T.D. (1992) Estimation of mesophyll conductance to CO_2 flux by three different methods. *Plant Physiology* **98,** 1437–1443.

Meir P., Kruijt B., Broadmeadow M., Barbosa E., Kull O., Carswell F., Norbre A. & Jarvis P.G. (2002) Acclimation of photosynthetic capacity to irradiance in tree canopies in relation to leaf nitrogen capacity and leaf mass per unit area. *Plant, Cell and En ironment* **25,** 343–357.

Miller J.B., Yakir D., White J.W.C. & Tans P.P. (1999) Measurement of O-18/O-16 in the soil-atmosphere CO_2 flux. *Global Biogeochemical Cycles* **13,** 761–774.

Miyazawa S.-I. & Terashima I. (2001) Slow development of leaf photosynthesis in an evergreen broad-leaved tree, *Castanopsis sieboldii*: relationships between leaf anatomical characteristics and photosynthetic rate. *Plant, Cell and En ironment* **24,** 279–291.

Nobel P.S. (1991) *Physicochemical and En ironmental Plant Physiology*. Academic Press, San Diego, CA, USA.

Nobel P.S., Zaragoza L.J. & Smith W.K. (1975) Relation between mesophyll surface area, photosynthetic rate, and illumination level during development for leaves of *Plectranthuis par iflorus* Henckel. *Plant Physiology* **55,** 1067–1070.

Parker G.G., Davis M.M. & Chapotin S.M. (2002) Canopy light transmittance in Douglas-fir–western hemlock stands. *Tree Physiology* **22,** 147–157.

Parkhurst D.F. & Mott K.A. (1990) Intercellular diffusion limits to CO_2 uptake in leaves. *Plant Physiology* **94,** 1024–1032.

Peisker M. & Apel H. (2001) Inhibition by light of CO_2 evolution from dark respiration: comparison of two gas exchange methods. *Photosynthesis Research* **70,** 291–298.

Roupsard O., Gross P. & Dreyer E. (1996) Limitation of photosynthetic activity by CO_2 availability in the chloroplasts of oak leaves from different species and during drought. *Annales Des Sciences Forestieres* **53,** 243–254.

Schoettle A.W. & Smith W.K. (1991) Interrelation between shoot characteristics and solar irradiance in the crown of *Pinus contorta* ssp. *latifolia*. *Tree Physiology* **9,** 245–254.

Serrano L., Gamon J.A. & Berry J. (1997) Estimation of leaf area with an integrating sphere. *Tree Physiology* **17,** 571–576.

Villar R., Held A.A. & Merino J. (1994) Comparison of methods to estimate dark respiration in the light in leaves of two woody species. *Plant Physiology* **105,** 167–172.

Vitousek P.M., Field C.B. & Matson P.A. (1990) Variation in foliar $\delta^{13}C$ in Hawaiian *Metrosideros polymorpha*: a case of internal resistance? *Oecologia* **84,** 362–370.

Warren C.R. & Adams M.A. (2001) Distribution of N, Rubisco and photosynthesis in *Pinus pinaster* and acclimation to light. *Plant, Cell and En ironment* **24,** 597–609.

Wellburn A.R. (1994) The spectral determination of chlorophylls *a* and *b*, as well as total carotenoids, using various solvents with spectrophotometers of different resolution. *Journal of Plant Physiology* **144,** 307–313.

Recei ed 7 October 2002; recei ed in re ised form 3 February 2003; accepted for publication 12 February 2003